TRMT1L-catalyzed $m^2{}_2G27$ on tyrosine tRNA is required for efficient mRNA translation and cell survival under oxidative stress.

Sseu-Pei Hwang[1, 2, †], Han Liao[1, †], Katherine Barondeau[1], Xinyi Han[1], Cassandra Herbert[3], Hunter McConie[1], Amirtha Shekar[1], Dimitri Pestov[4], Patrick A Limbach[3], Jeffrey T Chang[1], and Catherine Denicourt[1, 5, *].

[1] Department of Integrative Biology and Pharmacology, McGovern Medical School, The University of Texas Health Science Center, Houston, TX, USA

[2] The University of Texas MD Anderson Cancer Center UTHealth Houston Graduate School of Biomedical Sciences, Houston, TX, USA

[3] Rieveschl Laboratories for Mass Spectrometry, Department of Chemistry, University of Cincinnati, Cincinnati, OH, USA

[4] Department of Cell Biology and Neuroscience, Virtua Health College of Medicine and Life Sciences, Rowan University, Stratford, NJ, USA

[5] Lead Contact

[†] The first two authors contributed equally to this work

Present address: Han Liao, CAS Key Laboratory of Separation Science for Analytical Chemistry, Dalian Institute of Chemical Physics, Chinese Academy of Sciences, Dalian, China, 116023

* To whom correspondence should be addressed. Tel: +1 713-500-5696; Fax: 713-500-7444; Email: Catherine.Denicourt@uth.tmc.edu

Keywords: TRMT1L, RNA methyltransferases, N2, N2-dimethylguanosine ($m^2{}_2G$), eCLIP-seq, tRNA, rRNA, mRNA translation, oxidative stress response.

ABSTRACT

Mapping of the epitranscriptome has revealed the chemical diversity of RNA modifications and their functional importance in regulating gene expression. Transfer RNAs (tRNAs) are one of the most modified cellular RNAs, containing on average 10-13 modifications per molecule. These modifications have been shown to be critical for several aspects of tRNA functions, such as decoding, folding, and stability. Here we report that the human RNA methyltransferase TRMT1L associates with components of the Rix1 ribosome biogenesis complex and co-sediments with pre-60S ribosomes. Using eCLIP-Seq, we show that TRMT1L binds to a subset of tRNAs and to the 28S rRNA. Additionally, we demonstrate that TRMT1L is responsible for catalyzing N2, N2-dimethylguanosine ($m^2{}_2G$) solely at position 27 of tRNA-Tyr-GUA by Nano-tRNAseq and RNA LC-MS. Surprisingly, TRMT1L depletion also impaired the deposition of acp^3U and dihydrouridine on tRNA-Tyr-GUA, Cys-GCA, and Ala-CGC. TRMT1L knockout cells have a marked decrease in tRNA-Tyr-GUA levels, coinciding with a reduction in global translation rates and hypersensitivity of oxidative stress. Our results establish TRMT1L as the elusive methyltransferase catalyzing the $m^2{}_2G27$ modification on tRNA Tyr, resolving a long-standing gap of knowledge and highlighting its potential role in a tRNA modification circuit crucial for translation regulation and stress response.

INTRODUCTION

Post-transcriptional modification of RNA molecules has emerged as a key regulatory component of eukaryotic gene expression (1,2). Around 170 different types of chemical modification have been reported on coding and non-coding RNAs from all three domains of cellular life (2). In eukaryotes, nuclear-encoded tRNAs are the most extensively modified RNA, containing on average 10-13 modifications per molecule (3). tRNAs are essential adapter molecules that deliver amino acids to the ribosome to translate the genetic information encoded by mRNA templates (4). Modification expands the chemical properties of RNA nucleosides, thereby having a direct influence on tRNA structure, stability, and decoding function (3,5). The type and position of nucleoside modification varies between the different tRNA species. While some modifications are found on most tRNAs, others decorate only a subset. Positions 34 and 37 located in the tRNA anticodon loop are often found to harbor various modifications that regulate the stability and specificity of codon recognition (3). Modifications clustered in the tRNA core structure outside of the anticodon loop, regulate tRNA folding and stability (6-9). Hence, proper modification of tRNAs is essential for accurate and efficient translation. As such, the deregulation of tRNA modification and the enzymes responsible for their catalysis have been linked with altered mRNA translation programs in several human diseases (10,11).

Within the landscape of tRNA modifications, methylation stands out as a prevalent process affecting the nitrogen base or sugar (ribose) backbone, and this modification is primarily facilitated by S-adenosyl-methionine (SAM)-dependent methyltransferases. Although various methyltransferases responsible for tRNA methylation have been well-characterized in prokaryotes and *Saccharomyces cerevisiae*, understanding of their roles in vertebrates has remained elusive (12). Among these, TRMT1L emerges as a vertebrate paralog of the evolutionarily conserved SAM-dependent methyltransferase, TRMT1 (13,14). TRMT1 catalyzes the deposition of N2, N2-dimethylguanosine ($m^2{}_2G$) at position 26 of cytosolic and mitochondrial tRNAs (14-19). Unlike TRMT1, which possesses a mitochondrial-targeting sequence and localizes to mitochondria, cytosol, and nucleus, TRMT1L predominantly resides in the nucleus and nucleolus (13,14). Noteworthy is the shared significance of TRMT1 and TRMT1L in regulating neuronal functions, as studies demonstrate that genetic deletion of TRMT1L in mice disrupts motor coordination and induces aberrant exploratory behaviors (13,14,20-22). While the activity and targets of TRMT1 have been extensively characterized across various organisms, including humans, the substrates and function of TRMT1L remain incompletely elucidated. Recent investigations examining mouse brains RNA-seq datasets for modifications-induced mismatch signatures, suggested that TRMT1L could catalyze the deposition of $m^2{}_2G$ at position 26 on tRNA-Ala (AGC) (13). These findings imply that, akin to TRMT1, TRMT1L may function as an N2, N2-dimethylguanosine RNA methyltransferase, potentially evolving to act upon a similar or distinct set of substrates.

The $m^2{}_2G$-modified nucleotide at position 26 is found in the structural hinge region formed between the dihydro-uridine stem (D-stem) and the anticodon stem loop (ASL) in the vast majority of eukaryotic tRNAs (23,24). The presence of a N2, N2 dimethyl group on G precludes its pairing with C and, consequently $m^2{}_2G$ pairs almost exclusively with A, U,

or G at position 44 of the canonical tRNA structure. Consistent with the crucial roles of modification in regulating tRNA structure, both molecular dynamic simulations and crystal structure determination studies revealed that $m^2{}_2G$ not only inhibits the pairing of G26 with C in the tRNA D-stem but also regulates the pairing mode with A, favoring a more stable imino-hydrogen bonded form (25-27). Additionally, it has been suggested that the presence of $m^2{}_2G$ in cytosolic tRNAs likely serves to deter their adoption of atypical structures observed in mitochondrial tRNAs (mtRNAs), which lack the six canonical base pairs within the anticodon stem (9).

Emerging evidence demonstrates the crucial involvement of tRNA modifications in cellular stress responses, suggesting a systemic regulation of tRNA function in orchestrating translational programs for stress adaptation (28-31). This systemic control encompasses the diverse array of tRNA modifications, indicating their multifaceted roles in governing cellular adaptation to environmental challenges. Notably, the $m^2{}_2G$ modification undergoes dynamic regulation in response to oxidative stress, DNA damage, and nutrient deprivation (32,33). Recent studies in human cells have revealed that depletion of TRMT1, the enzyme responsible for catalyzing the $m^2{}_2G$ modification in both cytoplasmic and mitochondrial tRNAs, results in diminished global protein translation, elevated cellular levels of reactive oxygen species (ROS), and increased susceptibility to oxidizing agents (14). These findings suggest a crucial role for $m^2{}_2G$ modification in maintaining protein synthesis efficiency and cellular redox balance, highlighting its significance in cellular homeostasis and stress response mechanisms.

Here, we report the functional characterization of TRMT1L in human cells. While performing a proteomic purification of the Rix1 60S ribosome biogenesis complex, we identified TRMT1L as an interacting component. We show that it co-sediments with pre-60S particles, indicating a potential role in ribosomal RNA (rRNA) regulation. Using an eCLIP-seq approach, we demonstrate that TRMT1L specifically binds to the 28S rRNA expansion segment ES7Lb and to a small subset of nuclear-encoded tRNAs, of which Cys-GCA and Tyr-GUA were the most abundantly enriched. Using CRISPR-generated TRMT1L knock-out (KO) cells, we find that TRMT1L is required to catalyze the deposition of $m^2{}_2G$ at position 27 of only tRNAs Tyr-GUA. TRMT1L-dependent $m^2{}_2G$ modifications were not detected of any other tRNAs nor the 28S rRNA, suggesting that it may have catalytically independent functions depending on the RNA substrate. Intriguingly, TRMT1L-deficiency also leads to a loss of 3-(3-amino-3-carboxypropyl) uridine (acp^3U) and dihydrouridine (D) modifications on Tyr-GUA, Cys-GCA and Ala-CGC tRNAs, suggesting that TRMT1L may be part of a modification circuit required for the deposition of acp^3U and D by DTWD1 and DUS enzymes, respectively. Quantitative analysis of tRNA abundance in TRMT1L KO cells revealed a significant decrease in tRNA-Tyr-GUA levels, which correlated with a decline in global mRNA translation and hypersensitivity to endoplasmic reticulum (ER) and oxidative stress compared to WT cells. Our findings reinforce the importance of $m^2{}_2G$ in tRNA regulation for stress response and suggest an essential role for TRMT1L in regulating tRNA functions and establishing an adaptive translational program in response to oxidative and ER stress.

MATERIAL AND METHODS

Reagents

Reagents and kits used in this study were: Amersham Hybond N+ nylon membrane (RPN303B, GE Healthcare), AMPure RNAClean XP beads (A63987, Beckman Coulter), AMV Reverse Transcriptase (M510A, Promega), AMV Reverse Transcriptase 5X Reaction Buffer (M515A, Promega), Aprotinin (BP250310, Fisher), AEBSF (BP635-500, Fisher), BCA assay kit (23225, Pierce), CX-5461 (C2954-2s, Cellagen Technologies), Direct RNA Sequencing Kit (SQK-RNA002, Oxford Nanopore technologies), DMEM (no glucose) (11966025, Gibco), EconoFit Macro-Prep DEAE columns (BioRad, 12009274), Exonuclease I (M0293S, NEB), FastAP Thermosensitive Alkaline Phosphatase (EF0651, Thermo Scientific), Fetal bovine serum (SV30014.03, Hyclone), G50 spin column (27-5330-01, GE Healthcare), High glucose DMEM (SH30022.01, HyClone), Immun-Star AP substrate (1705018, Bio-rad), Lipofectamine RNAi Max (13778150, Invitrogen), Monarch RNA Cleanup kit (T2030L, NEB), Murine RNase inhibitor (M0314, NEB), Nitrocellulose membrane (1620115, Bio-rad), Penicillin-Streptomycin (SH40003.01, Hyclone), Protease inhibitor cocktail (78437, Thermo Scientific), Protinase K (46-7185, Invitrogen), Protein G Dynabeads (10003D, Invitrogen), Puromycin (P8833, Sigma), pCp-Biotin (NU-1706-Bio, Jena Bioscience), Q5 Site-Directed Mutagenesis Kit (E0554S, NEB), Recombinant protein G sepharose beads (101242, Invitrogen), RNase T1 (EN0541, Thermo Scientific), Silver stain kit (24612, Pierce), Streptavidin-alkaline pohsophatase conjugate (434322, Invitrogen), Streptavidin Magnetic Beads (S1420S, NEB), Streptavidin-IR800 (926-32230, LI-COR), SYBR Gold Nucleic Acid Gel Stain (S11494, Invitrogen), Thapsigargin (586006, Sigma), SuperScript IV Reverse Transcriptase (18090010, Invitrogen), TRIzol reagent (15596026, Invitrogen), Turbo DNase (AM2239, Invitrogen), TurboDNase buffer (AM2238, Invitrogen), T4 polynucleotide kinase (M0201S, NEB), T4 polynucleotide kinase reaction buffer (B0201S, NEB), T4 RNA ligase (M0204S, NEB), T4 RNA ligase 2 (M0239S, NEB), Leupeptin (PI78435, Fisher), [γ-^{32}P]ATP (NEG502A250UC, Perkin-Elmer). Antibodies used were: Anti-PELP1 (A300-180A, Bethyl), Anti-TRMT1L (Western blot) (A305-120A, Bethyl), Anti-TRMT1L (immunofluorescence staining) (SAB1408048-50UG, Sigma), Anti-SENP3 (5591, Cell Signaling), Anti-WDR18 (described in (34)), Anti-NPM1 (sc-56622, Santa Cruz Biotechnology), Anti-uL5 (RPL11) (SAB1402896, Sigma), Anti-Myc 9E10 (sc-40, Santa Cruz Biotechnology), Anti-TRMT1 (A304-205A, Bethyl), Anti-FBL (A303-891A, Bethyl), Anti-DDX21 (A300-627A), Anti-$m^2{}_2G$ (ab211488, Abcam), Anti-normal rabbit immunoglobulin G (IgG) (NI01, Millipore), Anti-GAPDH (sc-47724, Santa Cruz Biotechnology), Anti-Puromycin (PMY-2A4-s, DSHB), Anti-Mouse IgG H&L (Alexa Fluor 488) (A11001, Invitrogen), Anti-Rabbit IgG H&L (Alexa Fluor 594) (A11012, Invitrogen).

Biological resources

HCT116 wildtype (WT), HeLa, HT1080, U2OS, and HEK293T cells were purchased from ATCC. pLentiCRISPR v2 plasmid was obtained from Addgene (52961). pCMV-Myc was purchased from Clontech.

Data availability/sequence data resources

The datasets generated and/or analyzed during the current study are publicly available at the GEO genomics data repository (accession number pending).

Cell culture, RNA interference, proliferation assay and stress conditions

HCT116 WT, HeLa, HT1080, U2OS and HEK293T cells were cultured under 5% CO_2 atmosphere at 37°C in high glucose Dulbecco's modified Eagle's medium (DMEM) supplement with 5% fetal bovine serum (FBS) and 100 U/ml penicillin, and 100 µg/ml streptomycin. Synthetic short interfering RNA (siRNA) oligonucleotides (Sigma) were reverse transfected into the cells with Lipofectamine RNAi Max following the manufacturer's instructions. For transfection, 20 nM of siRNA oligonucleotide was mixed with 6 µl of Lipofectamine RNAi Max per well (6-well plate). The suspension cells were then mixed with the siRNA transfection mixture and incubate under 5% CO_2 atmosphere at 37°C. The sequences of the siRNAs utilized are listed in Supplementary Table S1. For the proliferation assay, 10,000 cells were plated into wells of a 48-well plate, and cultured for 6 days. The cells in each well were counted every 24 h. For the cellular stress assays the following treatments were applied. For oxidative stress, cells were incubated with growth media supplemented with 0 or 500 µM of H2O2 for 30 min. The cells were washed twice with phosphate buffered saline (PBS) and incubated in regular growth media for 48h. For endoplasmic reticulum (ER) stress, the cells were treated with 0 or 2 µM Thapsigargin for 48h. For the low glucose condition, the cells were washed three times with PBS and incubated in glucose-free DMEM supplemented with 5% FBS and 2.5 mM glucose for 48h. The cells were washed three times with PBS and grown in serum free DMEM for 48h for serum starvation. The cells were counted with trypan blue exclusion for all conditions at the 48h timepoint.

Immunoprecipitation and immunoblotting

For immunoprecipitation experiments, cells were lysed in ELB buffer (50 mM HEPES, pH 7.2, 250 mM NaCl, 2 mM EDTA, 0.5% NP-40) supplemented with protease inhibitors (aprotinin, leupeptin, AEBSF) on ice for 15 minutes. Lysates were then cleared by centrifugation at 22,000 × g for 10 minutes at 4°C, and the supernatant was incubated with 1 µg of normal rabbit IgG, anti-PELP1 antibody, or anti-TRMT1L antibody for 1 hour with rotation at 4°C. Protein G Sepharose beads were added for an additional 1 hour with rotation at 4°C. For immunoblotting, cells were lysed using RIPA buffer (25mM Tris-HCl pH 7.6, 150 mM NaCl, 1% NP-40, 1% Triton X-100, 1% sodium deoxycholate, and 0.1% SDS) and protease inhibitors on ice for 15 min. Lysates were cleared by centrifugation at 15,000 rpm for 10 minutes at 4°C. Protein concentrations were quantified using a BCA kit. Equal amounts of proteins were separated by SDS-PAGE and transferred to a 0.45 µm nitrocellulose membrane. The antibodies used for detection are listed in the reagent section.

Proteomic mass spectrometry analysis

HEK293T cells were lysed in ELB buffer (50 mM HEPES, pH 7.2, 250 mM NaCl, 2 mM EDTA, 0.5% NP-40) containing protease inhibitors (aprotinin, leupeptin, AEBSF) on ice

for 15 min, and lysates were cleared by centrifugation at 22,000 × *g* for 10 min at 4°C. The supernatants were incubated with 2 µg of normal rabbit IgG or anti-PELP1 antibody for 1 h with rotation at 4°C. Protein G Sepharose beads were added for another 1 h with rotation at 4°C. Precipitated complexes were eluted in SDS–PAGE sample buffer and separated on a 10% SDS–PAGE. The gel was silver-stained (Pierce silver stain kit) and proteins present only in the anti-PELP1 lane were cut out, digested with trypsin, and analyzed by mass spectrometry on an Orbitrap Exploris 480 instrument (Whitehead Institute Quantitative Proteomic Core).

Generation of TRMT1L knockout (KO) cells

To establish CRISPR-KO cell lines, guide RNAs targeting TRMT1L were designed with CHOPCHOP (35). A non-targeting sgRNA control was used to establish cells labeled as WT: 5'-AACCTACGGGCTACGATACG-3', KO1 targeting region: 5'-GTAGTTGTGAGAGTTTTGAG-3', KO2 targeting region: 5'-TGTTACATCCGTAGTGACGC-3'. The oligo sequences, available in Supplementary Table S1, were cloned into pLentiCRISPR v2 as described previously (36,37). To produce viral particles, the lentiviral vector containing the guide RNA was co-transfected to HEK-293T cells along with lentiviral packaging vectors, pMDL, pVSVG, and pREV in a ratio of 3:1:1:1 (38). 24 h following transfection, the media was replaced, and the virus-containing media was collected at 48 and 72 h post transfection. The TRMT1L KO cells were generated by incubating HCT116 cells with the virus-containing media for 24 h. The infected cells were selected by puromycin. Gene deletion was assessed by DNA genotyping. Genomic DNA was extracted, and the TRMT1L targeted region was amplified with NEB Q5 polymerase and target-specific primers with Illumina adaptor overhangs. The PCR product was purified by gel extraction and sequenced on the Mi-Seq platform with 2x250 paired-end mode (Genewiz EZ Amplicon sequencing).

RNA extraction and Northern blot analysis

Total RNA was extracted using TRIzol reagent following manufacturer's instructions. Total RNA (2-3 µg) was mixed with an equal volume of 2X urea-PAGE loading dye (2X: 95% formamide, 0.02% Bromophenol blue, 5 mM EDTA-NaOH (pH 8)) and denatured at 70C for 5 min. Denatured RNAs were separated on a 12% denaturing (8 M urea) polyacrylamide gel followed by SYBR gold staining and visualization by transillumination at 302 nm UV. To analyze native tRNA structure, 2 µg of total RNA was combined with an equal volume of 2X native PAGE loading dye (2X: 20% glycerol, 0.012% bromophenol blue, 0.012% xylene cyanol, 10 mM MgCl2) and separated on 20% non-denaturing THEM (Tris/HEPES/EDTA/$MgCl_2$) polyacrylamide gel at 4°C overnight as described by Woodson *et al.* (39). For the pre-rRNA processing analysis, total RNA was separated on 0.8% formaldehyde denaturing agarose gel as described in (40). After electrophoretic separation, the RNA was transferred to an Amersham Hybond N+ nylon membrane and crosslinked to the membrane by 120 mJ/cm^2 UV exposure. Northern blotting was performed as described previously (41). Briefly, membranes were pre-hybridized in hybridization buffer (0.6 M NaCl, 60 mM sodium citrate pH 7, 0.5% SDS, 0.1% BSA, 0.1% polyvinyl pyrrolidone, 0.1% Ficoll 400) at 50°C for 1 h and hybridized with 5 µM 5'-biotin-

labeled probe in fresh hybridization buffer overnight. After hybridization and washes, probes were detected using streptavidin-alkaline phosphatase conjugate and Immun-Star AP substrate. Probes for Northern blot are listed in Supplementary Table S1. Densitometry analysis was performed using ImageJ. The membranes were stripped for other rounds of blotting by incubating the membrane in boiling stripping buffer (0.1X SSC, 0.1% SDS) twice.

Analysis of aminoacyl-tRNAs

The analysis of the aminoacylation status of tRNAs was performed according to protocols described in (42) and (43). Briefly, total RNA was extracted with TRIzol and stored in acidic conditions to preserve aminoacyl-tRNAs (10 mM NaOAc (pH 5.0), 1 mM EDTA). As a control, a fraction of total RNA was deacylated in 50 µl of 100 mM Tris-HCl (pH 9.0) with incubation at 37°C for 30 min and purified using the Monarch RNA Cleanup kit. 2.5 ug of RNA samples were combined with an equal volume of 2X acid loading dye (2X: 8 M urea, 0.1 M HOAc/NaOAc, pH 4.8, 0.05% bromophenol blue, 0.05% xylene cyanol), denatured at 95°C for 3 min and separated on a 12% acid denaturing PAGE gel (8.3 M urea, 100 mM NaOAc (pH 5), 1 mM EDTA) in pre-chilled running buffer (100 mM sodium acetate (pH 5.0), 1 mM EDTA) at 16 W at 4°C for 24 h. The RNA was transferred to Amersham Hybond N+ nylon membrane and analyzed by Northern blotting as described in the section above.

Exogenous expression of wildtype, NLS mutant and NoLS mutant TRMT1L

To overexpress exogenous Myc-tagged TRMT1L, the TRMT1L CDS cDNA was cloned into pCMV-Myc. The nuclear localization signal (NLS) and nucleolar localization signal (NoLS) sequence of TRMT1L were predicted with cNLS Mapper (44) and NoD tool (45,46), respectively. PCR mutagenesis was performed using the Q5 Site-Directed Mutagenesis Kit with primers listed in Supplementary Table S1. Two lysine to alanine mutations (K621A and K622A) were introduced for the NLS mutant. For the NoLS mutant, R138A, R139A, H135A, and K136A mutations were made. Sequences of TRMT1L WT, NLS mutant, and NoLS mutant constructs were confirmed by Sanger sequencing (Genewiz).

Immunofluorescence staining

To localize endogenous TRMT1L by immunofluorescence, U2OS cells cultured on the cover glass and transfected with nontargeting scramble or TRMT1L siRNA for 72h were fixed with 4% formaldehyde and immunostained with anti-TRMT1L and anti-FBL antibodies. Cells were treated with a DMSO vehicle or 500 nM CX-5461 to inhibit rRNA transcription for 1h before immunostaining. HCT116 cells transfected with Myc-tagged WT, NLS mutant, or NoLS mutant TRMT1L expressing plasmids on cover glasses were fixed with 4% formaldehyde and immunostained anti-Myc and anti-DDX21 antibodies. Primary antibodies were detected with Goat Anti-Mouse IgG H&L (Alexa Fluor 488) and Goat Anti-Rabbit IgG H&L (Alexa Fluor 594). Nuclei were stained with DAPI and visualized by fluorescence microscopy as previously described (47).

Sucrose gradient density centrifugation for co-sedimentation assays

For the co-sedimentation assay, frozen HT1080 cells were incubated for 30 min on ice in lysis buffer (20 mM HEPES-NaOH pH 7.6, 150 mM NaCl, 0.5% Igepal CA-630, 1× protease inhibitor cocktail). The lysates were cleared by centrifugation at 18,400 × *g* for 20 min. The supernatant was loaded on a 10%-30% (wt/wt) sucrose gradient made in 10 mM HEPES-NaOH pH 7.6, 150 mM NaCl, 0.1 mM $MgCl_2$, 1 mM DTT, and 0.01% Brij 35, and ultra-centrifuged at 36,000 RPM for 4 h at 4ºC with a Beckman SW 41 Ti rotor. Each 1-ml fraction was thoroughly mixed, and RNA was isolated from 200 µl using TRI Reagent LS (Molecular Research Center, Inc), while the rest of each fraction was processed as described in Pestov *et al.,* (48) to precipitate proteins for Western blot analysis. To assess defects in pre-ribosomal particle biogenesis, WT and TRMT1L KO cells were harvested and incubated in low salt buffer (10 mM HEPES-NaOH, pH 7.5, 10 mM NaCl, 2 mM MgCl2, 1 mM ethylene glycol tetraacetic acid) for 10 min and lysed by the addition of Igepal CA-630 and sodium deoxycholate to final concentrations of 0.3% and 0.2%, respectively as described in (48). Nuclei were sedimented by centrifugation at 1000 × *g* for 5 min and resuspended in sonication buffer (25 mM Tris-HCl, pH 7.5, 100 mM KCl, 1 mM NaF, 2 mM EDTA, 0.05% Igepal CA-630, 1 mM dithiothreitol [DTT]). Protease inhibitors (aprotinin, leupeptin, AEBSF) and RNase inhibitors were added, and nuclei were disrupted by sonication. The lysate was cleared by centrifugation at 15,000 × *g* for 15 min and was then separated on a 10–30% (wt/vol) sucrose gradient made in 25 mM Tris-HCl (pH 7.5), 100 mM KCl, 2 mM EDTA, and 1 mM DTT for 3 h at 160,000 × *g* using a Beckman SW 41 Ti rotor. Fractions were collected using a piston gradient fractionator (BioComp), and the absorbance at 255 nm was measured.

Polysome analysis

Polysome profiling was performed as described in (49). Cells were treated with 100 µg/ml cycloheximide for 5 min and lysed in polysome buffer (25 mM Tris–HCl pH 7.5, 150 mM NaCl, 15 mM $MgCl_2$, 8% glycerol, 1% Triton X-100, 0.5% sodium deoxycholate, 1 mM DTT, 100 µg/ml cycloheximide, 100U/ml murine RNase inhibitor, 25 U/ml Turbo DNase, 1× protease inhibitor cocktail). The lysate was loaded on a 10-50% sucrose gradient and centrifuged at 40,000 rpm for 2.5h at 4°C. The fractions were collected by piston gradient fractionator (BioComp) and the absorbance at 255 nm was measured.

eCLIP-sequencing and biotin-labeling of immunoprecipitated RNA

The eCLIP-sequencing pipeline was adapted from procedures described by Van Nostrand et *al*. (50). Cells were initially crosslinked with 400 mJ/cm^2 UV on ice and lysed in CLIP buffer (50 mM Tris-HCl pH 7.4, 100 mM NaCl, 1% NP-40, 0.1% SDS, 0.5% sodium deoxycholate, 1× protease inhibitor cocktail) for 15 min. RNA fragmentation was accomplished through sonication, followed by treatment with RNase T1 and Turbo DNase at 37°C for 5 minutes. The nuclease-treated lysate was immunoprecipitated with protein G Dynabeads pre-bound with anti-TRMT1L antibody or rabbit IgG overnight. The co-precipitated complex was washed sequentially with high salt wash buffer (50 mM Tris-

HCl pH 7.4, 1 M NaCl, 1% NP-40,0.1% SDS, 0.5% sodium deoxycholate, 1 mM EDTA) and wash buffer (20 mM Tris-HCl pH 7.4, 0.2% Tween-20). The RNA-ends were repaired on beads by treatment with Fast-AP and T4 PNK. For testing RNA binding activity of TRMT1L, a proportion of the dephosphorylated RNA was ligated to biotinylated cytidine (bis)phosphate (pCp-Biotin) by T4 RNA ligase. The biotin-labeled RNA samples were separated on an 8% SDS-PAGE gel, transferred to a nitrocellulose membrane, and bound RNA was detected using Streptavidin-IR800 on a LI-COR Odyssey DLx Imager. For eCLIP-seq, the rest of the dephosphorylated RNA was ligated to a 3' RNA adaptor (/5Phos/rArGrArUrCrGrGrArArGrArGrCrArCrArCrGrUrC/3SpC3/) by T4 RNA ligase on beads. The co-precipitated complex and the samples for SMInputs were resolved on an 8% SDS-PAGE gel and transferred to a nitrocellulose membrane for size selection. Samples ranging from the TRMT1L band to 75 kDa above on the membrane were excised, recovered, and prepared into libraries for paired-end sequencing on an Illumina Hi-Seq 4000 platform (Novogene). The raw fastq data were first trimmed to remove the adaptor sequence with CutAdapt (51). fastp was then used to remove and append the unique molecular identifier (UMI) to the read names (52). Reads shorter than 18 nt after trimming were discarded and the rest were aligned to the human genome (hg38) and human repetitive elements using the family-aware mapping approach developed by Van Nostrand *et al.* (53). Peak calling was conducted using the PEAKachu peak calling tool (https://github.com/tbischler/PEAKachu) within the pipeline, with parameters set as follows: --paired_end --max_insert_size 220. The deduplication was performed using UMI-tools (54) with the parameter --read-length. Mapping profiles and statistics were extracted by Samtools (55).

Puromycin labeling assay

HCT116 cells were transfected with non-targeting scramble or TRMT1L siRNAs for 72 hours and treated with 5 µg/ml of puromycin for 0, 15, and 30 min. Cells were harvested and processed for Western blotting analysis using an anti-puromycin antibody.

tRNA purification and single tRNA iso-decoder isolation

tRNAs were isolated from total RNA by ion exchange chromatography. The RNA samples were brought to a final concentration of 20 mM HEPES-KOH (pH 7.5) and loaded onto a Bio-Rad EconoFit Macro-Prep DEAE columns (BioRad, 12009274) pre-equilibrated sequentially with the following buffers: 6 column volumes (CV) of low salt buffer (200 mM NaCl, 8 mM $MgCl_2$, 20 mM HEPES-KOH pH 7.5), followed by 15 CV of high salt buffer (450 mM NaCl, 16 mM $MgCl_2$, 20 mM HEPES-KOH pH 7.5), then 15 CV of low salt buffer, and finally, 15 CV of binding buffer (100 mM NaCl, 20 mM HEPES-KOH pH 7.5). After loading the RNA, the column was washed with 10 CV of binding buffer and eluted with a step gradient of 200 mM NaCl, 8 mM $MgCl_2$, 20 mM HEPES-KOH to 500 mM NaCl, 16 mM $MgCl_2$, 20 mM HEPES-KOH. A final elution step was conducted with 1 M NaCl. After elution, the collected fractions were analyzed by on urea-PAGE, and the fractions containing pure tRNA were pooled and subsequently recovered by precipitation with 1/10 volume of 3M sodium acetate (pH 5.2), 20 ug/ml Glycogen and 1.5 volume of isopropanol.

Individual tRNAs were isolated from the purified tRNA using specific biotin-labeled DNA probes listed in Supplementary Table S1. tRNAs were incubated with specific isoacceptor probes in binding buffer (0.5 M NaCl, 50 mM Tris-HCl (pH 7.5)) for 2 minutes at 98°C, followed by annealing at 80°C for 30 seconds and gradual cooling (-0.1°C/s) to 25°C. The annealed tRNAs were then captured on streptavidin magnetic beads, washed four times in binding buffer and eluted in RNase-free water. The remaining trace amounts of biotin-labeled DNA probes were removed by treating the eluate with Exonuclease I for 45 minutes at room temperature. This was followed by purification on the NEB RNA clean up column. The isolated tRNAs were analyzed for purity by Northern blot before further mass spectrometry analysis of modifications.

Mass spectrometry analysis of RNA modifications

For the oligonucleotide analysis, purified tRNA iso-decoders were digested with RNase T1 (50 U/ug) at 37°C for 1.5 hrs RNase A (0.01 U/ug) at 37°C for 1 hr. Analysis was done as previously described (56). The Synapt G2-S (Waters) coupled to a Dionex Ultimate 3000 RSLNano UHPLC (Thermo Scientific) was equipped with an Acquity UPLC BEH C18 column (1.7 µm, 0.3 × 150 mm, Waters). RNA digestion products were eluted at a 5 µl/min flow rate and 60°C column temperature with mobile phase A (8mM TEA and 200mM HFIP, pH = 7.8 in water) and mobile phase B (8mM TEA and 200mM HFIP in 50% methanol) with a linear gradient (3–55% of B over 70 min). Data was collected in sensitivity mode. MS scans were collected over 0.5 s in the *m/z* range of 545–2000, and MS/MS scans over 1 s period in the *m/z* range 250–2000. Three of the most abundant MS events were selected for MS/MS. A collision energy ramp (20–23 V at *m/z* 545; 51–57 V at *m/z* 2000) was applied in a precursor *m/z* dependent manner, and the accumulated TIC threshold was set to 3.5×10^5 counts. Oligonucleotide digestion products MS and MS/MS *m/z* were determined using the Mongo Oligo Mass Calculator v2.06 (http://rna.rega.kuleuven.be/masspec/mongo.htm) (57). Data was collected and relative quantification was performed with MassLynx v4.2.

For the nucleoside analysis, tRNA iso-decoders were digested to nucleosides using a previously described method (58). The RNA was denatured by heating at 95 °C for 3 mins with an immediate cooling. The denatured RNA was incubated in 0.01 M ammonium acetate for 2 h with nuclease P1 (0.1 U/µg RNA) (Sigma-Aldrich). The RNA was then digested for 2 hr at 37 °C in 1/10 volume of 1 M ammonium bicarbonate with snake venom phosphodiesterase (1.2×10−4 U/µg RNA) and bacterial alkaline phosphatase (0.1U/ µg RNA) (Worthington Biochemical corporation). Analysis was performed on a TSQ Quantiva Triple Quadrupole (Thermo Fisher Scientific) coupled to a Vanquish Flex Quaternary (Thermo Fisher Scientific) with an Acquity UPLC HSS T3, 1.8 µm, 1.0 mm x 100 mm column (Waters). The nucleoside species were eluted at a 0.1 mL/min flow rate and 30 °C column temperature. Mobile phase A (5.3 mM ammonium acetate (pH = 4.5)) and mobile phase B (5.3 mM ammonium acetate, pH = 4.5, in 40% acetonitrile) were used with a previously described LC elution method (59). An SRM method was used for data collection to relatively quantify RNA modifications in samples using selected SRM transitions (supplemental table). Analysis was done in positive polarity with an H-ESI source. The Q1 and Q3 resolution was 0.7, and a Dwell Time of 150 ms. For collision

induced dissociation (CID), nitrogen gas was used at 1.5 mTorr achieving fragmentation. The sheath gas, auxiliary gas, and sweep gas of 35, 10, and 0 arbitrary units, respectively achieving; ion transfer tube temperature of 200 °C; vaporizer temperature of 260 °C; and spray voltage of 3.5 kV was used for analysis. Data processing and relative quantification was done with Xcalibur 4.2 (Thermo Fisher Scientific). The 28S rRNA was isolated from total RNA by sucrose gradient fractionation followed by hydrolysis to single nucleosides, dephosphorylation and LC–MS analysis was performed at Arraystar Inc.

Primer extension assay

For preparing 5'-^{32}P-labeled oligonucleotide, 20 pmol of oligonucleotide was incubated with 20 µCi [γ-^{32}P]ATP and 10 U T4 polynucleotide kinase in 1× T4 polynucleotide kinase reaction buffer at 37°C for 45 min. The reaction was heat-inactivated for 10 min at 68°C. Labeled primers were purified on a microspin G50 column (Cytiva 27-5330-01) per the manufacturer's protocol. For the reverse transcription reaction, 3.3 µg of total RNA was mixed with 0.6 pmol of the 5'-^{32}P-labeled oligonucleotides (Supplementary Table S1) in 1X AMV Reverse Transcriptase buffer and incubated at 95°C for 3 min and slowly cooled to 42°C. 1.6 nmol of dNTP mix and 10 U AMV reverse transcriptase were added to the reaction and incubated at 42°C for 1 h. The reaction was stopped by adding an equal volume of 2X urea-PAGE loading dye (2X: 95% formamide, 0.02% Bromophenol blue, 5 mM EDTA-NaOH (pH 8)). The reverse transcribed product was separated on a 15% urea-PAGE gel and exposed to x-ray films.

Nano-tRNAseq

The tRNA samples purified from total RNA were prepared into libraries following the Nano-tRNAseq protocol developed by Lucas *et al.* (60). Initially, the tRNAs were deacylated in 100 mM Tris-HCl (pH 9.0) at 37°C for 30 minutes. After recovery using the NEB RNA Cleanup kit, the tRNAs were ligated to pre-annealed 5' and 3' splint adaptors (5' RNA splint adapter: 5'-rCrCrUrArArGrArGrCrArArGrArArGrArArGrCrCrUrGrGrN, 3' splint adapter: 5'-Phos-rGrGrCrUrUrCrUrUrCrUrUrGrCrUrCrUrUrArGrGrArArArArArArArArArAAAA-3') with T4 RNA 2 Ligase followed by purification on AMPure RNAClean XP beads. The splint adaptor-ligated tRNAs were reverse transcribed using SuperScript IV Reverse Transcriptase at 60 °C for 1 hour followed by 85 °C for 5 minutes to linearize the tRNAs. The linearized tRNAs were cleaned up with AMPure RNAClean XP beads and then prepared into libraries following the standard protocol of the Direct RNA Sequencing Kit (SQK-RNA002) before being sequenced on a MinION flow cell (FLO-MIN-106). The bulk files were saved during sequencing for subsequent simulation runs using the alternative configuration described by Lucas *et al.* (60). Fastq files generated by the simulation run were aligned to high confidence mature tRNA sequences retrieved from GtRNAdb (61) using the bwa alignment tool with parameters set as follows: -W 13 -k 6 -x ont2d -T20. Sequence alignments in bam files were extracted by BEDTools (62). One tRNA gene was selected for each iso-decoder based on the read counts in this alignment to generate a reference file containing only one gene per tRNA iso-decoder. Differential expression of

tRNAs was analyzed by aligning the fastq files to the one iso-decoder reference with the bwa alignment tool, using parameters set as follows: -W 13 -k 6 -x ont2d -T20, and extracting the alignment read counts by BEDTools. Mismatches and deletions at each position of tRNA iso-decoders were extracted using Samtools (55). The sum of base calling errors for each tRNA iso-decoders position in TRMT1L depleted cells relative to WT was calculated by adding the rate of deletions to the rate of mismatches. An arbitrary weight of 1 for deletions and 0.6 for mismatches was assigned to identify tRNA modifications causing deletions. Sequence alignments were visualized using Integrative Genomics Viewer (IGV) (63).

Statistics

Data were shown as mean ± standard deviation. Each dot on dot-bar plot represents an independent biological replicate. A two-tailed Student's t-test determined the difference between the two groups.

RESULTS

TRMT1L interacts with components of the Rix1 complex and co-sediments with pre-60S particles.

In a mass spectrometry-based proteomic analysis of the Rix1 60S biogenesis complex through immunoprecipitation of endogenous PELP1, we identified the RNA methyltransferase TRMT1L as an interacting component (Figure 1A). Immunoprecipitation of PELP1 followed by TRMT1L Western blot analysis was used to validate this interaction (Figure 1B). Reversely, we also show that immunoprecipitated endogenous TRMT1L interacts with PELP1 and other components of the larger Rix1 complex, namely WDR18 and SENP3 and with the ribosome biogenesis factor nucleophosmin (NPM1) (34,64) (Figure 1C). TRMT1L has previously been reported to localize to the nucleus, with an enrichment to the nucleolar compartment, which is the site of ribosome biogenesis (13,14). Immunostaining analysis on U2OS cells treated with control and TRMT1L siRNAs validated the localization of endogenous TRMT1L in both the nucleus and nucleolus (Figure 2B). Using the cNLS Mapper (44) and NoD tool (45,46), we predicted potential protein domains responsible for regulating the subcellular localization of TRMT1L (Figure 2A and Supplementary Figure S1A). Our analysis unveiled putative nucleolar (NoLS) and nuclear (NLS) localization sequences situated at the N- and C-terminus of TRMT1L, respectively (Supplementary Figure S1A). Mutation of key basic residues within the NoLS domain resulted in a redistribution of TRMT1L in the nucleoplasm. In contrast, mutation of basic residues in the NLS domain resulted in cytosolic redistribution of TRMT1L, indicating these regions act as critical regulatory elements governing its subcellular distribution (Supplementary Figure S1B-C). Interestingly, the nucleolar localization of TRMT1L appears to depend on active rRNA transcription as inhibition of RNA Pol I activity with CX-5461 resulted in its redistribution to the nucleoplasm (Figure 2C).

PELP1 and the Rix1 complex regulate important rRNA processing steps required for 60S ribosomal subunit biogenesis (34,64). As we co-purified TRMT1L with Rix1 components, this suggests that TRMT1L may have a role in ribosome synthesis. To test this, we first determined whether TRMT1L co-sediments with nucleolar pre-ribosomal particles by sucrose gradient sedimentation profiling. Similarly to PELP1 and WDR18, we find that TRMT1L specifically co-sediment with only the pre-60S subunit enriched with the 28S rRNA precursors (32S and 12S), 5S rRNA and the large subunit protein uL5 (formerly RPL11) (Figure 3A). However, upon TRMT1L depletion by RNAi, we did not observe any significant rRNA processing defects apart from a slight reduction in the levels of the 32S and 12S rRNA precursors (Supplementary Figure S2A-C). Nuclear 40S and 60S pre-ribosomal particle levels were also not affected by TRMT1L depletion (Figure 3B-C). Collectively, these findings suggest that while TRMT1L co-sediments with pre-60S ribosomes, it is unlikely to be directly involved in rRNA processing or is indispensable for ribosome biogenesis. This observation is consistent with the limited evolutionary conservation of TRMT1L and the viability of TRMT1L gene knockout mice (22), suggesting a regulatory rather than essential role for TRMT1L in ribosome function.

TRMT1L binds to tRNAs and 28S rRNA expansion segments.

To further elucidate TRMT1L functions and identify its potential RNA substrates, we performed a genome-wide eCLIP-seq analysis (50,65) of endogenous TRMT1L in two different cell lines (HCT116 and HeLa) in duplicates and with respective size-matched input (SMInput) controls. We first tested whether TRMT1L binds to RNA by performing an immunoprecipitation in UV cross-linked vs. non-cross-linked conditions. Ligation-mediated labeling of immunoprecipitated (IP) endogenous TRMT1L in HCT116 cells with pCp-Biotin (Cytidine-5'-phosphate-3'-(6-aminohexyl) phosphate labeled with Biotin) (53), followed by detection with fluorescence imaging of streptavidin-conjugated-IR800 was used to confirm the presence of trapped TRMT1L-RNA complexes. The pCp-Biotin signal was detected only in the cross-linked TRMT1L IP, not in the non-crosslinked condition or the control IgG IP, indicating specificity (Figure 4A-B). Having validated the binding of TRMT1L to RNA, cells were processed for large scale eCLIP-seq analysis as depicted in Figure 4C. Following limited RNase digestion and immunoprecipitation with an IgG control or TRMT1L antibody, co-precipitated RNA from HCT116 and HeLa cells (as well as their respective paired size-matched input (SMInput)) were purified by separation on SDS-PAGE and then transferred onto a membrane. Protein-RNA complexes from a 75 kDa region above TRMT1L were excised from the membrane (Figure 4C). The recovered RNA was further prepared into paired-end libraries for high-throughput sequencing on Illumina Hi-Seq 4000 platform. Only samples from biological duplicates of TRMT1L immunoprecipitates and respective paired SMInput were processed for sequencing as the IgG control immunoprecipitated samples did not recover enough RNA to be amplified for library preparation. Reads were processed using an established eCLIP-seq pipeline (53). The numbers of reads identified as binding sites in the TRMT1L eCLIP samples were normalized to SMInput and significance and fold enrichment were calculated.

Most eCLIP reads in TRMT1L samples corresponded to rRNAs and tRNAs (Figure 5A and Supplementary Table S3), which also showed peaks of significant enrichments when

normalized to SMInput (Figure 5B-C, Supplementary Figure S3 and Figure 6). For tRNAs, the majority of enriched reads in both HCT116 and HeLa cells corresponded to a small subset of nuclear-encoded tRNAs, mainly tRNA-Cys-GCA, Tyr-GUA followed by Arg-UCG, Arg-CCU, and Asn-GUU genes (Figure 5B-C and Supplementary Figure S3). Although in lower abundance, other various isoacceptors were found in HCT116 vs. HeLa cells differently, indicating that the range of tRNA substrates is cell specific (Supplementary Figure S3). Remarkably, the reads enriched in the TRMT1L immunoprecipitation (IP) for tRNA-Cys-GCA and Tyr-GUA corresponded to precursor tRNAs that retained their 3' trailer sequence. In contrast, most other tRNAs appeared mature, with their 3' trailer processed and containing the CCA addition (Supplementary Figure S4). For tRNA-Tyr-GUA, most reads retaining the 3' trailer exhibited intron removal, suggesting that TRMT1L binds to these tRNAs during an early processing stage. Surprisingly, for rRNA, a main peak of enrichment aligned to a very narrow region of the 28S rRNA corresponding to expansion segments ES7Lb (Figure 6). Our CLIP-seq analysis indicates that a specific subset of tRNAs and 28S rRNA expansion segment ES7Lb may be methylation substrates of TRMT1L.

TRMT1L is required for the deposition of $m^2{}_2G$ at position 27 of tRNA-Tyr-GUA

Expansion segments in ribosomal RNA (rRNA) represent additional sequences acquired by eukaryotes during evolution. One notable characteristic of these segments is their positioning outside the catalytic cores of the ribosome, instead extending as elongated and flexible protrusions on its surface (66,67). Analysis of the rRNA chemical modification landscape of the human 80S ribosome using quantitative mass spectrometry has revealed that the majority of modifications occur in functionally conserved regions within the core catalytic centers, with very few modifications observed at the periphery and none on expansion segments (68). Although not confirmed through mass spectrometry, cryo-electron microscopy studies have suggested the potential presence of several human-specific modifications forming an extended shell, distinguishing human ribosomes from their bacterial counterparts (69). Among the 52 newly identified human-specific modification sites, two m^2G modifications were proposed on expansion segment ES7L (m^2G729: ES7Lb, m^2G978: ES7Lc), located just a few nucleotides away from the TRMT1L binding region identified by the eCLIP analysis (Figure 6). To test the presence of TRMT1L-catalyzed modification on rRNA, we established CRISPR Cas9-mediated TRMT1L knockout HCT116 cells with two different guide RNAs (TRMT1L KO1 and KO2) (Supplementary Figure S5). As expected, immunoblotting revealed the absence of detectable TRMT1L protein in both KO1 and KO2 cell lines. Importantly, we did not observe any significant effect on the levels of the paralog TRMT1, indicating the suitability of these cells lines to specifically assess TRMT1L functions (Supplementary Figure S5C). We next isolated total RNA as well as purified 28S rRNA from WT (non-targeting control guide RNA) and TRMT1L KO1 and KO2 cells for quantitative liquid chromatography-tandem mass spectrometry (LC-MS/MS) of modified ribonucleosides (Arraystar Inc). Among the 53 RNA modification levels measured, which included m^2G and $m^2{}_2G$, no significant differences were detected in the TRMT1L knockouts (KOs) compared to the control wild-type (WT) RNA samples (data not shown). Importantly, m^2G and $m^2{}_2G$ modifications were not detected on 28S rRNA. This observation aligns with previous LC-

MS/MS analysis and more recent cryoEM studies (68,70), which did not uncover any m^2G or $m^2{}_2G$ on human ribosomes. Additionally, previous studies comparing WT and TRMT1L KO cells did not detect any significant differences in the levels of 27 distinct RNA modifications across various RNA pools (13). Several studies have suggested that certain rRNA bases may not always undergo complete modification, leading to heterogeneity within ribosomes of the same cell type (68,71-74). It is, therefore, conceivable that the modification catalyzed by TRMT1L may exist at sub-stoichiometric levels, potentially falling below the detection threshold.

To evaluate the occurrence of TRMT1L-catalyzed modifications on tRNAs, a significant potential substrate revealed in the eCLIP-seq analysis, we initially employed a Northern blot-based PHA approach (Positive Hybridization in Absence of modification) (75,76), comparing total RNA from WT and TRMT1L KO cells. This assay relies on the differential hybridization efficiency of a probe due to the presence or absence of a bulky modification, which affects base pairing. We detected an elevated PHA signal exclusively for tRNAs Cys-GCA and Tyr-GUA from the TRMT1L KO cells (Figure 7A-C). This signal was observed when using a probe covering the D-loop side of the tRNAs, while no such signal was detected with a probe pairing with the T-loop side, which served as a normalization control. Other tRNA tested did not show any PHA effect in the TRMT1L KO cells (Supplementary Figure S6). This suggests a potential loss of modification on the D-loop side of tRNAs Cys-GCA and Tyr-GUA (Figure 7A-C and Supplementary Figure S6). Notably, ectopic re-expression of TRMT1L in the KO background markedly rescued the heightened PHA signal, implying that the potential loss of modification is TRMT1L-dependent (Figure 7D-F). We also generated a catalytically inactive TRMT1L mutant based on key conserved residues in the paralog TRMT1 that were shown to abolish its activity (15). However, these mutants were dramatically unstable and could not reach the levels of WT TRMT1L expression, making them unsuitable to use in the re-expression rescue experiments (data not shown). Nonetheless, our results indicate that TRMT1L likely catalyzes modification on the D-loop side of tRNAs Cys-GCA and Tyr-GUA.

To uncover TRMT1L-catalyzed modifications on tRNAs, we employed Nano-tRNAseq, a Nanopore-based direct RNA sequencing method (60). This approach allows for the direct detection and quantification of native tRNA modifications without the necessity for reverse transcription or PCR amplification. Direct RNA nanopore sequencing has been validated in numerous studies for its ability to detect RNA modifications with near-single nucleotide precision. This is achieved by identifying positions showing base calling errors upon alignment to reference transcriptome (60,77-85). Purified tRNAs isolated from WT and TRMT1L KO cells were processed for Nano-tRNAseq and the base calling errors (base mismatch, insertion and deletion) for each nucleotide position and tRNA iso-decoder reference were calculated for each duplicate sample. Relative to WT, TRMT1L KO cells showed a significant decrease in base calling errors for specific positions mainly for tRNA-Tyr-GUA and Cys-GCA (Figure 8A), the top two iso-decoders found to have the highest enrichment for binding to TRMT1L in the eCLIP-Seq analysis (Figure 5B-C). Although not found to be significantly enriched in the TRMT1L eCLIP-Seq data, Ala-CGC and Ala-UCG also showed positions with decreased base calling errors (Figure 8A), suggesting the loss of modification on these tRNAs in the TRMT1L KO cells. A closer examination of specific

nucleotide positions with decreased base calling errors in the TRMT1L KO revealed potential loss of $m^2{}_2G27$ and surprisingly 3-(3-amino-3-carboxypropyl) uridine (acp^3U) 20 and dihydrouridine (D) 17, modifications reported to be present at these positions on tRNA-Tyr-GUA (86,87). Both tRNAs Cys-GCA and Ala-CGC/UCG from TRMT1L KO cells showed a significant increase in quality reads at position 20, suggesting loss of acp^3U and D modifications that were reported on these tRNAs, respectively (86,88,89).

tRNA-Tyr-GUA from human placenta and bovine liver is known to harbor two consecutive $m^2{}_2G$ modifications at positions 26 and 27 (87,90). While human TRMT1, the close relative of TRMT1L, has been demonstrated to catalyze the dimethylation at position G26, the enzyme responsible for catalyzing $m^2{}_2G$ at position 27 has yet to be identified (15). The Nano-tRNAseq analysis detected the presence of $m^2{}_2G26$ and $m^2{}_2G27$ on tRNA-Tyr-GUA from WT cells, which appeared as deletions instead of mismatches at both positions. While the percentage of deletions was significantly decreased for both positions in TRMT1L KO cells, position G26 showed increased mismatch frequency, and position G27 showed an overall decrease in base calling errors (Figure 8A-B and Supplementary Table S4). These findings suggest that TRMT1L is likely responsible for the deposition of $m^2{}_2G27$ on tRNA-Tyr-GUA. To validate this finding, we employed a primer extension assay capable of detecting RNA modifications with precise nucleotide resolution (91-93). This method can specifically identify $m^2{}_2G$, which impedes the elongation of the reverse transcriptase (RT) at the nucleotide carrying the modification (94), in this instance, position 27 (Supplementary Figure S7A). As expected, we observed an RT stop at position G27 in WT cells, imposed by the $m^2{}_2G$ modification reported at this position (Supplementary Figure S7B). In contrast, this RT block was relieved in TRMT1L KO cells, which showed instead a stop at G26, a position known to harbor the $m^2{}_2G$ catalyzed by the paralog TRMT1 (Supplementary Figure S7B). No changes between WT and TRMT1L KO cells were detected for tRNAs Arg-UCG and Asn-GUU, both reported to contain $m^2{}_2G26$ catalyzed by TRMT1 (Supplementary Figure S7B). A partial reduction, rather than complete loss, of $m^2{}_2G$ on tRNA-Tyr in TRMT1L KO cells was further validated via an immune-Northern assay employing an anti-$m^2{}_2G$ antibody. This analysis confirms the loss of $m^2{}_2G$ at position 27 in TRMT1L KO cells, while position 26 retained the modification accounting for the remaining signal (Supplementary Figure S7C). Consistently, purified tRNA-Cys-GCA and tRNA-Arg-CCU were not detected by the anti-$m^2{}_2G$ antibody, as previous reports have indicated the absence of $m^2{}_2G$ modification in these tRNAs (23).

The Nano-tRNAseq data also suggest loss of acp^3U at positions 20 on tRNA-Tyr-GUA and tRNA-Cys-GCA in TRMT1L KO cells, which was detected as a decrease in mismatch errors in both cases (Figure 8A-C). tRNA-Cys-GCA was previously reported to lack $m^2{}_2G$ at position 26 and our data did not identify any other potential modification showing a significant decrease in base calling errors in the TRMT1L KO cells for this tRNA. By primer extension assay, an RT block at position 20 on tRNA-Cys-GCA was observed in WT cells, confirming the presence of a modification likely to be acp^3U20. In the TRMT1L KO cells, this RT block was substantially reduced but not completely absent (Supplementary Figure S7B). This partial loss indicates that TRMT1L does not catalyze but is likely required to facilitate the deposition of acp^3U20. The Nano-tRNAseq analysis further reveals that

tRNA-Tyr-GUA appears to lack the D modification previously reported at position 17 (87). In contrast, tRNAs Ala-CGC and Ala-UCG exhibit a less pronounced reduction of this reported modification at 20 in the TRMT1L KO cells (Figures 8A and 8D) (88,89).

Earlier studies examining modification changes in total tRNAs from TRMT1L KO cells using LC-MS/MS did not reveal significant alterations compared to WT cells (13). Our discovery that TRMT1L binds to and affects only a very limited subset of tRNAs may explain this finding. As an alternative approach, we isolated individual tRNAs Tyr-GUA and Cys-GCA and assessed their modification status using LC–MS/MS analysis of RNAse A (tRNA Tyr) or RNAse T1 (tRNA Cys)-generated fragments. For tRNA-Tyr-GUA, the fragment containing $m^2{}_2G27$ and $m^2{}_2G26$ observed in the WT cells was absent in the TRMT1L KO which showed instead a fragment containing only one $m^2{}_2G$ modification predicted by the mapping software to be at position 26 (Figure 9A). Based on our Nano-tRNAseq and primer extension results, the fragment from the TRMT1L KO cells correspond to a loss of $m^2{}_2G27$ while $m^2{}_2G26$ is maintained. In the TRMT1L KO cells, the level of acp^3U was drastically reduced on tRNA-Tyr-GUA, and to a lesser extent on Cys-GCA. Instead, the loss or reduction in acp^3U20 was accompanied by the modified bases converted to either D20 or U20 (Figure 9B-C). This is consistent with previous studies showing that acp^3U formation inhibits D20 formation on tRNA-Tyr-GUA and Cys-GCA (86). Collision-induced dissociation spectrum was performed to confirm the modification identified on each fragment (not shown). Additionally, nucleoside analysis of purified tRNA-Tyr-GUA further confirms a reduction of $m^2{}_2G$ by about 50% while acp3U is almost completely absent in the TRMT1L KO cells (Supplementary Figure S7D). The absence of D17 on tRNA-Tyr-GUA in TRMT1L KO cells requires further investigation, as we could not confidently confirm the presence of this modified position in the experimental condition tested.

The high conservation of homology between the methyltransferase domains of TRMT1L and TRMT1 together with our findings indicate that TRMT1L is an $m^2{}_2G$ methyltransferase with only one major catalytic substrate, $m^2{}_2G27$ on tRNA-Tyr-GUA. The acp3U modification on tRNAs Tyr-GUA and Cys-GCA is facilitated by the uridine aminocarboxypropyltransferase DTWD1, while DTWD2 is responsible for catalyzing acp^3U deposition in tRNAs Asn-GUU, Ile-AAU, and Ile-UAU (86). Our Nano-tRNAseq did not reveal any decrease in the abundance of acp^3U on tRNAs Asn-GUU, Ile-AAU, and Ile-UAU in TRMT1L knockout cells (Figure 8A), indicating that the depletion of TRMT1L specifically impacts the targets of DTWD1. In contrast, dihydrouridine synthases (DUS), which comprise four family members in eukaryotes, are responsible for introducing the D modification localized in the characteristic tRNA "D arm" (12,95). Our comprehensive analysis suggests that, besides catalyzing $m^2{}_2G$ on tRNA-Tyr-GUA, TRMT1L may participate in a modification circuit with the DTW1 and DUS enzymes, regulating the deposition of acp^3U and D on a select subset of tRNAs. While TRMT1L does not catalyze the deposition of $m^2{}_2G$ on other tRNAs such as tRNA-Cys-GCA, our data suggest that it may have a chaperone function, facilitating tRNA folding or the recruitment of other modifying enzymes to specific tRNAs.

TRMT1L-depleted cells have reduced levels of tRNA-Tyr-GUA and increased tRFs.

To examine whether depletion of TRMT1L affects tRNA levels, we utilized the data from the Nano-tRNAseq analysis, a method shown to accurately quantify tRNA abundances (96). Normalized read counts of individual iso-decoders from both WT and TRMT1L KO samples showed a good correlation across biological replicates (Figure 10A-B). Compared to the WT cells, we observed a notable impact of TRMT1L depletion on the abundance of only one tRNA, namely tRNA-Tyr-GUA (Figure 10C). This nearly 2-fold reduction in tRNA-Tyr-GUA levels was validated through Northern blotting (Figure 10D-F). This outcome further supports our finding that TRMT1L specifically catalyzes the deposition of $m^2{}_2G$ on tRNA-Tyr-GUA, which appears to be required for the deposition of acp^3U20 and D17, a process crucial for maintaining the stability of this tRNA. To determine whether the decrease in tRNA-Tyr-GUA level could be due to impaired structural stability due to its hypomethylation status, we analyzed RNA derived from WT and TRMT1L KO cells on native gel electrophoresis. The migration pattern of both tRNAs Tyr-GUA and Cys-GCA were unremarkably changed, indicating that the folding of these tRNAs was not dramatically altered or below the detection capacity of this method (Supplementary Figure S8A).

As tRNA modifications have been shown to regulate the binding and activity of aminoacyl-tRNA synthetases (97-99), we assessed the aminoacylation status of different tRNA, including tRNA-Tyr-GUA and Cys-GCA, in WT vs. TRMT1L KO cells. RNAs extracted from both WT and TRMT1L KO cells were purified and reconstituted under acidic conditions to maintain the covalently bound amino acids. A subset of the RNA samples was subjected to deacylation under alkaline conditions to provide deacylated controls. Subsequently, the RNAs were separated via acidic polyacrylamide gel electrophoresis (PAGE), where aminoacylated tRNAs exhibit a slower migration rate than their deacylated counterparts (42,43). This difference in migration rate arises from the protonation of the α-amino group of the amino acid attached to the 3′ ends of the tRNA under acidic conditions. Intriguingly, tRNAs Tyr-GUA and Cys-GCA from TRMT1L KO cells migrated faster than the ones from WT cells in both deacylated and acylated conditions. As a control, tRNA-Leu from TRMT1L KO cells migrated similarly to the ones from WT cells. However, under acidic conditions, both Tyr-GUA and Cys-GCA, as well as the Leu control from TRMT1L KO cells, appeared fully aminoacylated, demonstrating that the hypomethylated state of tRNAs Tyr-GUA and Cys-GCA does not affect amino acid charging (Supplementary Figure S8B). The precise reason why tRNAs Tyr and Cys from TRMT1L KO cells exhibit faster migration in the acid denaturing gel is presently unclear. However, a plausible explanation could be attributed to the absence of the acp^3U modification, which acquires a positive charge under acidic conditions. This charge difference may result in the tRNAs from WT cells migrating more slowly in the gel than those from TRMT1L KO cells lacking acp^3U.

Interestingly, we observed that TRMT1L KO cells displayed an increased abundance of small tRNA-derived RNA fragments (tRFs), specifically for tRNA-Tyr-GUA and Cys-GCA (Figure 11) and not for other tRNAs tested (Supplementary Figure S9). These fragments are generally products of precursors or mature tRNAs cleaved by different ribonucleases at specific positions (100). tRFs were observed in the TRMT1L KO cells, with probes specific for both the D and T-loop regions and ranged from approximately 35 to 55

nucleotides in length. Some of the most abundant fragments observed to be unique to TRMT1L KO cells could correspond to potential cleavage sites of the precursor tRNA-Tyr-GUA transcript at position 26/27 (fragments of 33 nt and 58 nt in length) (Figure 11B-C). Presumably, such fragments would originate from a spliced tRNA-Tyr-GUA precursor that still contains the 5' leader and 3' trailer sequences. While the precise nature of these observed tRFs needs to be confirmed by sequencing analysis, our data suggest that the absence of $m^2{}_2G27$ could render tRNA-Tyr-GUA more susceptible to cleavage at this position, possibly due to structural alterations, thereby contributing to its depletion in TRMT1L KO cells. Although we did not observe significant changes in tRNA-Cys-GCA levels, our findings indicate that depletion of TRMT1L also makes this tRNA more susceptible to cleavage potentially due to a reduction in acp^3U20. It is also possible that TRMT1L may function as a chaperone, protecting tRNA from cleavage, which will need further investigation.

TRMT1L is required for efficient mRNA translation and cell survival under oxidative and ER stress.

Several tRFs, including tRF Tyr-GUA, have demonstrated roles in trans, regulating cellular processes such as mRNA translation and cell division (101-107). The decrease in tRNA-Tyr-GUA levels and the elevated presence of tRFs observed in the TRMT1L KO cells prompted us to investigate whether the depletion of TRMT1L influenced translation and proliferation. Polysome profiling on sucrose density gradient reveals that cells depleted of TRMT1L slightly reduce mRNA translation efficiency, as observed by their lower polysome profiles compared to WT cells (Figure 12A). Because the TRMT1L KO cells were generated through puromycin selection, we used siRNA delivery to perform a puromycilation assay as a second means of measuring translation efficiency. Compared to control siRNA-treated cells, TRMT1L knockdown cells showed a noticeable reduction in global translation rate (Figure 12B), corroborating our polysome profiling observations. Surprisingly, given the decrease in mRNA translation observed, TRMT1L KO cells showed no significant proliferation defects compared to WT cells (Figure 13A).

tRNA modifications have been demonstrated to dynamically change in response to stress stimuli. Specifically, levels of $m^2{}_2G$ have been shown to increase under oxidative stress conditions (32,33,108,109). Interestingly, human cells depleted of the paralog TRMT1 exhibit heightened sensitivity to oxidizing agents (14). To test whether TRMT1L also plays an important role in stress response, we subjected WT and TRMT1L KO cells to different stressors. Similarly to what was reported for TRMT1-depleted cells (14), TRMT1L KO cells also displayed hypersensitivity to oxidative stress (low dose of H_2O_2) as well as endoplasmic reticulum (ER) stress (Thapsigargin) but not nutrient deprivation stresses (serum deprivation and low glucose) (Figure 13B). These findings highlight the pivotal role of TRMT1L in maintaining the homeostasis of a specific subset of tRNAs by catalyzing $m^2{}_2G$ and likely coordinating the deposition of acp^3U20 and D17 modifications by DTWD1 and DUS enzymes, respectively. These functions are essential for efficient protein translation and the cellular response to oxidative and ER stress.

Discussion

The presence of two consecutive $m^2{}_2G$ modifications, occurring at positions 26 and 27, is relatively rare and has been observed in only a few tRNAs, such as tRNA-Tyr purified from bovine liver and human placenta, as well as on *A. aeolicus* tRNA-Cys (87,90,110). While TRM1 has been identified as the enzyme responsible for catalyzing both $m^2{}_2G26$ and $m^2{}_2G27$ on *A. aeolicus* tRNA-Cys, human TRMT1 has been found to catalyze only $m^2{}_2G26$ tRNA-Tyr (15,110), leaving the identity of the methyltransferase responsible for depositing $m^2{}_2G$ at position 27 unresolved. In this study, we demonstrate that TRMT1L functions as the elusive methyltransferase catalyzing $m^2{}_2G27$ on human tRNA-Tyr-GUA. While our eCLIP-seq analysis revealed binding to a broader spectrum of tRNA and rRNA expansion segments, we found that TRMT1L exhibits catalytic activity only towards tRNA-Tyr-GUA. This observation suggests that TRMT1L may have additional catalytically independent functions depending on the RNA substrate.

Ensuring the proper folding of tRNAs into functional structures is vital for their role in translation. This process relies on the assistance of specialized proteins known as tRNA chaperones (6). Among these, the La protein, one of the most characterized tRNA chaperones, aids in the folding of nascent RNA polymerase III transcripts and shielding the 3' end of pre-tRNAs from degradation (111,112). Recent investigations have unveiled additional roles for RNA-modifying enzymes beyond their catalytic functions, hinting at a dual role as tRNA chaperones (6). Notably, in bacterial systems, enzymes like the tRNA pseudouridine synthase TruB and the methyltransferase TrmA have been found to facilitate tRNA folding independently of their enzymatic activities (113,114). Instead of merely catalyzing modifications, they actively contribute to the structural integrity of tRNAs, suggesting a broader functional repertoire. While primarily known for its role in catalyzing $m^2{}_2G26$ modification, TRMT1L's yeast paralog, TRM1, functions redundantly with La protein, stabilizing pre-tRNA *in vitro* and *in vivo* (111,112). Recent studies in fission yeast have uncovered chaperone-like activities for TRM1 where both WT and catalytically inactive mutants have been shown to facilitate RNA strand annealing and dissociation, indicating a direct involvement in tRNA folding beyond the deposition of $m^2{}_2G$ (115). Similarly, our study suggests a potential conservation of dual catalytic and chaperone functions for TRMT1L, whereby certain tRNAs may rely more heavily on one activity over the other. Our findings reveal distinct pools of substrates for TRMT1L: a group of modified substrates, primarily represented by tRNA-Tyr-GUA isoforms, and unmodified tRNAs (Cys, Arg, Asn, etc.) that may engage in chaperone-like interactions. These activities could exhibit tissue-specific variations, with the balance between catalytic and non-catalytic substrates varying across different cell types. In light of these observations, TRMT1L has been implicated in the deposition of $m^2{}_2G$ at position 26 on a subset of tRNA-Ala-AGC iso-decoders in mouse brain tissue (13), a function that does not appear to be conserved in the HCT116 colon carcinoma cells used in our experiments. Future work will be needed to experimentally test whether TRMT1L has a chaperone or tRNA folding function independent from catalytic activity.

Our quantification of tRNA abundance revealed that the levels of only tRNA-Tyr-GUA were affected by the depletion of TRMT1L, indicating that the presence of $m^2{}_2G27$ is critical for the stability of this particular tRNA. An integral aspect of tRNA structural stability revolves around the strategic positioning of stabilizing modifications, particularly at the

junctures between stems called hinge regions. Position 26 and 27, located at the convergence of the D-stem and anticodon stem, alongside positions 44 and 43, situated at the interface of the anticodon and variable arms, serves as a key point of flexibility, facilitating controlled conformational changes essential for tRNA engagement with the ribosome during translation (116). Numerous studies have shown the significant impact of $m^2{}_2G$ presence within the hinge region on the conformational dynamics of tRNA molecules (24-27). The incorporation of dimethylguanosine at position 26 disrupts potential base-pairing interactions with cytidine, thereby playing a crucial role in stabilizing the canonical tRNA structure and preventing alternative folding conformations (9). Experimental evidence suggests that tRNAs devoid of $m^2{}_2G26$ exhibit notable structural alterations within their core architecture, characterized by a lack of base-stacking interactions and consequential loss of tertiary structural stability (117). In the case of tRNA-Tyr-GUA, the deposition of $m^2{}_2G$ at position 26 would favor interaction with A44, while this modification at G27 would allow pairing with U43 in the stem region. The lack of $m^2{}_2G27$ is expected to compromise the structural integrity of tRNA-Tyr-GUA, potentially resulting in misfolding and subsequent degradation. While native gel analysis did not reveal significant conformational abnormalities in tRNA-Tyr from TRMT1L KO cells, further *in vivo* chemical probing is warranted for a finer assessment of the accessibility of the hinge region in tRNA-Tyr-GUA lacking $m^2{}_2G27$.

While numerous studies in yeast have suggested that most individual modifications are not essential, the collective presence of specific modification combinations on a tRNA appears to exert a more significant influence on tRNA function and structural stability (118-121). Our Nano-seq analysis surprisingly revealed that in addition to lacking $m^2{}_2G27$, tRNA-Tyr-GUA from TRMT1L KO cells also showed impaired deposition of acp^3U20 and likely D17. Similarly, this was observed for tRNA-Cys-GCA, which also showed a decreased presence of acp^3U20, and for tRNA-Ala potentially lacking D20. In eukaryotes, including humans, the acp^3U modification catalyzed by DTWD1 and DTWD2 enzymes occurs at positions 20 and 20a within the D-loop of nuclear-encoded tRNAs such as Tyr-GUA, Cys-GCA, Asn-GUU, and Ile-AAU/UAU (86). The attachment of the 3-amino-3-carboxypropyl (ACP) group to the N3 ring position of the uracil base inhibits Watson–Crick base pairing, thereby contributing to the maintenance of the D-loop structure. While the presence of acp^3U at position 47 of E. coli tRNAs has been demonstrated to enhance thermal stability, the loss of acp^3U at position 20 or 20a in human cells does not appear to adversely affect tRNA stability (86).

On the other hand, D (dihydrouridine) modifications on tRNAs, also located in the D-loop, are formed through the reduction of the uridine C5-C6 bond catalyzed by the DUS family of NADPH-dependent reductases (122). The presence of dihydrouridine influences D-loop structure by promoting the formation of a hairpin with a stable stem and flexible loop and facilitates tertiary interactions that contribute to three-dimensional tRNA folding (123). In budding yeast, strains with mutations in Dus2, which modifies U20, have been shown to have reduced levels of a mutant allele of tRNA Ser-CGA, suggesting a role for D modification in imparting tRNA stability (124). Recent studies investigating the role of human DUS proteins have shown that although D is abundant across many tRNAs, only a subset of tRNA species show impaired expression levels upon DUS enzyme depletion

(89). Thus, loss of acp^{3}U and D modification on tRNA-Tyr-GUA, in addition to the loss of m$^2{}_2$G, could contribute to its instability and reduced levels in the TRMT1L KO cells. Similarly, the functions of tRNA-Cys-GCA and Ala-CGC/UGC could also be impaired, potentially leading to translational defects on their cognate codons, which will be the focus of our future research.

Our findings that TRMT1L is necessary for the deposition of acp^{3}U and D modifications on tRNA-Tyr and Cys suggest its involvement in a potential tRNA modification circuit, wherein the introduction of modifications likely follows a specific order. Modification circuits on tRNAs have primarily been elucidated in bacteria and yeast, where modifications are typically installed in a sequential manner (125,126). For instance, pseudouridylation (Ψ) at position 55 of tRNA-Phe commonly occurs early during nascent tRNA maturation, facilitating the subsequent deposition of 2'-O-methylthymidine (Tm) at nucleotide 54, followed by the catalysis of m^{1}A58 (126,127). Similarly, in vertebrate tRNAs, studies using microinjected frog oocytes have revealed a sequential order of modifications on tRNA-Tyr that correlates with leader and trailer processing and intron removal. Alongside the early appearance of Ψ55, Tm54, and m^{1}A58, traces of m$^2{}_2$G begin to emerge on the unprocessed tRNA-Tyr precursor. Upon leader and trailer removal, the intermediate precursor becomes fully m$^2{}_2$G modified, simultaneous with the appearance of acp^{3}U and D, suggesting the potential requirement of m$^2{}_2$G for the deposition of acp^{3}U and D modifications on tRNA-Tyr (128,129). Upon closer examination of our eCLIP-seq data, we discovered that TRMT1L exhibits binding affinity towards pre-tRNA-Tyr-GUA and Cys-GCA, which both contain 3’ trailer sequences. This observation suggests that TRMT1L binding is an early event in tRNA maturation. Interestingly, many of the TRMT1L eCLIP reads associated with tRNA-Tyr lacked the intron sequence but retained the 3’ trailer region. This finding indicates that intron splicing precedes leader and trailer removal, contradicting previous observations from Xenopus oocyte microinjection studies, which proposed the opposite sequence of events where splicing would occur before tRNA end processing (128). Since TRMT1L does not exhibit catalytic activity towards tRNA-Cys-GCA, our cumulative results indicate that it may not be the m$^2{}_2$G modification itself, but rather the binding of TRMT1L to tRNA-Tyr or -Cys that is crucial for possibly recruiting DTWD1 and DUS enzymes, which are responsible for catalyzing the deposition of acp^{3}U and D on these tRNAs. Future experiments will be required to determine whether TRMT1L forms a complex with these tRNA modifying enzymes and how it would coordinate such a modification circuit.

Another contributing factor to the decrease in tRNA-Tyr-GUA levels could be attributed to the elevated abundance of tRNA-derived small RNA fragments (tRFs) observed in TRMT1L KO cells. tRFs represent a newly recognized category of small non-coding RNAs derived from the cleavage of mature or precursor tRNAs (130). They can be categorized into specific groups based on their site of origin on the corresponding tRNA: 5'-derived tRFs (5'-tRFs), 3'-derived tRFs (3'-tRFs) and internally derived tRFs (i-tRFs) (131-133). The sizes of tRFs vary, with shorter tRFs typically ranging from 15 to 22 nucleotides, constitutively produced in various tissues and cell lines under normal growth conditions (134-136). Conversely, longer tRFs, spanning 31 to 55 nucleotides, are predominantly observed in response to stress (106,137,138). The fragments observed in

the TRMT1L KO cells, detected with probes specific for the D and T-loop regions, ranged from approximately 33 to 58 nucleotides, similar to the length of tRFs generated under stress conditions. Although it is commonly understood that only a small fraction of mature cytoplasmic tRNAs are cleaved into tRFs during stress (138), studies in human cells have shown that oxidative stress can lead to the generation of tRNA-Tyr-GUA fragments, resulting in a notable depletion of its precursor tRNA (102). In this case, predominant tRNA-Tyr-derived fragments of around 45 nt in length were found to be generated under oxidative stress from the cleavage of the precursors in or close to the intron junction in a DIS3L2 exoribonuclease-dependent manner. In TRMT1L KO cells, the presence of 45 nt tRFs, similar to those previously described, suggests a potential increase in reactive oxygen species (ROS) production. Additionally, unique tRFs observed in TRMT1L KO cells, measuring approximately 33 and 58 nt in length, correspond to cleavage events at positions 26-27 of precursor tRNA-Tyr, precisely where TRMT1L catalyzes $m^2{}_2G$ deposition. While tRFs were also identified for tRNA-Cys-GCA, other tRNAs did not exhibit elevated tRF levels, indicating specificity in tRF production, particularly for tRNA-Tyr and Cys, which were the most enriched tRNAs bound by TRMT1L according to eCLIP-seq data. Previous studies have highlighted the role of tRNA modifications in modulating tRNA cleavage, notably by angiogenin (31,139-143). These modifications typically inhibit cleavage, extending beyond the anticodon loop, where angiogenin primarily acts. Various ribonucleases, including Dicer, have been implicated in tRF biogenesis (130). Further investigations are warranted to elucidate whether the observed tRFs in TRMT1L KO cells arise from nonspecific stress signals like ROS or result from specific ribonuclease recognition. Our findings suggest that TRMT1L activity likely contributes to stabilizing tRNA tertiary structures, thereby preventing their fragmentation into tRFs.

It is becoming increasingly clear that different forms of stress can alter the modification pattern of tRNAs. Notably, studies in budding yeast exposed to oxidative stress have shown increased levels of 2'-O-methylcytidine (Cm), 5-methylcytidine (m^5C), $m^2{}_2G$ on tRNAs. Deletion of the enzymes catalyzing these modifications renders cells hypersensitive to oxidative stress, indicating the crucial role of such modifications in modulating tRNA function during stress (108). Notably, cells deficient in TRMT1 have demonstrated defects in redox homeostasis and heightened sensitivity to oxidizing agents (14). While we have not directly measured the redox state of TRMT1L-depleted cells, we have observed increased sensitivity to oxidative and ER stresses. Our findings suggest that the functions of TRMT1L are likely essential for orchestrating a translational response to cope with these stressors effectively. The significant reduction in tRNA-Tyr levels in TRMT1L KO cells suggests that translation defects may arise from inefficiencies in translating mRNAs enriched in this specific cognate codon. Considering its association with oxidative stress, it is conceivable that TRMT1L may become activated to methylate a broader range of tRNA substrates upon stress induction, although this hypothesis requires further investigation.

While the studies presented here focused on tRNAs, our CLIP-seq analysis (Figure 6) also showed that TRMT1L binds to the 28S rRNA expansion segment ES7L, revealing a previously unexplored connection between the tRNA and ribosome biogenesis

machineries. Expansion segments are extra sequences found in eukaryotic rRNA, which are believed to reflect the complex regulation of protein synthesis associated with organismal complexity (144). Previous studies suggested that expansion segments can serve as interaction platforms for ribosome-associated factors, binding with specific mRNAs, regulating translation fidelity, and controlling compartment-specific translation (145-149). ES7L, the largest eukaryotic expansion segment, contains a highly conserved core signature fold and long tentacle-like extensions that undergo rapid evolutionary changes (150). In yeast, the rRNA expansion segment ES7L was proposed to bind aminoacyl tRNA synthetases, potentially modulating translation efficiency (146). Additionally, under sublethal levels of oxidative stress, yeast 25S rRNA undergoes strand cleavage due to the binding of redox-active iron to ES7L, suggesting a potential role for this process in the adaptive oxidative stress response (151). While a previous cryo-EM study predicted m^2G modifications on mammalian ES7L (69), we did not observe posttranscriptional modifications of ES7L catalyzed by TRMT1L. It is possible that such modifications might be restricted to specific cell types or occur under conditions different from those we examined. Alternatively, the interaction detected in the CLIP-seq analysis might reflect a distinct regulatory role of ES7L in the nucleolus. Although previous studies have primarily focused on the roles of expansion segments in mature ribosomes, the extensions in ES7L could also assist in the recruitment of proteins to pre-ribosomal complexes or play a role in mediating complex formation between rRNA and nuclear proteins under stress conditions. Future investigation will explore the interactions of TRMT1L with pre-ribosomes in regulating tRNA and rRNA functions, providing insight into translation programs reliant on its activities for adaptive responses to stress.

Data Availability/Sequence Data Resources

The datasets generated and/or analyzed during the current study are available in the GEO (Gene Expression Omnibus) data repository (accession number pending).

REFERENCES

1. Gilbert, W.V. and Nachtergaele, S. (2023) mRNA Regulation by RNA Modifications. *Annu Rev Biochem*, **92**, 175-198.
2. Wiener, D. and Schwartz, S. (2021) The epitranscriptome beyond m(6)A. *Nat Rev Genet*, **22**, 119-131.
3. Suzuki, T. (2021) The expanding world of tRNA modifications and their disease relevance. *Nat Rev Mol Cell Biol*, **22**, 375-392.
4. Kirchner, S. and Ignatova, Z. (2015) Emerging roles of tRNA in adaptive translation, signalling dynamics and disease. *Nat Rev Genet*, **16**, 98-112.
5. Ohira, T. and Suzuki, T. (2024) Transfer RNA modifications and cellular thermotolerance. *Mol Cell*, **84**, 94-106.
6. Porat, J., Kothe, U. and Bayfield, M.A. (2021) Revisiting tRNA chaperones: New players in an ancient game. *RNA*, **27**, 543-559.
7. Helm, M., Giege, R. and Florentz, C. (1999) A Watson-Crick base-pair-disrupting methyl group (m1A9) is sufficient for cloverleaf folding of human mitochondrial tRNALys. *Biochemistry*, **38**, 13338-13346.

8. Kobitski, A.Y., Hengesbach, M., Seidu-Larry, S., Dammertz, K., Chow, C.S., van Aerschot, A., Nienhaus, G.U. and Helm, M. (2011) Single-molecule FRET reveals a cooperative effect of two methyl group modifications in the folding of human mitochondrial tRNA(Lys). *Chem Biol*, **18**, 928-936.
9. Steinberg, S. and Cedergren, R. (1995) A correlation between N2-dimethylguanosine presence and alternate tRNA conformers. *RNA*, **1**, 886-891.
10. Chujo, T. and Tomizawa, K. (2021) Human transfer RNA modopathies: diseases caused by aberrations in transfer RNA modifications. *FEBS J*, **288**, 7096-7122.
11. Orellana, E.A., Siegal, E. and Gregory, R.I. (2022) tRNA dysregulation and disease. *Nat Rev Genet*, **23**, 651-664.
12. de Crecy-Lagard, V., Boccaletto, P., Mangleburg, C.G., Sharma, P., Lowe, T.M., Leidel, S.A. and Bujnicki, J.M. (2019) Matching tRNA modifications in humans to their known and predicted enzymes. *Nucleic Acids Res*, **47**, 2143-2159.
13. Jonkhout, N., Cruciani, S., Santos Vieira, H.G., Tran, J., Liu, H., Liu, G., Pickford, R., Kaczorowski, D., Franco, G.R., Vauti, F. *et al.* (2021) Subcellular relocalization and nuclear redistribution of the RNA methyltransferases TRMT1 and TRMT1L upon neuronal activation. *RNA Biol*, 1-15.
14. Dewe, J.M., Fuller, B.L., Lentini, J.M., Kellner, S.M. and Fu, D. (2017) TRMT1-Catalyzed tRNA Modifications Are Required for Redox Homeostasis To Ensure Proper Cellular Proliferation and Oxidative Stress Survival. *Mol Cell Biol*, **37**.
15. Liu, J. and Straby, K.B. (2000) The human tRNA(m(2)(2)G(26))dimethyltransferase: functional expression and characterization of a cloned hTRM1 gene. *Nucleic Acids Res*, **28**, 3445-3451.
16. Xiong, Q.P., Li, J., Li, H., Huang, Z.X., Dong, H., Wang, E.D. and Liu, R.J. (2023) Human TRMT1 catalyzes m(2)G or m(2)(2)G formation on tRNAs in a substrate-dependent manner. *Sci China Life Sci*, **66**, 2295-2309.
17. Ellis, S.R., Morales, M.J., Li, J.M., Hopper, A.K. and Martin, N.C. (1986) Isolation and characterization of the TRM1 locus, a gene essential for the N2,N2-dimethylguanosine modification of both mitochondrial and cytoplasmic tRNA in Saccharomyces cerevisiae. *J Biol Chem*, **261**, 9703-9709.
18. Stanford, D.R., Martin, N.C. and Hopper, A.K. (2000) ADEPTs: information necessary for subcellular distribution of eukaryotic sorting isozymes resides in domains missing from eubacterial and archaeal counterparts. *Nucleic Acids Res*, **28**, 383-392.
19. Phillips, J.H. and Kjellin-Straby, K. (1967) Studies on microbial ribonucleic acid. IV. Two mutants of Saccharomyces cerevisiae lacking N-2-dimethylguanine in soluble ribonucleic acid. *J Mol Biol*, **26**, 509-518.
20. Najmabadi, H., Hu, H., Garshasbi, M., Zemojtel, T., Abedini, S.S., Chen, W., Hosseini, M., Behjati, F., Haas, S., Jamali, P. *et al.* (2011) Deep sequencing reveals 50 novel genes for recessive cognitive disorders. *Nature*, **478**, 57-63.
21. Davarniya, B., Hu, H., Kahrizi, K., Musante, L., Fattahi, Z., Hosseini, M., Maqsoud, F., Farajollahi, R., Wienker, T.F., Ropers, H.H. *et al.* (2015) The Role of a Novel TRMT1 Gene Mutation and Rare GRM1 Gene Defect in Intellectual Disability in Two Azeri Families. *PLoS One*, **10**, e0129631.
22. Vauti, F., Goller, T., Beine, R., Becker, L., Klopstock, T., Holter, S.M., Wurst, W., Fuchs, H., Gailus-Durner, V., de Angelis, M.H. *et al.* (2007) The mouse Trm1-like

gene is expressed in neural tissues and plays a role in motor coordination and exploratory behaviour. *Gene*, **389**, 174-185.
23. Clark, W.C., Evans, M.E., Dominissini, D., Zheng, G. and Pan, T. (2016) tRNA base methylation identification and quantification via high-throughput sequencing. *RNA*, **22**, 1771-1784.
24. Edqvist, J., Grosjean, H. and Straby, K.B. (1992) Identity elements for N2-dimethylation of guanosine-26 in yeast tRNAs. *Nucleic Acids Res*, **20**, 6575-6581.
25. Pallan, P.S., Kreutz, C., Bosio, S., Micura, R. and Egli, M. (2008) Effects of N2,N2-dimethylguanosine on RNA structure and stability: crystal structure of an RNA duplex with tandem m2 2G:A pairs. *RNA*, **14**, 2125-2135.
26. Bavi, R.S., Sambhare, S.B. and Sonawane, K.D. (2013) MD simulation studies to investigate iso-energetic conformational behaviour of modified nucleosides m(2)G and m(2) 2G present in tRNA. *Comput Struct Biotechnol J*, **5**, e201302015.
27. Bavi, R.S., Kamble, A.D., Kumbhar, N.M., Kumbhar, B.V. and Sonawane, K.D. (2011) Conformational preferences of modified nucleoside N(2)-methylguanosine (m(2)G) and its derivative N(2), N(2)-dimethylguanosine (m(2)(2)G) occur at 26th position (hinge region) in tRNA. *Cell Biochem Biophys*, **61**, 507-521.
28. Nedialkova, D.D. and Leidel, S.A. (2015) Optimization of Codon Translation Rates via tRNA Modifications Maintains Proteome Integrity. *Cell*, **161**, 1606-1618.
29. Fernandez-Vazquez, J., Vargas-Perez, I., Sanso, M., Buhne, K., Carmona, M., Paulo, E., Hermand, D., Rodriguez-Gabriel, M., Ayte, J., Leidel, S. *et al.* (2013) Modification of tRNA(Lys) UUU by elongator is essential for efficient translation of stress mRNAs. *PLoS Genet*, **9**, e1003647.
30. Blanco, S., Bandiera, R., Popis, M., Hussain, S., Lombard, P., Aleksic, J., Sajini, A., Tanna, H., Cortes-Garrido, R., Gkatza, N. *et al.* (2016) Stem cell function and stress response are controlled by protein synthesis. *Nature*, **534**, 335-340.
31. Blanco, S., Dietmann, S., Flores, J.V., Hussain, S., Kutter, C., Humphreys, P., Lukk, M., Lombard, P., Treps, L., Popis, M. *et al.* (2014) Aberrant methylation of tRNAs links cellular stress to neuro-developmental disorders. *EMBO J*, **33**, 2020-2039.
32. Chan, C.T., Dyavaiah, M., DeMott, M.S., Taghizadeh, K., Dedon, P.C. and Begley, T.J. (2010) A quantitative systems approach reveals dynamic control of tRNA modifications during cellular stress. *PLoS Genet*, **6**, e1001247.
33. Yoluc, Y., van de Logt, E. and Kellner-Kaiser, S. (2021) The Stress-Dependent Dynamics of Saccharomyces cerevisiae tRNA and rRNA Modification Profiles. *Genes (Basel)*, **12**.
34. Castle, C.D., Cassimere, E.K. and Denicourt, C. (2012) LAS1L interacts with the mammalian Rix1 complex to regulate ribosome biogenesis. *Mol Biol Cell*, **23**, 716-728.
35. Labun, K., Montague, T.G., Krause, M., Torres Cleuren, Y.N., Tjeldnes, H. and Valen, E. (2019) CHOPCHOP v3: expanding the CRISPR web toolbox beyond genome editing. *Nucleic Acids Res*, **47**, W171-W174.

36. Sanjana, N.E., Shalem, O. and Zhang, F. (2014) Improved vectors and genome-wide libraries for CRISPR screening. *Nat Methods*, **11**, 783-784.
37. Shalem, O., Sanjana, N.E., Hartenian, E., Shi, X., Scott, D.A., Mikkelson, T., Heckl, D., Ebert, B.L., Root, D.E., Doench, J.G. *et al.* (2014) Genome-scale CRISPR-Cas9 knockout screening in human cells. *Science*, **343**, 84-87.
38. Tiscornia, G., Singer, O. and Verma, I.M. (2006) Production and purification of lentiviral vectors. *Nat Protoc*, **1**, 241-245.
39. Woodson, S.A. (2001) Probing RNA folding pathways by RNA fingerprinting. *Curr Protoc Nucleic Acid Chem*, **Chapter 11**, Unit 11 14.
40. Mansour, F.H. and Pestov, D.G. (2013) Separation of long RNA by agarose-formaldehyde gel electrophoresis. *Anal Biochem*, **441**, 18-20.
41. Liao, H., Gaur, A., McConie, H., Shekar, A., Wang, K., Chang, Jeffrey T., Breton, G. and Denicourt, C. (2022) Human NOP2/NSUN1 regulates ribosome biogenesis through non-catalytic complex formation with box C/D snoRNPs. *Nucleic Acids Research*.
42. Janssen, B.D., Diner, E.J. and Hayes, C.S. (2012) Analysis of aminoacyl- and peptidyl-tRNAs by gel electrophoresis. *Methods Mol Biol*, **905**, 291-309.
43. Zhang, W., Xu, R., Matuszek, Z., Cai, Z. and Pan, T. (2020) Detection and quantification of glycosylated queuosine modified tRNAs by acid denaturing and APB gels. *RNA*, **26**, 1291-1298.
44. Kosugi, S., Hasebe, M., Tomita, M. and Yanagawa, H. (2009) Systematic identification of cell cycle-dependent yeast nucleocytoplasmic shuttling proteins by prediction of composite motifs. *Proc Natl Acad Sci U S A*, **106**, 10171-10176.
45. Scott, M.S., Boisvert, F.M., McDowall, M.D., Lamond, A.I. and Barton, G.J. (2010) Characterization and prediction of protein nucleolar localization sequences. *Nucleic Acids Res*, **38**, 7388-7399.
46. Scott, M.S., Troshin, P.V. and Barton, G.J. (2011) NoD: a Nucleolar localization sequence detector for eukaryotic and viral proteins. *BMC Bioinformatics*, **12**, 317.
47. Liao, H., Gaur, A., Mauvais, C. and Denicourt, C. (2021) p53 induces a survival transcriptional response after nucleolar stress. *Mol Biol Cell*, **32**, ar3.
48. Pestov, D.G., Lapik, Y.R. and Lau, L.F. (2008) Assays for ribosomal RNA processing and ribosome assembly. *Curr Protoc Cell Biol*, **Chapter 22**, Unit 22 11.
49. Simsek, D., Tiu, G.C., Flynn, R.A., Byeon, G.W., Leppek, K., Xu, A.F., Chang, H.Y. and Barna, M. (2017) The Mammalian Ribo-interactome Reveals Ribosome Functional Diversity and Heterogeneity. *Cell*, **169**, 1051-1065 e1018.
50. Van Nostrand, E.L., Nguyen, T.B., Gelboin-Burkhart, C., Wang, R., Blue, S.M., Pratt, G.A., Louie, A.L. and Yeo, G.W. (2017) Robust, Cost-Effective Profiling of RNA Binding Protein Targets with Single-end Enhanced Crosslinking and Immunoprecipitation (seCLIP). *Methods Mol Biol*, **1648**, 177-200.
51. Martin, M. (2011) Cutadapt removes adapter sequences from high-throughput sequencing reads. *2011*, **17**, 3.
52. Chen, S., Zhou, Y., Chen, Y. and Gu, J. (2018) fastp: an ultra-fast all-in-one FASTQ preprocessor. *Bioinformatics*, **34**, i884-i890.
53. Van Nostrand, E.L., Pratt, G.A., Yee, B.A., Wheeler, E.C., Blue, S.M., Mueller, J., Park, S.S., Garcia, K.E., Gelboin-Burkhart, C., Nguyen, T.B. *et al.* (2020)

Principles of RNA processing from analysis of enhanced CLIP maps for 150 RNA binding proteins. *Genome Biol*, **21**, 90.
54. Smith, T., Heger, A. and Sudbery, I. (2017) UMI-tools: modeling sequencing errors in Unique Molecular Identifiers to improve quantification accuracy. *Genome Res*, **27**, 491-499.
55. Li, H. (2011) A statistical framework for SNP calling, mutation discovery, association mapping and population genetical parameter estimation from sequencing data. *Bioinformatics*, **27**, 2987-2993.
56. D'Ascenzo, L., Popova, A.M., Abernathy, S., Sheng, K., Limbach, P.A. and Williamson, J.R. (2022) Pytheas: a software package for the automated analysis of RNA sequences and modifications via tandem mass spectrometry. *Nat Commun*, **13**, 2424.
57. Rozenski, J., Crain, P.F. and McCloskey, J.A. (1999) The RNA Modification Database: 1999 update. *Nucleic Acids Res*, **27**, 196-197.
58. Jora, M., Burns, A.P., Ross, R.L., Lobue, P.A., Zhao, R., Palumbo, C.M., Beal, P.A., Addepalli, B. and Limbach, P.A. (2018) Differentiating Positional Isomers of Nucleoside Modifications by Higher-Energy Collisional Dissociation Mass Spectrometry (HCD MS). *J Am Soc Mass Spectrom*, **29**, 1745-1756.
59. Kelley, M., Uhran, M., Herbert, C., Yoshida, G., Watts, E.R., Limbach, P.A. and Benoit, J.B. (2022) Abundances of transfer RNA modifications and transcriptional levels of tRNA-modifying enzymes are sex-associated in mosquitoes. *Insect Biochem Mol Biol*, **143**, 103741.
60. Lucas, M.C., Pryszcz, L.P., Medina, R., Milenkovic, I., Camacho, N., Marchand, V., Motorin, Y., Ribas de Pouplana, L. and Novoa, E.M. (2024) Quantitative analysis of tRNA abundance and modifications by nanopore RNA sequencing. *Nat Biotechnol*, **42**, 72-86.
61. Chan, P.P. and Lowe, T.M. (2016) GtRNAdb 2.0: an expanded database of transfer RNA genes identified in complete and draft genomes. *Nucleic Acids Res*, **44**, D184-189.
62. Quinlan, A.R. and Hall, I.M. (2010) BEDTools: a flexible suite of utilities for comparing genomic features. *Bioinformatics*, **26**, 841-842.
63. Thorvaldsdottir, H., Robinson, J.T. and Mesirov, J.P. (2013) Integrative Genomics Viewer (IGV): high-performance genomics data visualization and exploration. *Brief Bioinform*, **14**, 178-192.
64. Finkbeiner, E., Haindl, M. and Muller, S. (2011) The SUMO system controls nucleolar partitioning of a novel mammalian ribosome biogenesis complex. *EMBO J*, **30**, 1067-1078.
65. Van Nostrand, E.L., Freese, P., Pratt, G.A., Wang, X., Wei, X., Xiao, R., Blue, S.M., Chen, J.Y., Cody, N.A.L., Dominguez, D. *et al.* (2020) A large-scale binding and functional map of human RNA-binding proteins. *Nature*, **583**, 711-719.
66. Armache, J.P., Jarasch, A., Anger, A.M., Villa, E., Becker, T., Bhushan, S., Jossinet, F., Habeck, M., Dindar, G., Franckenberg, S. *et al.* (2010) Cryo-EM structure and rRNA model of a translating eukaryotic 80S ribosome at 5.5-A resolution. *Proc Natl Acad Sci U S A*, **107**, 19748-19753.

67. Anger, A.M., Armache, J.P., Berninghausen, O., Habeck, M., Subklewe, M., Wilson, D.N. and Beckmann, R. (2013) Structures of the human and Drosophila 80S ribosome. *Nature*, **497**, 80-85.
68. Taoka, M., Nobe, Y., Yamaki, Y., Sato, K., Ishikawa, H., Izumikawa, K., Yamauchi, Y., Hirota, K., Nakayama, H., Takahashi, N. *et al.* (2018) Landscape of the complete RNA chemical modifications in the human 80S ribosome. *Nucleic Acids Res*, **46**, 9289-9298.
69. Natchiar, S.K., Myasnikov, A.G., Kratzat, H., Hazemann, I. and Klaholz, B.P. (2017) Visualization of chemical modifications in the human 80S ribosome structure. *Nature*, **551**, 472-477.
70. Faille, A., Dent, K.C., Pellegrino, S., Jaako, P. and Warren, A.J. (2023) The chemical landscape of the human ribosome at 1.67 A resolution. *bioRxiv*.
71. Krogh, N., Jansson, M.D., Häfner, S.J., Tehler, D., Birkedal, U., Christensen-Dalsgaard, M., Lund, A.H. and Nielsen, H. (2016) Profiling of 2′-O-Me in human rRNA reveals a subset of fractionally modified positions and provides evidence for ribosome heterogeneity. *Nucleic Acids Research*, **44**, 7884-7895.
72. Sharma, S., Marchand, V., Motorin, Y. and Lafontaine, D.L.J. (2017) Identification of sites of 2'-O-methylation vulnerability in human ribosomal RNAs by systematic mapping. *Sci Rep*, **7**, 11490.
73. Erales, J., Marchand, V., Panthu, B., Gillot, S., Belin, S., Ghayad, S.E., Garcia, M., Laforêts, F., Marcel, V., Baudin-Baillieu, A. *et al.* (2017) Evidence for rRNA 2′-O-methylation plasticity: Control of intrinsic translational capabilities of human ribosomes. *Proceedings of the National Academy of Sciences*, **114**, 12934-12939.
74. Marcel, V., Kielbassa, J., Marchand, V., Natchiar, K.S., Paraqindes, H., Nguyen Van Long, F., Ayadi, L., Bourguignon-Igel, V., Lo Monaco, P., Monchiet, D. *et al.* (2020) Ribosomal RNA 2'O-methylation as a novel layer of inter-tumour heterogeneity in breast cancer. *NAR Cancer*, **2**, zcaa036.
75. Hiley, S.L., Jackman, J., Babak, T., Trochesset, M., Morris, Q.D., Phizicky, E. and Hughes, T.R. (2005) Detection and discovery of RNA modifications using microarrays. *Nucleic Acids Res*, **33**, e2.
76. Lamichhane, T.N., Blewett, N.H. and Maraia, R.J. (2011) Plasticity and diversity of tRNA anticodon determinants of substrate recognition by eukaryotic A37 isopentenyltransferases. *Rna*, **17**, 1846-1857.
77. Thomas, N.K., Poodari, V.C., Jain, M., Olsen, H.E., Akeson, M. and Abu-Shumays, R.L. (2021) Direct Nanopore Sequencing of Individual Full Length tRNA Strands. *ACS Nano*, **15**, 16642-16653.
78. Jenjaroenpun, P., Wongsurawat, T., Wadley, T.D., Wassenaar, T.M., Liu, J., Dai, Q., Wanchai, V., Akel, N.S., Jamshidi-Parsian, A., Franco, A.T. *et al.* (2021) Decoding the epitranscriptional landscape from native RNA sequences. *Nucleic Acids Res*, **49**, e7.
79. Price, A.M., Hayer, K.E., McIntyre, A.B.R., Gokhale, N.S., Abebe, J.S., Della Fera, A.N., Mason, C.E., Horner, S.M., Wilson, A.C., Depledge, D.P. *et al.* (2020) Direct RNA sequencing reveals m(6)A modifications on adenovirus RNA are necessary for efficient splicing. *Nat Commun*, **11**, 6016.

80. Liu, H., Begik, O., Lucas, M.C., Ramirez, J.M., Mason, C.E., Wiener, D., Schwartz, S., Mattick, J.S., Smith, M.A. and Novoa, E.M. (2019) Accurate detection of m(6)A RNA modifications in native RNA sequences. *Nat Commun*, **10**, 4079.
81. Smith, A.M., Jain, M., Mulroney, L., Garalde, D.R. and Akeson, M. (2019) Reading canonical and modified nucleobases in 16S ribosomal RNA using nanopore native RNA sequencing. *PLoS One*, **14**, e0216709.
82. Huang, S., Zhang, W., Katanski, C.D., Dersh, D., Dai, Q., Lolans, K., Yewdell, J., Eren, A.M. and Pan, T. (2021) Interferon inducible pseudouridine modification in human mRNA by quantitative nanopore profiling. *Genome Biol*, **22**, 330.
83. Begik, O., Lucas, M.C., Pryszcz, L.P., Ramirez, J.M., Medina, R., Milenkovic, I., Cruciani, S., Liu, H., Vieira, H.G.S., Sas-Chen, A. *et al.* (2021) Quantitative profiling of pseudouridylation dynamics in native RNAs with nanopore sequencing. *Nature Biotechnology*, **39**, 1278-1291.
84. Parker, M.T., Knop, K., Sherwood, A.V., Schurch, N.J., Mackinnon, K., Gould, P.D., Hall, A.J., Barton, G.J. and Simpson, G.G. (2020) Nanopore direct RNA sequencing maps the complexity of Arabidopsis mRNA processing and m(6)A modification. *Elife*, **9**.
85. Fleming, A.M., Bommisetti, P., Xiao, S., Bandarian, V. and Burrows, C.J. (2023) Direct Nanopore Sequencing for the 17 RNA Modification Types in 36 Locations in the E. coli Ribosome Enables Monitoring of Stress-Dependent Changes. *ACS Chem Biol*, **18**, 2211-2223.
86. Takakura, M., Ishiguro, K., Akichika, S., Miyauchi, K. and Suzuki, T. (2019) Biogenesis and functions of aminocarboxypropyluridine in tRNA. *Nat Commun*, **10**, 5542.
87. van Tol, H., Stange, N., Gross, H.J. and Beier, H. (1987) A human and a plant intron-containing tRNATyr gene are both transcribed in a HeLa cell extract but spliced along different pathways. *EMBO J*, **6**, 35-41.
88. Cappannini, A., Ray, A., Purta, E., Mukherjee, S., Boccaletto, P., Moafinejad, S.N., Lechner, A., Barchet, C., Klaholz, B.P., Stefaniak, F. *et al.* (2024) MODOMICS: a database of RNA modifications and related information. 2023 update. *Nucleic Acids Res*, **52**, D239-D244.
89. Yu, N.J., Dai, W., Li, A., He, M. and Kleiner, R.E. (2023) Cell type-specific translational regulation by human DUS enzymes. *bioRxiv*.
90. Johnson, G.D., Pirtle, I.L. and Pirtle, R.M. (1985) The nucleotide sequence of tyrosine tRNAQ* psi A from bovine liver. *Arch Biochem Biophys*, **236**, 448-453.
91. Hagenbuchle, O., Santer, M., Steitz, J.A. and Mans, R.J. (1978) Conservation of the primary structure at the 3' end of 18S rRNA from eucaryotic cells. *Cell*, **13**, 551-563.
92. Youvan, D.C. and Hearst, J.E. (1979) Reverse transcriptase pauses at N2-methylguanine during in vitro transcription of Escherichia coli 16S ribosomal RNA. *Proc Natl Acad Sci U S A*, **76**, 3751-3754.
93. Moazed, D., Stern, S. and Noller, H.F. (1986) Rapid chemical probing of conformation in 16 S ribosomal RNA and 30 S ribosomal subunits using primer extension. *J Mol Biol*, **187**, 399-416.

94. Kristen, M., Plehn, J., Marchand, V., Friedland, K., Motorin, Y., Helm, M. and Werner, S. (2020) Manganese Ions Individually Alter the Reverse Transcription Signature of Modified Ribonucleosides. *Genes*, **11**, 950.
95. Kato, T., Daigo, Y., Hayama, S., Ishikawa, N., Yamabuki, T., Ito, T., Miyamoto, M., Kondo, S. and Nakamura, Y. (2005) A novel human tRNA-dihydrouridine synthase involved in pulmonary carcinogenesis. *Cancer Res*, **65**, 5638-5646.
96. Lucas, M.C., Pryszcz, L.P., Medina, R., Milenkovic, I., Camacho, N., Marchand, V., Motorin, Y., Ribas de Pouplana, L. and Novoa, E.M. (2023) Quantitative analysis of tRNA abundance and modifications by nanopore RNA sequencing. *Nat Biotechnol*.
97. Pütz, J., Florentz, C., Benseler, F. and Giegé, R. (1994) A single methyl group prevents the mischarging of a tRNA. *Nature Structural Biology*, **1**, 580-582.
98. Nureki, O., Niimi, T., Muramatsu, T., Kanno, H., Kohno, T., Florentz, C., Giege, R. and Yokoyama, S. (1994) Molecular recognition of the identity-determinant set of isoleucine transfer RNA from Escherichia coli. *J Mol Biol*, **236**, 710-724.
99. Muramatsu, T., Nishikawa, K., Nemoto, F., Kuchino, Y., Nishimura, S., Miyazawa, T. and Yokoyama, S. (1988) Codon and amino-acid specificities of a transfer RNA are both converted by a single post-transcriptional modification. *Nature*, **336**, 179-181.
100. Magee, R. and Rigoutsos, I. (2020) On the expanding roles of tRNA fragments in modulating cell behavior. *Nucleic Acids Res*, **48**, 9433-9448.
101. Goodarzi, H., Liu, X., Nguyen, H.C., Zhang, S., Fish, L. and Tavazoie, S.F. (2015) Endogenous tRNA-Derived Fragments Suppress Breast Cancer Progression via YBX1 Displacement. *Cell*, **161**, 790-802.
102. Huh, D., Passarelli, M.C., Gao, J., Dusmatova, S.N., Goin, C., Fish, L., Pinzaru, A.M., Molina, H., Ren, Z., McMillan, E.A. *et al.* (2021) A stress-induced tyrosine-tRNA depletion response mediates codon-based translational repression and growth suppression. *EMBO J*, **40**, e106696.
103. Saikia, M., Jobava, R., Parisien, M., Putnam, A., Krokowski, D., Gao, X.H., Guan, B.J., Yuan, Y., Jankowsky, E., Feng, Z. *et al.* (2014) Angiogenin-cleaved tRNA halves interact with cytochrome c, protecting cells from apoptosis during osmotic stress. *Mol Cell Biol*, **34**, 2450-2463.
104. Luo, S., He, F., Luo, J., Dou, S., Wang, Y., Guo, A. and Lu, J. (2018) Drosophila tsRNAs preferentially suppress general translation machinery via antisense pairing and participate in cellular starvation response. *Nucleic Acids Res*, **46**, 5250-5268.
105. Kumar, P., Kuscu, C. and Dutta, A. (2016) Biogenesis and Function of Transfer RNA-Related Fragments (tRFs). *Trends Biochem Sci*, **41**, 679-689.
106. Ivanov, P., Emara, M.M., Villen, J., Gygi, S.P. and Anderson, P. (2011) Angiogenin-induced tRNA fragments inhibit translation initiation. *Mol Cell*, **43**, 613-623.
107. Muthukumar, S., Li, C.T., Liu, R.J. and Bellodi, C. (2024) Roles and regulation of tRNA-derived small RNAs in animals. *Nat Rev Mol Cell Biol*, **25**, 359-378.
108. Chan, C.T., Pang, Y.L., Deng, W., Babu, I.R., Dyavaiah, M., Begley, T.J. and Dedon, P.C. (2012) Reprogramming of tRNA modifications controls the oxidative stress response by codon-biased translation of proteins. *Nat Commun*, **3**, 937.

109. Pang, Y.L., Abo, R., Levine, S.S. and Dedon, P.C. (2014) Diverse cell stresses induce unique patterns of tRNA up- and down-regulation: tRNA-seq for quantifying changes in tRNA copy number. *Nucleic Acids Res*, **42**, e170.
110. Awai, T., Kimura, S., Tomikawa, C., Ochi, A., Ihsanawati, Bessho, Y., Yokoyama, S., Ohno, S., Nishikawa, K., Yokogawa, T. *et al.* (2009) Aquifex aeolicus tRNA (N2,N2-guanine)-dimethyltransferase (Trm1) catalyzes transfer of methyl groups not only to guanine 26 but also to guanine 27 in tRNA. *J Biol Chem*, **284**, 20467-20478.
111. Vakiloroayaei, A., Shah, N.S., Oeffinger, M. and Bayfield, M.A. (2017) The RNA chaperone La promotes pre-tRNA maturation via indiscriminate binding of both native and misfolded targets. *Nucleic Acids Res*, **45**, 11341-11355.
112. Copela, L.A., Chakshusmathi, G., Sherrer, R.L. and Wolin, S.L. (2006) The La protein functions redundantly with tRNA modification enzymes to ensure tRNA structural stability. *RNA*, **12**, 644-654.
113. Keffer-Wilkes, L.C., Soon, E.F. and Kothe, U. (2020) The methyltransferase TrmA facilitates tRNA folding through interaction with its RNA-binding domain. *Nucleic Acids Res*, **48**, 7981-7990.
114. Keffer-Wilkes, L.C., Veerareddygari, G.R. and Kothe, U. (2016) RNA modification enzyme TruB is a tRNA chaperone. *Proc Natl Acad Sci U S A*, **113**, 14306-14311.
115. Porat, J., Vakiloroayaei, A., Remnant, B.M., Talebi, M., Cargill, T. and Bayfield, M.A. (2023) Crosstalk between the tRNA methyltransferase Trm1 and RNA chaperone La influences eukaryotic tRNA maturation. *J Biol Chem*, **299**, 105326.
116. Biela, A., Hammermeister, A., Kaczmarczyk, I., Walczak, M., Koziej, L., Lin, T.Y. and Glatt, S. (2023) The diverse structural modes of tRNA binding and recognition. *J Biol Chem*, **299**, 104966.
117. Sonawane, K.D., Bavi, R.S., Sambhare, S.B. and Fandilolu, P.M. (2016) Comparative Structural Dynamics of tRNA(Phe) with Respect to Hinge Region Methylated Guanosine: A Computational Approach. *Cell Biochem Biophys*, **74**, 157-173.
118. De Zoysa, T. and Phizicky, E.M. (2020) Hypomodified tRNA in evolutionarily distant yeasts can trigger rapid tRNA decay to activate the general amino acid control response, but with different consequences. *PLoS Genet*, **16**, e1008893.
119. Alexandrov, A., Chernyakov, I., Gu, W., Hiley, S.L., Hughes, T.R., Grayhack, E.J. and Phizicky, E.M. (2006) Rapid tRNA decay can result from lack of nonessential modifications. *Mol Cell*, **21**, 87-96.
120. Kadaba, S., Wang, X. and Anderson, J.T. (2006) Nuclear RNA surveillance in Saccharomyces cerevisiae: Trf4p-dependent polyadenylation of nascent hypomethylated tRNA and an aberrant form of 5S rRNA. *RNA*, **12**, 508-521.
121. Kadaba, S., Krueger, A., Trice, T., Krecic, A.M., Hinnebusch, A.G. and Anderson, J. (2004) Nuclear surveillance and degradation of hypomodified initiator tRNAMet in S. cerevisiae. *Genes Dev*, **18**, 1227-1240.
122. Finet, O., Yague-Sanz, C., Marchand, F. and Hermand, D. (2022) The Dihydrouridine landscape from tRNA to mRNA: a perspective on synthesis, structural impact and function. *RNA Biol*, **19**, 735-750.

123. Dyubankova, N., Sochacka, E., Kraszewska, K., Nawrot, B., Herdewijn, P. and Lescrinier, E. (2015) Contribution of dihydrouridine in folding of the D-arm in tRNA. *Org Biomol Chem*, **13**, 4960-4966.
124. Xu, F., Zhou, Y., Bystrom, A.S. and Johansson, M.J.O. (2018) Identification of factors that promote biogenesis of tRNA(CGA)(Ser). *RNA Biol*, **15**, 1286-1294.
125. Sokolowski, M., Klassen, R., Bruch, A., Schaffrath, R. and Glatt, S. (2018) Cooperativity between different tRNA modifications and their modification pathways. *Biochim Biophys Acta Gene Regul Mech*, **1861**, 409-418.
126. Barraud, P., Gato, A., Heiss, M., Catala, M., Kellner, S. and Tisne, C. (2019) Time-resolved NMR monitoring of tRNA maturation. *Nat Commun*, **10**, 3373.
127. Schultz, S.K. and Kothe, U. (2020) tRNA elbow modifications affect the tRNA pseudouridine synthase TruB and the methyltransferase TrmA. *RNA*, **26**, 1131-1142.
128. Nishikura, K. and De Robertis, E.M. (1981) RNA processing in microinjected Xenopus oocytes. Sequential addition of base modifications in the spliced transfer RNA. *J Mol Biol*, **145**, 405-420.
129. Melton, D.A., De Robertis, E.M. and Cortese, R. (1980) Order and intracellular location of the events involved in the maturation of a spliced tRNA. *Nature*, **284**, 143-148.
130. Kuhle, B., Chen, Q. and Schimmel, P. (2023) tRNA renovatio: Rebirth through fragmentation. *Mol Cell*, **83**, 3953-3971.
131. Kumar, P., Mudunuri, S.B., Anaya, J. and Dutta, A. (2015) tRFdb: a database for transfer RNA fragments. *Nucleic Acids Res*, **43**, D141-145.
132. Loher, P., Telonis, A.G. and Rigoutsos, I. (2017) MINTmap: fast and exhaustive profiling of nuclear and mitochondrial tRNA fragments from short RNA-seq data. *Sci Rep*, **7**, 41184.
133. Pliatsika, V., Loher, P., Magee, R., Telonis, A.G., Londin, E., Shigematsu, M., Kirino, Y. and Rigoutsos, I. (2018) MINTbase v2.0: a comprehensive database for tRNA-derived fragments that includes nuclear and mitochondrial fragments from all The Cancer Genome Atlas projects. *Nucleic Acids Res*, **46**, D152-D159.
134. Kumar, P., Anaya, J., Mudunuri, S.B. and Dutta, A. (2014) Meta-analysis of tRNA derived RNA fragments reveals that they are evolutionarily conserved and associate with AGO proteins to recognize specific RNA targets. *BMC Biol*, **12**, 78.
135. Peng, H., Shi, J., Zhang, Y., Zhang, H., Liao, S., Li, W., Lei, L., Han, C., Ning, L., Cao, Y. *et al.* (2012) A novel class of tRNA-derived small RNAs extremely enriched in mature mouse sperm. *Cell Res*, **22**, 1609-1612.
136. Zhang, Y., Zhang, Y., Shi, J., Zhang, H., Cao, Z., Gao, X., Ren, W., Ning, Y., Ning, L., Cao, Y. *et al.* (2014) Identification and characterization of an ancient class of small RNAs enriched in serum associating with active infection. *J Mol Cell Biol*, **6**, 172-174.
137. Thompson, D.M., Lu, C., Green, P.J. and Parker, R. (2008) tRNA cleavage is a conserved response to oxidative stress in eukaryotes. *RNA*, **14**, 2095-2103.
138. Yamasaki, S., Ivanov, P., Hu, G.F. and Anderson, P. (2009) Angiogenin cleaves tRNA and promotes stress-induced translational repression. *J Cell Biol*, **185**, 35-42.

139. Tuorto, F., Liebers, R., Musch, T., Schaefer, M., Hofmann, S., Kellner, S., Frye, M., Helm, M., Stoecklin, G. and Lyko, F. (2012) RNA cytosine methylation by Dnmt2 and NSun2 promotes tRNA stability and protein synthesis. *Nat Struct Mol Biol*, **19**, 900-905.
140. Schaefer, M., Pollex, T., Hanna, K., Tuorto, F., Meusburger, M., Helm, M. and Lyko, F. (2010) RNA methylation by Dnmt2 protects transfer RNAs against stress-induced cleavage. *Genes Dev*, **24**, 1590-1595.
141. Cosentino, C., Toivonen, S., Diaz Villamil, E., Atta, M., Ravanat, J.L., Demine, S., Schiavo, A.A., Pachera, N., Deglasse, J.P., Jonas, J.C. *et al.* (2018) Pancreatic beta-cell tRNA hypomethylation and fragmentation link TRMT10A deficiency with diabetes. *Nucleic Acids Res*, **46**, 10302-10318.
142. Rashad, S., Han, X., Sato, K., Mishima, E., Abe, T., Tominaga, T. and Niizuma, K. (2020) The stress specific impact of ALKBH1 on tRNA cleavage and tiRNA generation. *RNA Biol*, **17**, 1092-1103.
143. Chen, Z., Qi, M., Shen, B., Luo, G., Wu, Y., Li, J., Lu, Z., Zheng, Z., Dai, Q. and Wang, H. (2019) Transfer RNA demethylase ALKBH3 promotes cancer progression via induction of tRNA-derived small RNAs. *Nucleic Acids Res*, **47**, 2533-2545.
144. Hariharan, N., Ghosh, S. and Palakodeti, D. (2023) The story of rRNA expansion segments: Finding functionality amidst diversity. *Wiley Interdiscip Rev RNA*, **14**, e1732.
145. Shankar, V., Rauscher, R., Reuther, J., Gharib, W.H., Koch, M. and Polacek, N. (2020) rRNA expansion segment 27Lb modulates the factor recruitment capacity of the yeast ribosome and shapes the proteome. *Nucleic Acids Res*, **48**, 3244-3256.
146. Gomez Ramos, L.M., Smeekens, J.M., Kovacs, N.A., Bowman, J.C., Wartell, R.M., Wu, R. and Williams, L.D. (2016) Yeast rRNA Expansion Segments: Folding and Function. *J Mol Biol*, **428**, 4048-4059.
147. Fujii, K., Susanto, T.T., Saurabh, S. and Barna, M. (2018) Decoding the Function of Expansion Segments in Ribosomes. *Mol Cell*, **72**, 1013-1020 e1016.
148. Knorr, A.G., Schmidt, C., Tesina, P., Berninghausen, O., Becker, T., Beatrix, B. and Beckmann, R. (2019) Ribosome-NatA architecture reveals that rRNA expansion segments coordinate N-terminal acetylation. *Nat Struct Mol Biol*, **26**, 35-39.
149. Pfeffer, S., Brandt, F., Hrabe, T., Lang, S., Eibauer, M., Zimmermann, R. and Forster, F. (2012) Structure and 3D arrangement of endoplasmic reticulum membrane-associated ribosomes. *Structure*, **20**, 1508-1518.
150. Biesiada, M., Hu, M.Y., Williams, L.D., Purzycka, K.J. and Petrov, A.S. (2022) rRNA expansion segment 7 in eukaryotes: from Signature Fold to tentacles. *Nucleic Acids Res*, **50**, 10717-10732.
151. Zinskie, J.A., Ghosh, A., Trainor, B.M., Shedlovskiy, D., Pestov, D.G. and Shcherbik, N. (2018) Iron-dependent cleavage of ribosomal RNA during oxidative stress in the yeast Saccharomyces cerevisiae. *J Biol Chem*, **293**, 14237-14248.

Figure Legend

Figure 1. TRMT1L interacts with components of the Rix1 60S biogenesis complex. **(A)** Mass spectrometry analysis of Pelp1-associated complexes identifies TRMT1L as an interacting partner. Pelp1 was affinity purified from HEK 293T cell lysate using an anti-Pelp1 antibody. Normal rabbit IgG was used as a negative control. Pelp1-associated complexes were separated on SDS-PAGE, silver stained, and bands present only in the Pelp1 immunoprecipitated (IP) lane were analyzed by mass spectrometry. Identified proteins are marked with an arrow. **(B)** Endogenous Pelp1 or **(C)** TRMT1L were immunoprecipitated (IP) with an anti-Pelp1 or TRMT1L specific antibody from HEK 293T cell lysates. Associated proteins were separated on SDS-PAGE and analyzed by Western blotting with specific antibodies as indicated on the left of each panel. Normal rabbit IgG was used as negative control. Asterisk indicates the presence of the IgG cross reactivity band.

Figure 2. TRMT1L nucleolar localization is dependent on active RNA Pol I transcription. **(A)** Schematic representation of TRMT1L and TRMT1 proteins with predicted domains and sub-cellular localization signals indicated. **(B)** Immunofluorescence detection of endogenous TRMT1L showing nuclear and nucleolar localization in U2OS cells. Fibrillarin (FBL) was used as a nucleolar marker and nuclear DNA was stained with DAPI. **(C)** Inhibition of rRNA transcription by CX-5461 (500 nM, 1h) impairs TRMT1L nucleolar localization in U2OS cells.

Figure 3. TRMT1L co-sediments with pre-60S ribosomes. **(A)** Pre-ribosomal particles from HT1080 cell extracts were separated on sucrose gradient ultra-centrifugation followed by fractionation. Proteins and RNA from each fraction were extracted and analyzed by Western blot with the indicated antibodies (top panel) or by Northern blot with the indicated probes (bottom panel), respectively. **(B)** Depletion of TRMT1L by RNAi does not impair ribosome biogenesis. Nuclear extracts from HCT116 cells treated with control (siC) or TRMT1L siRNA were separated on sucrose gradient ultra-centrifugation and processed on a fractionator equipped with a UV monitor to visualize the pre-40S and pre-60S ribosomes as indicated. **(C)** A small fraction of the cells from (B) were collected before fractionation and analyzed by Western blotting to monitor TRMT1L depletion.

Figure 4. eCLIP-seq approach to identify TRMT1L RNA substrates. **(A)** UV crosslinked and non-crosslinked HCT116 cells were lysed, digested with RNase, immunoprecipitated with TRMT1L or IgG control antibody, and 3'-end labeled with pCp-biotin for detection of co-precipitated RNA. After separation by SDS-PAGE and membrane transfer, the pCp-biotin labeled RNA was detected with Streptavidin-IR800 as indicated by the white box. **(B)** Immunoprecipitated TRMT1L was detected by immunoblotting with a specific antibody. **(C)** Schematic representation of the eCLIP-seq approach utilized to identify endogenous TRMT1L substrate.

Figure 5. TRMT1L binds to tRNAs and rRNA. Immunoprecipitated TRMT1L and size-matched inputs (SMInputs) associated RNAs from HCT116 and HeLa cells were subject to eCLIP-sequencing analysis (two biological replicates for each sample). CLIP-sequencing reads were aligned to the human genome (hg38) and a database of repetitive elements families. Reads mapping equally well to more than one family were discarded.

CLIP peaks were called using Peakachu. **(A)** Percentage of reads in SMInputs and TRMT1L IP samples mapped to CLIP peak regions in each indicated RNA category for HCT116 cells. **(B)** Log_2 fold enrichment of TRMT1L IP over size-matched input (SMInput) with cut-offs of adjusted significance *P* values < 0.05, fold change over size-matched input (SMInput) >= 2 and basemean >= 1000 from HCT116 replicates or **(C)** HeLa replicates for different tRNA iso-decoders.

Figure 6. TRMT1L binds to rRNA expansion segments. eCLIP-sequencing reads of TRMT1L IP and SMInputs from HCT116 and HeLa replicates aligned to human 47S rRNA (NR_146144.1 (RNA45SN2)) was extracted from the whole genome alignment data using Samtools. Dashed boxes mark the location of expansion segment ES7Lb.

Figure 7. Depletion of TRMT1L is associated with loss of modifications on tRNAs Cys-GCA and Tyr-GUA. **(A)** Positive hybridization in absence (PHA) of modification assay. The PHA probe covers the tRNAs 5' half (D-loop region). A probe recognizing the 3' half (T-loop region) was used as an internal control for normalization. **(B)** Total RNAs from HCT116 WT and TRMT1L KO cells were analyzed by Northern blot using the indicated probes. **(C)** Densitometry quantification of PHA signal from (B) normalized to Control probe signal. **(D)** Rescue re-expression of TRMT1L WT in TRMT1L KO cells was confirmed by immunoblotting with TRMT1L antibody. **(E)** Total RNAs from HCT116 WT, TRMT1L KO and TRMT1L KO cells with exogenous re-expression of TRMT1L were analyzed by Northern blot using the indicated probes as described in (A). **(F)** Densitometry quantification of PHA signal from (E) normalized to Control probe signal. The data is presented as the mean of 3 independent biological replicates ± standard deviation (SD). Statistical significance between TRMT1L KO and WT PHA signal intensities was calculated using a 2-tailed independent student t-test.

Figure 8. Nano-tRNAseq identifies potential tRNA modification changes in TRTM1L-depleted cells. **(A)** Heat map of summed base calling error of biological replicates of TRMT1L KO cells relative to WT, for each nucleotide (*x-axis*) and for each tRNA (*y-axis*, tRNA iso-decoder genes with the highest read counts are shown. Triangles indicate position with decreased base calling errors in the TRMT1L KO cells. **(B)** Zoomed snapshots of IGV tracks for tRNA-Tyr-GTA-2-1, **(C)** tRNA-Cys-GCA-3-1, and **(D)** tRNA-Ala-CGC-2-1 alignments in the replicated WT and KO samples. Positions with a mismatch frequency greater than thresholds of 0.2 (Ala-CGC-2-1), 0.3 (Tyr-GTA-2-1), and 0.35 (Cys-GCA-3-1) are colored, whereas those lower than the set thresholds are shown in gray. Known modifications according to Modomics (88) and previous studies (86,89,90) are indicated.

Figure 9. LC-MS/MS modification analysis of tRNA-Tyr-GUA and tRNA-Cys-GCA isolated from WT and TRMT1L KO cells. **(A)** Extracted ion chromatograms of tRNA-Tyr-GUA RNase A digestion products containing the $m^2{}_2G26$ and $m^2{}_2G27$ fragments including "[$m^2{}_2G$][$m^2{}_2G$]AGGACp" (*m/z* 1207.696 (z = -2), 804.797 (z = -3), 603.338 (z = -4)), "[$m^2{}_2G$]GAGGACp" (*m/z* 1193.678 (z = -2), 795.444 (z = -3), 596.332 (z = -4)) and "GGAGGACp" (*m/z* 1179.666 (z = -2), 786.109 (z = -3), 589.325 (z = -4)) and **(B)** the acp^3U20, D20, and U20-containing fragments including "GG[acp^3U]AGAGCp" (*m/z*

1383.214 (z = -2), 921.800 (z = -3), 691.090 (z = -4), 552.678 (z = -5)), “GG[D]p” *(m/z* 1015.145 (z = -1)), and “GGUp” (*m/z* 1013.139 (z = -1)). **(C)** Extracted ion chromatograms of tRNA-Cys-GCA RNase T1 digestion products containing the acp^{3}U20, D20, and U20 fragments including “[acp^{3}U]AGp” (*m/z* 1098.187 (z = -1), 548.583 (z = -2)), “[D]AGp” (*m/z* 999.155 (z = -1)) and “UAGp” (*m/z* 997.138 (z = -1)). Peak intensities are normalized to the sum of modified and unmodified digestion products.

Figure 10. TRMT1L-depleted cells show a reduced abundance in tRNA-Tyr. **(A)** Nano-tRNAseq scatter plots of tRNA abundances of WT and **(B)** TRMT1L KO cells across biological replicates. Each colored point represents a tRNA alloacceptor type. The correlation strength is indicated by the Pearson correlation coefficient (r). **(C)** Volcano plot showing differential expression of tRNAs in TRMT1L KO relative to WT. The threshold of differential expression was set as $p < 0.5$ and absolute log2 fold change > 0.6. **(D)** Diagram showing the location of the Tyr-GUA probe utilized for Northern blotting. **(E)** Total RNAs from HCT116 WT and TRMT1L KO cells were analyzed by Northern blot using the indicated Tyr-GUA and U6 probes. **(F)** Densitometry quantification of Tyr-GUA signal normalized to U6 probe signal from (E). The data is presented as the mean of 3 independent biological replicates ± standard deviation (SD). Statistical significance between TRMT1L KO and WT Tyr-GUA signal intensities was calculated using a 2-tailed independent student t-test.

Figure 11. TRTM1L-depleted cells have higher levels of tRNA-derived small RNA fragments. **(A)** Diagram showing the probes designed to cover different regions of tRNA-Tyr. **(B-C)** Total RNAs from HCT116 WT and TRMT1L KO cells were analyzed by Northern blot using the depicted tRNA-Tyr probes. Approximate sizes of fragments detected in nucleotides are indicated on the side of each panel. Diagram showing the speculative fragments generated from a cut at position 26/27 **(D)** Diagram showing the probes designed to cover different regions of the tRNA-Cys. **(E-F)** Total RNAs from HCT116 WT and TRMT1L KO cells were analyzed by Northern blot using the depicted tRNA-Cys probes. Approximate sizes of fragments detected in nucleotides are indicated on the side of each panel.

Figure 12. Depletion of TRMT1L reduces the global translation rate. **(A)** WT and TRMT1L KO HCT116 cells were lyzed and processed on sucrose gradient ultra-centrifugation for polysome profiling. **(B)** HCT116 cells were transfected with non-targeting control (siCtrl) or TRMT1L siRNAs. 72h after transfection, cells were treated with 5 µg/ml puromycin for the indicated time. Puromycylation of nascent peptides, as well as TRMT1L depletion efficiency, was determined by Western blot with the indicated antibodies.

Figure 13. TRMT1L-depleted cells exhibit increased sensitivity to oxidative and ER stresses. **(A)** WT and TRMT1L KO HCT116 cells were monitored for proliferation by cell counting. Relative cell counts were normalized to the cell counts on day 1. Data are presented as the mean of triplicated independent biological experiments ± standard deviation (SD). Statistical significance values relative to WT were calculated using a 2-tailed independent Student’s t-test. ns: $p > 0.05$. **(B)** WT and TRMT1L KO HCT116 cells were subjected to different stress conditions as indicated. Live cells were counted by

trypan blue exclusion after 48 h of treatment. Data are presented as the mean of three independent biological replicates ± standard deviation (SD). Statistical significance values relative to non-treated cells were calculated using a 2-tailed independent Student's t-test.

Supplementary Figure S1. The subcellular localization of TRMT1L is dependent on its functional NLS and NoLS sequences. **(A)** The schematic representation of TRMT1L protein with predicted sub-cellular localization signals and the indicated NoLs and NLS mutation sites. **(B)** HCT116 cells were transfected with Myc-tagged constructs of TRMT1L WT, NLS and NoLS mutants. The subcellular localization was detected by immunofluorescence with a Myc antibody. DDX21 was used as a nucleolar marker and nuclear DNA was stained with DAPI. **(C)** Quantification of the percentage of cells showing nuclear, nucleolar or cytosolic fluorescence signal for each construct from (B). 100 transfected cells were quantified for each construct.

Supplementary Figure S2. TRMT1L is not required for efficient pre-rRNA processing. **(A)** Schematic overview of the human pre-rRNA processing pathway and the location of probes used for northern blotting are indicated by the cream-color-shaded area. **(B)** The total RNA of HCT116 cells transfected with non-targeting control (siCtrl) or TRMT1L siRNAs for 72 h were resolved on formaldehyde denaturing agarose gel and analyzed by Northern blot with probes targeting to 5′ETS, ITS1 and ITS2. **(C)** The TRMT1L expression in a fraction of cells from (B) was analyzed by Western blot with TRMT1L antibody.

Supplementary Figure S3. TRMT1L binds to tRNAs. **(A)** Complete list of tRNA isodecoders identified by eCLIP-seq in HCT116 cells and **(B)** HeLa cells. Log2 fold enrichment of TRMT1L IP over size-matched input (SMInput) with cut-offs of adjusted significance *P* values < 0.05, fold change over size-matched input (SMInput) >= 2 and basemean >= 100.

Supplementary Figure S4. The eCLIP-seq reads coverage of selected tRNA isodecoders. Plots of normalized reads mapped to each tRNA iso-decoder gene as indicated for IP and Input replicates. Aligned reads per 1000 mapped reads are represented.

Supplementary Figure S5. TRMT1L depletion does not affect the level of TRMT1.
(A) Diagram of the human TRMT1L genes and the designed guide RNAs (sgRNA) sequences and their targeting sites. **(B)** DNA genotypes of TRMT1L KO cell lines generated for each guide RNA by CRISPR Cas9. The targeting sequences are indicated in bold font, and the insertions and deletions in each are shown in red. **(C)** The TRMT1L and TRMT1 expression in HCT116 TRMT1L KO cells was analyzed by Western blot with TRMT1L and TRMT1 antibody as indicated.

Supplementary Figure S6. TRMT1L depletion does not affect the signals of tRNAs Leu, Arg-TCG, Asn-GTT and Arg-CTT as observed by Northern blot using PHA (D-loop) and Control (T-loop) probes. **(A)** Total RNAs from HCT116 WT and TRMT1L KO cells were analyzed by Northern blot using the indicated probes. **(B)** Densitometry quantification of PHA probe signal from (A) normalized to Control probe signal. The data is presented as

the mean of 3 independent biological replicates ± standard deviation (SD). Statistical significance between TRMT1L KO and WT PHA signal intensities was calculated using a 2-tailed independent student t-test.

Supplementary Figure S7. Primer extension assay showing loss of modification-induced reverse transcription (RT) block on tRNA Tyr-GUA and Cys-GCA in TRMT1L KO cells. **(A)** The position of RT primers for each tRNA is indicated. **(B)** The total RNA from HCT116 WT and TRMT1L KO cells were reverse transcribed with 32P-labeled oligonucleotide primers. RT products were resolved on urea-PAGE gel and exposed to radiographic film. The position of the labeled probe and RT stops is indicated on the left of each panel. **(C)** $m^2{}_2G$ immuno-northern blot. The total RNA or isolated tRNA Tyr-GUA, Cys-GCA and Arg-CCU iso-decoders from the total RNA of HCT116 WT and TRMT1L KO cells were analyzed by immuno-Northern blotting with an $m^2{}_2G$ antibody. Densitometry quantification of the $m^2{}_2G$ signals normalized to SYBR gold signal for tRNA-Tyr isolated from WT and TRMT1L KO cells. **(D)** Mass spectrometric nucleoside analyses of tRNA-Tyr modifications from WT and TRMT1L KO cells. The relative abundance of each type of nucleoside is normalized to the anticipated nucleoside numbers in WT according to Modomics (88).

Supplementary Figure S8. Northern blots analysis from native-PAGE and acid urea-PAGE. **(A)** The total RNA from HCT116 WT and TRMT1L KO cells were separated on native PAGE and detected by Northern blot with the indicated tRNA iso-decoder probes. **(B)** The deacylated total RNA control and non-deacylated total RNA from WT and TRMT1L KO cells were resolved on 12% acid urea-PAGE gel and analyzed by Northern Blot using the indicated tRNA iso-decoder probes.

Supplementary Figure S9. TRMT1L depletion does not affect the level of tRFs derived from tRNA-Leu, tRNA-Asn-GUU, tRNA-Arg-UCG and tRNA-Arg-CCU. The total RNA from HCT116 WT and TRMT1L KO cells were analyzed by Northern blot using **(A)** tRNA-Leu probes **(B)** tRNA-Asn-GTT probes **(C)** tRNA-Arg-TCG probes **(D)** tRNA-Arg-CCT probes. For each tRNA, blots were consecutively hybridized with D-loop and T-loop specific probes. The blots are shown at a high exposure to detect the presence of tRFs.

Supplementary Table 1. The sequence of primers and probes used in this paper.

Supplementary Table 2. The selected SRM transitions of the RNA modifications used in nucleoside analysis.

Supplementary Table 3. TRMT1L eCLIP sequencing peaks with IP vs SMInput fold-change >= 2 and adjusted P value < 0.05.

Supplementary Table 4. Basecalling errors of each position of tRNA in Nano-tRNAseq.

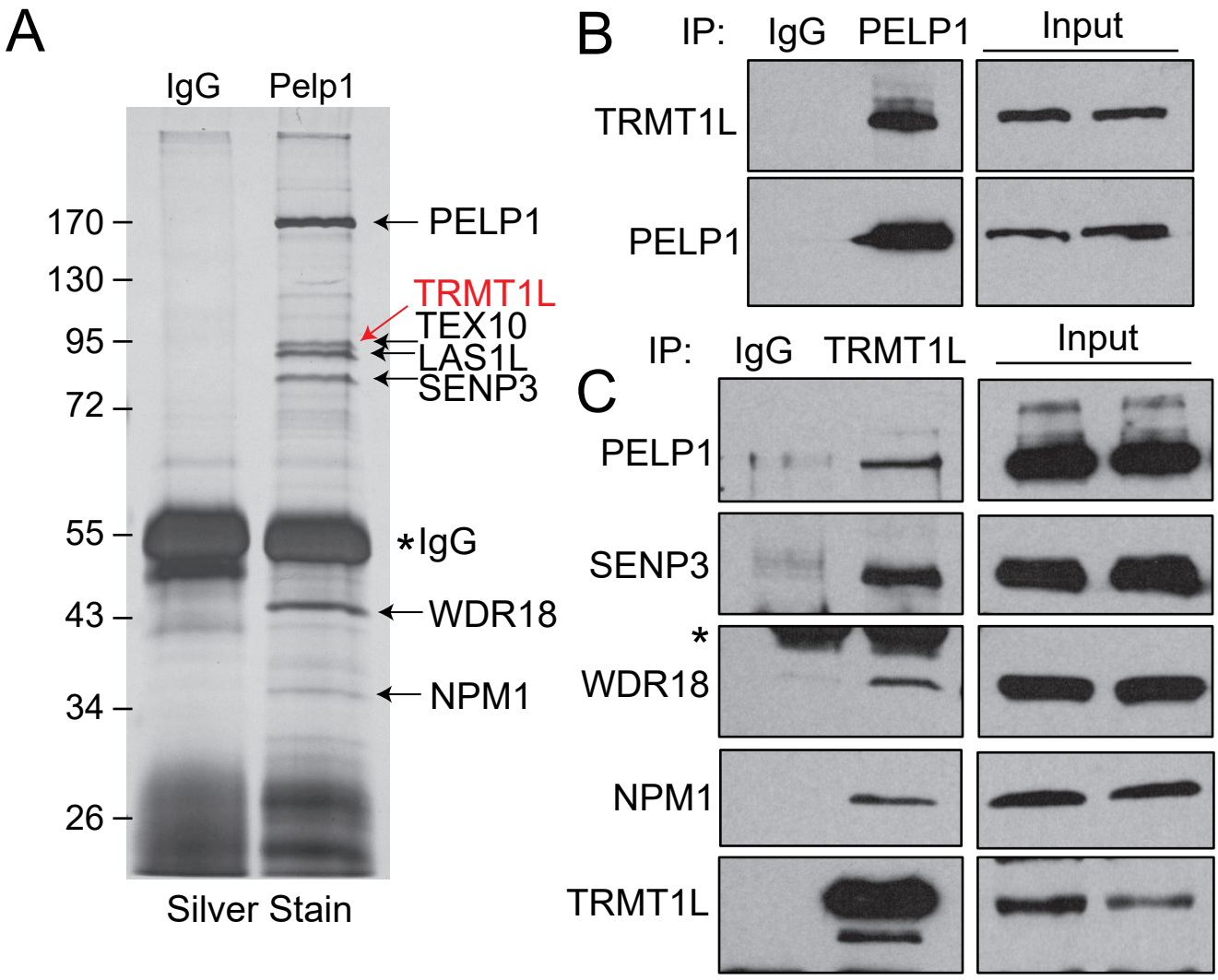
A
IgG
Pelp1
170
130
95
72
55
43
34
26
PELP1
TRMT1L
TEX10
LAS1L
SENP3
*IgG
WDR18
NPM1
Silver Stain
B
IP:
IgG
PELP1
Input
TRMT1L
PELP1
C
IP:
IgG
TRMT1L
Input
PELP1
SENP3
*
WDR18
NPM1
TRMT1L

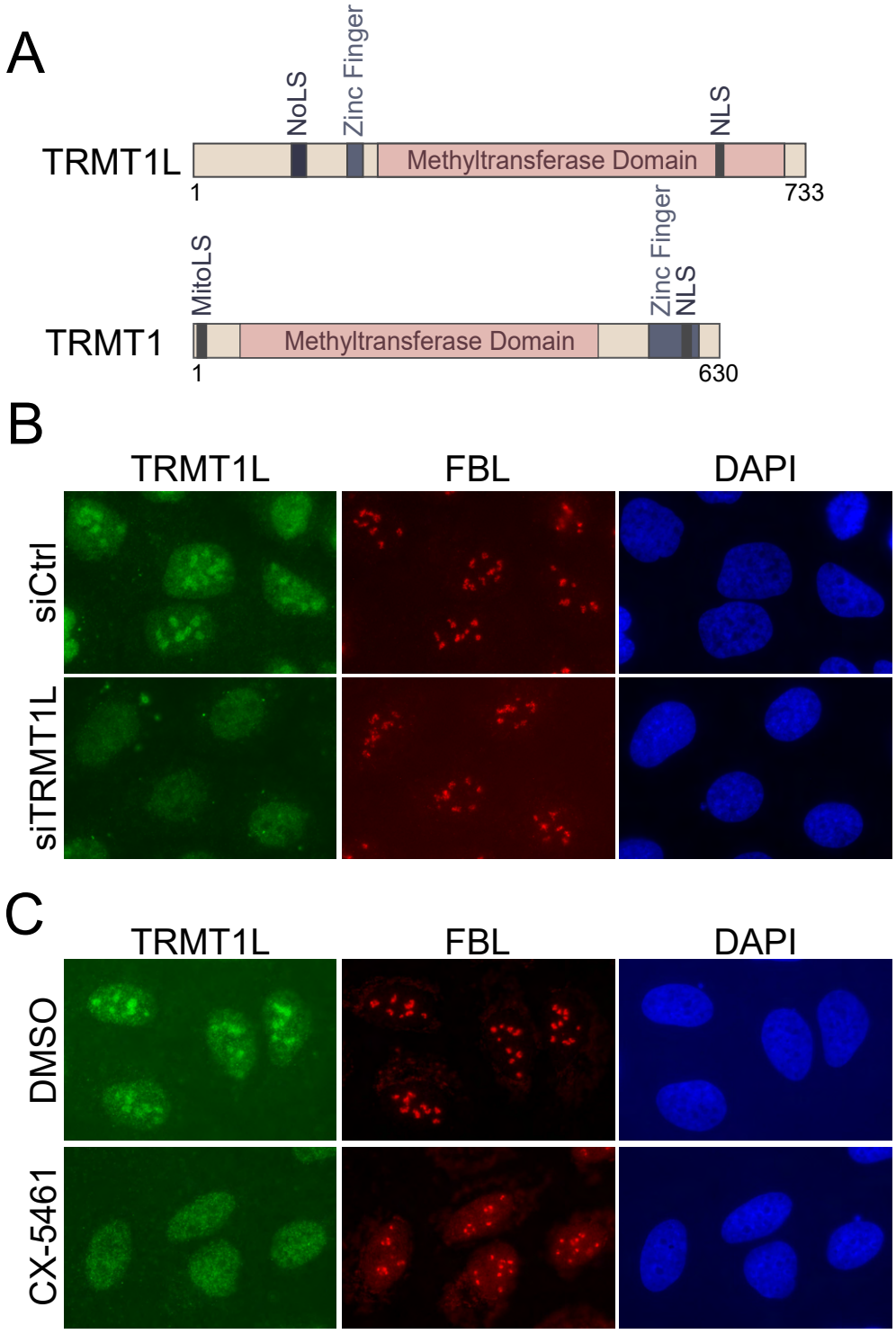
A
NoLS
Zinc Finger
NLS
TRMT1L
Methyltransferase Domain
1
733
MitoLS
Zinc Finger
NLS
TRMT1
Methyltransferase Domain
1
630
B
TRMT1L
FBL
DAPI
siCtrl
siTRMT1L
C
TRMT1L
FBL
DAPI
DMSO
CX-5461

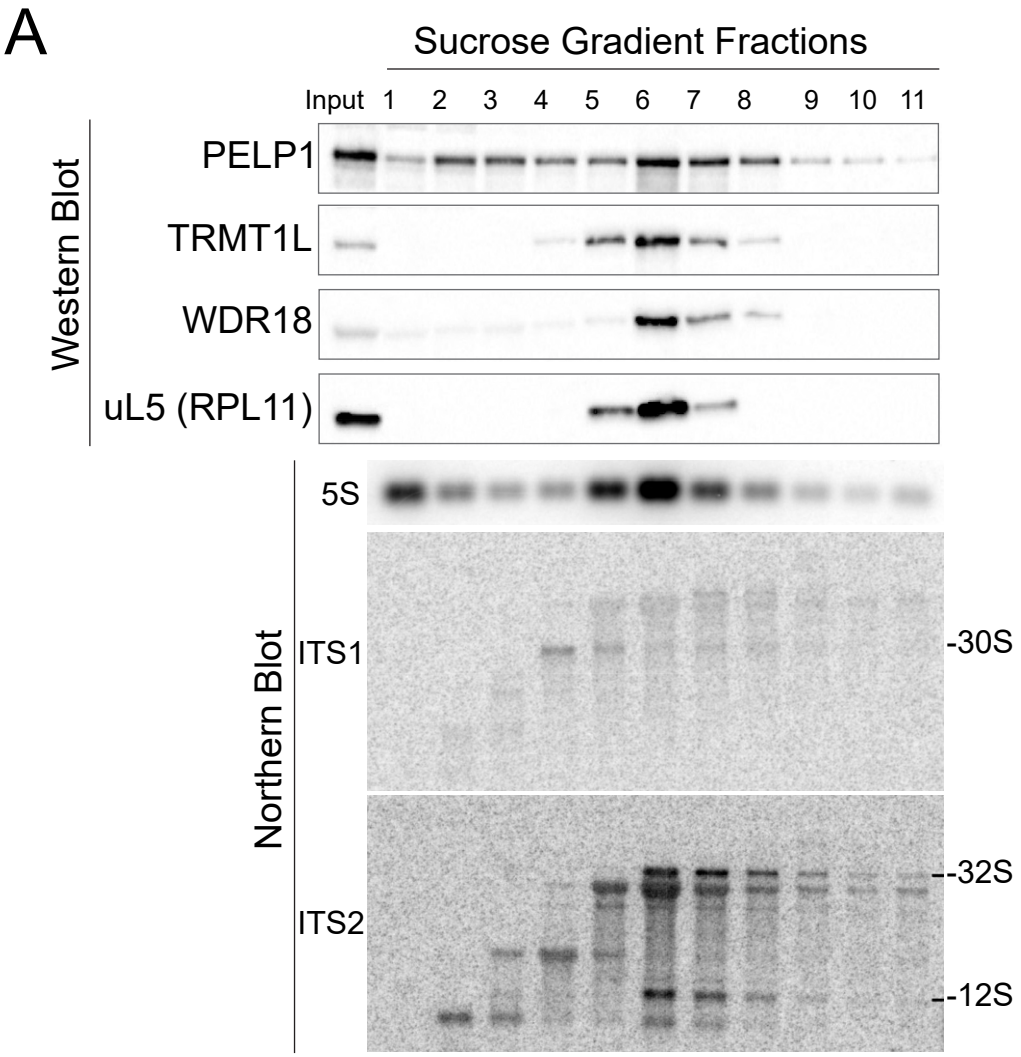
A
Sucrose Gradient Fractions
Input 1 2 3 4 5 6 7 8 9 10 11
Western Blot
PELP1
TRMT1L
WDR18
uL5 (RPL11)
Northern Blot
5S
ITS1
-30S
ITS2
--32S
--12S

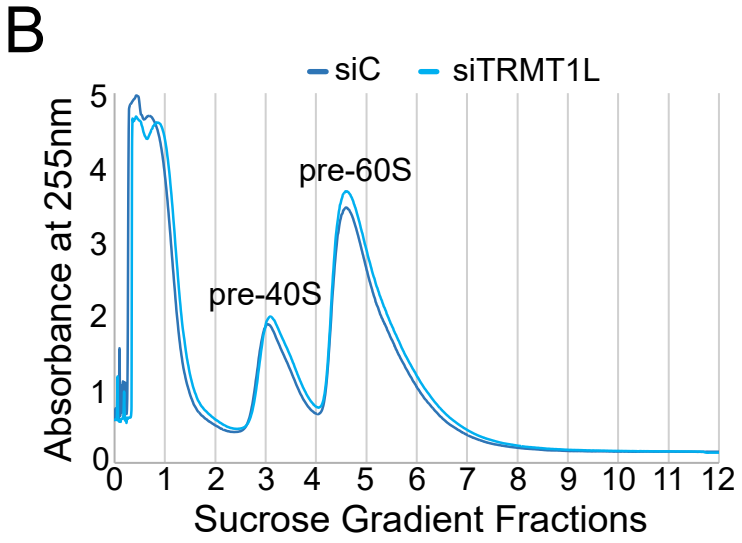
B
siC
siTRMT1L
Absorbance at 255nm
0 1 2 3 4 5
pre-60S
pre-40S
0 1 2 3 4 5 6 7 8 9 10 11 12
Sucrose Gradient Fractions

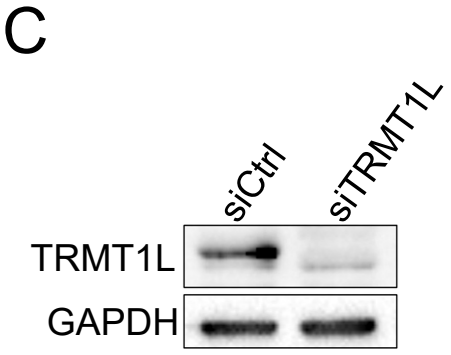
C
siCtrl
siTRMT1L
TRMT1L
GAPDH

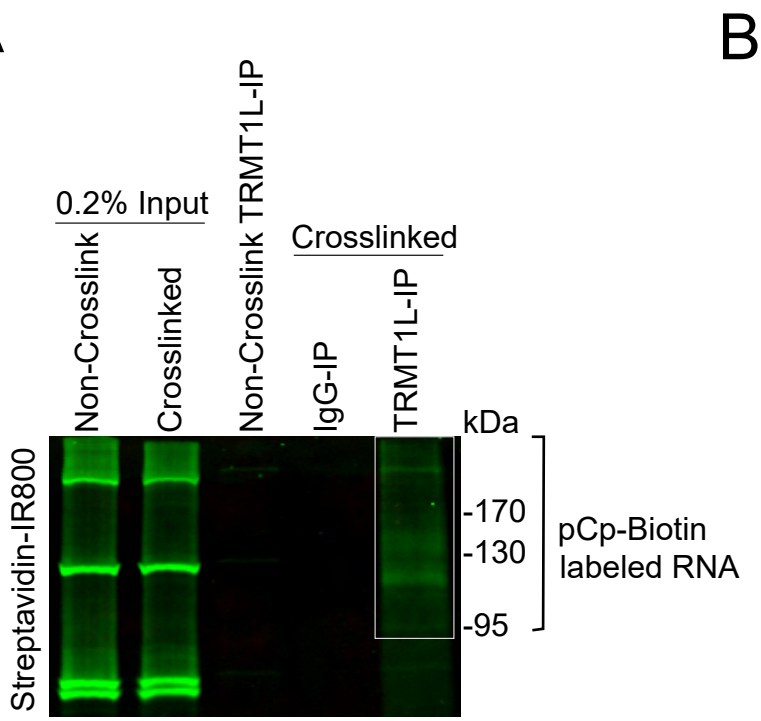
A
0.2% Input
Crosslinked
Non-Crosslink
Crosslinked
Non-Crosslink
TRMT1L-IP
IgG-IP
TRMT1L-IP
kDa
Streptavidin-IR800
-170
-130
-95
pCp-Biotin
labeled RNA

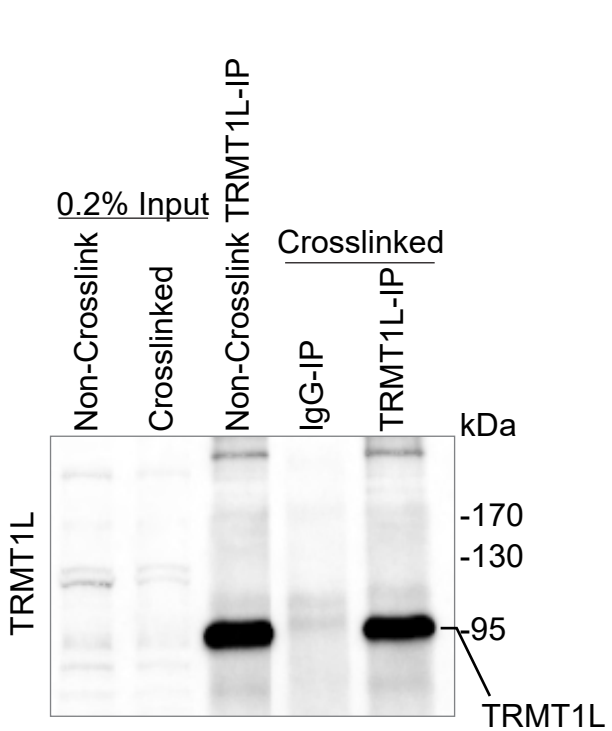
B
0.2% Input
Crosslinked
Non-Crosslink
Crosslinked
Non-Crosslink
TRMT1L-IP
IgG-IP
TRMT1L-IP
kDa
TRMT1L
-170
-130
-95
TRMT1L

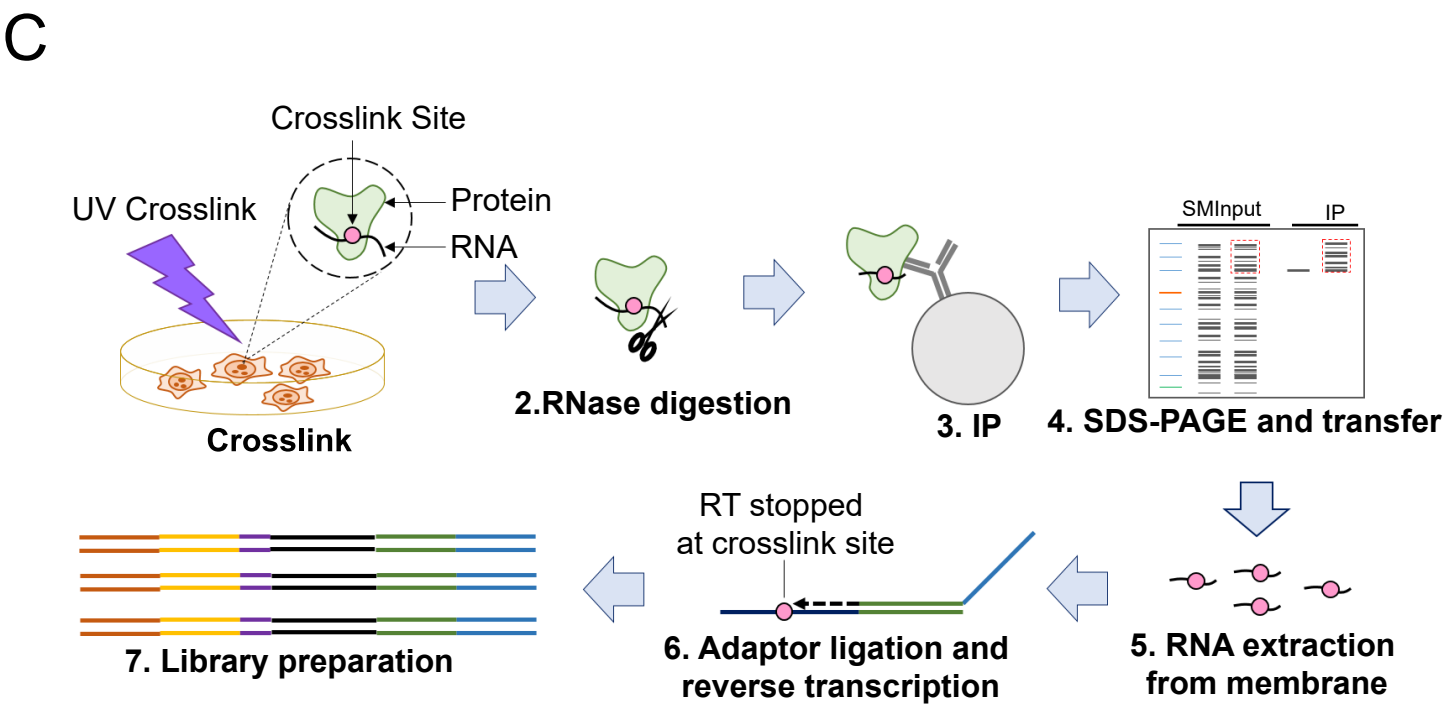
C
Crosslink Site
UV Crosslink
Protein
RNA
Crosslink
2.RNase digestion
3. IP
SMInput
IP
4. SDS-PAGE and transfer
5. RNA extraction
from membrane
RT stopped
at crosslink site
6. Adaptor ligation and
reverse transcription
7. Library preparation

A

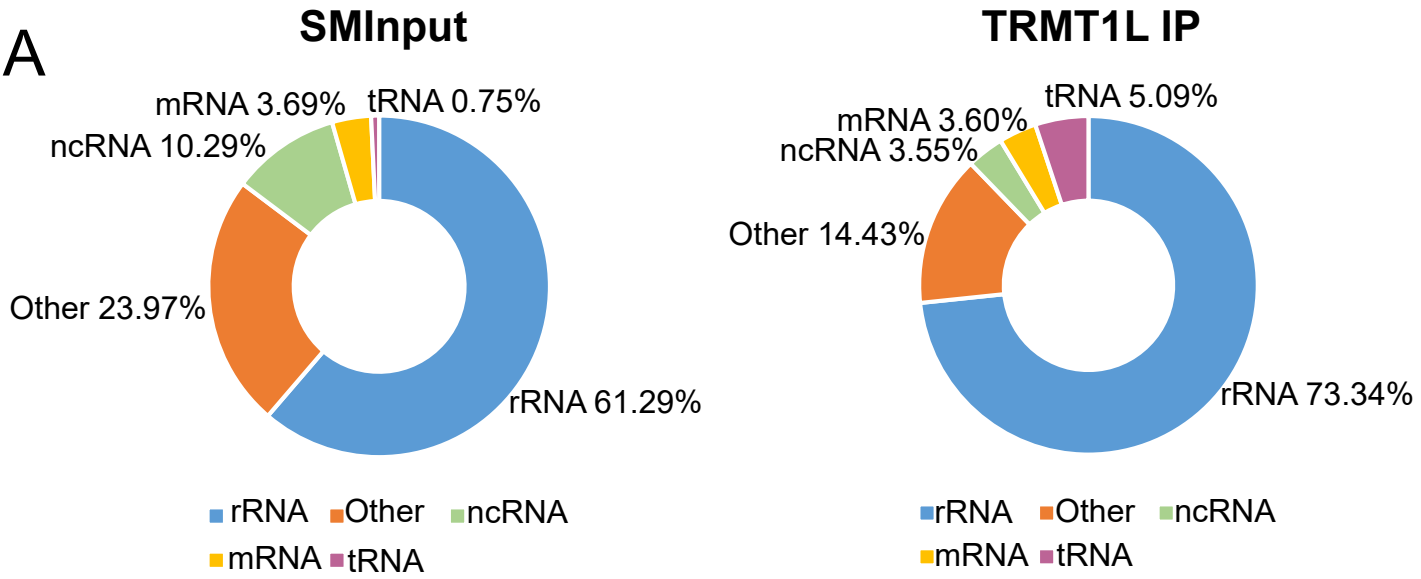
SMInput
mRNA 3.69%
tRNA 0.75%
ncRNA 10.29%
Other 23.97%
rRNA 61.29%
rRNA
Other
ncRNA
mRNA
tRNA
TRMT1L IP
tRNA 5.09%
mRNA 3.60%
ncRNA 3.55%
Other 14.43%
rRNA 73.34%
rRNA
Other
ncRNA
mRNA
tRNA

B

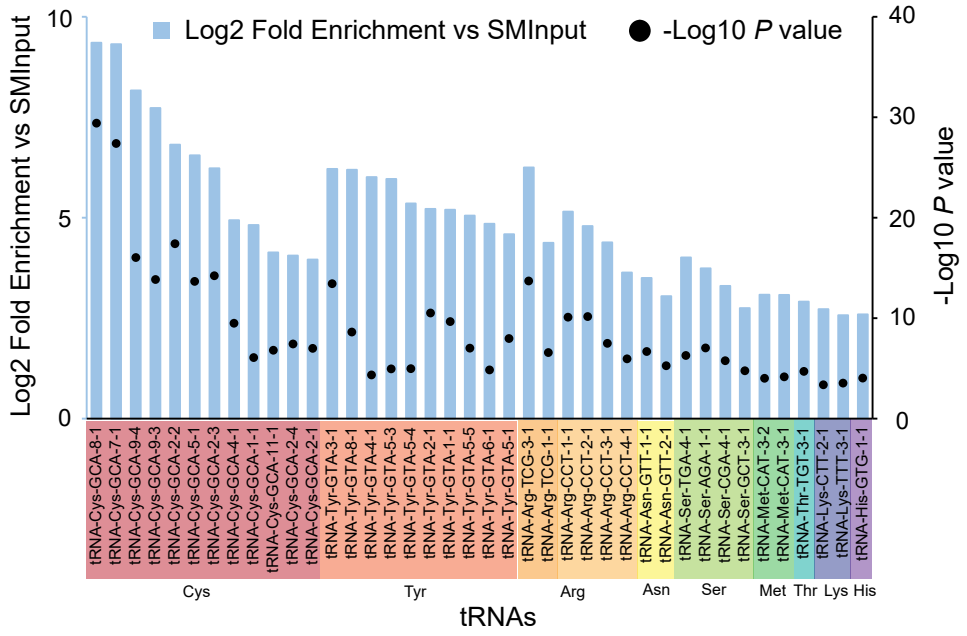
Log2 Fold Enrichment vs SMInput
-Log10 P value
Log2 Fold Enrichment vs SMInput
-Log10 P value
10
5
0
40
30
20
10
0
tRNA-Cys-GCA-8-1
tRNA-Cys-GCA-7-1
tRNA-Cys-GCA-9-4
tRNA-Cys-GCA-9-3
tRNA-Cys-GCA-2-2
tRNA-Cys-GCA-5-1
tRNA-Cys-GCA-2-3
tRNA-Cys-GCA-4-1
tRNA-Cys-GCA-1-1
tRNA-Cys-GCA-11-1
tRNA-Cys-GCA-2-4
tRNA-Cys-GCA-2-1
tRNA-Tyr-GTA-3-1
tRNA-Tyr-GTA-8-1
tRNA-Tyr-GTA-4-1
tRNA-Tyr-GTA-5-3
tRNA-Tyr-GTA-5-4
tRNA-Tyr-GTA-2-1
tRNA-Tyr-GTA-1-1
tRNA-Tyr-GTA-5-5
tRNA-Tyr-GTA-6-1
tRNA-Tyr-GTA-5-1
tRNA-Arg-TCG-3-1
tRNA-Arg-TCG-1-1
tRNA-Arg-CCT-1-1
tRNA-Arg-CCT-2-1
tRNA-Arg-CCT-3-1
tRNA-Arg-CCT-4-1
tRNA-Asn-GTT-1-1
tRNA-Asn-GTT-2-1
tRNA-Ser-TGA-4-1
tRNA-Ser-AGA-1-1
tRNA-Ser-CGA-4-1
tRNA-Ser-GCT-3-1
tRNA-Met-CAT-3-2
tRNA-Met-CAT-3-1
tRNA-Thr-TGT-3-1
tRNA-Lys-CTT-2-1
tRNA-Lys-TTT-3-1
tRNA-His-GTG-1-1
Cys
Tyr
Arg
Asn
Ser
Met
Thr
Lys
His
tRNAs

C

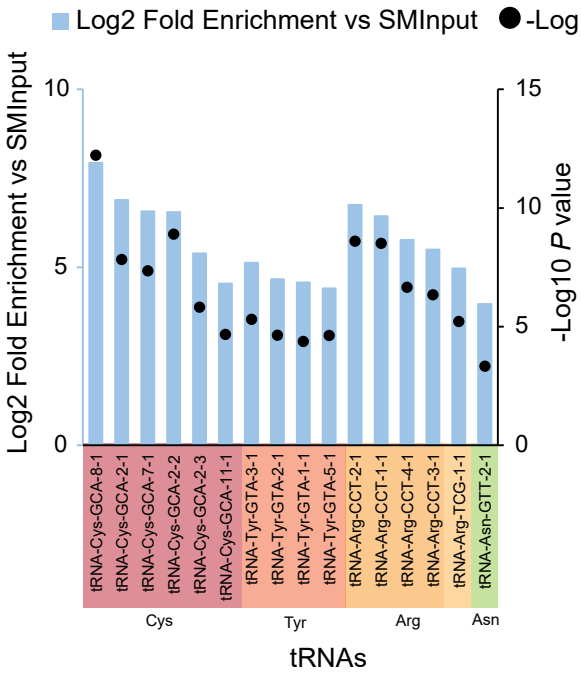
Log2 Fold Enrichment vs SMInput
-Log10 P value
Log2 Fold Enrichment vs SMInput
-Log10 P value
10
5
0
15
10
5
0
tRNA-Cys-GCA-8-1
tRNA-Cys-GCA-2-1
tRNA-Cys-GCA-7-1
tRNA-Cys-GCA-2-2
tRNA-Cys-GCA-2-3
tRNA-Cys-GCA-11-1
tRNA-Tyr-GTA-3-1
tRNA-Tyr-GTA-2-1
tRNA-Tyr-GTA-1-1
tRNA-Tyr-GTA-5-1
tRNA-Arg-CCT-2-1
tRNA-Arg-CCT-1-1
tRNA-Arg-CCT-4-1
tRNA-Arg-CCT-3-1
tRNA-Arg-TCG-1-1
tRNA-Asn-GTT-2-1
Cys
Tyr
Arg
Asn
tRNAs

Hwang *et al.* Fig. 6

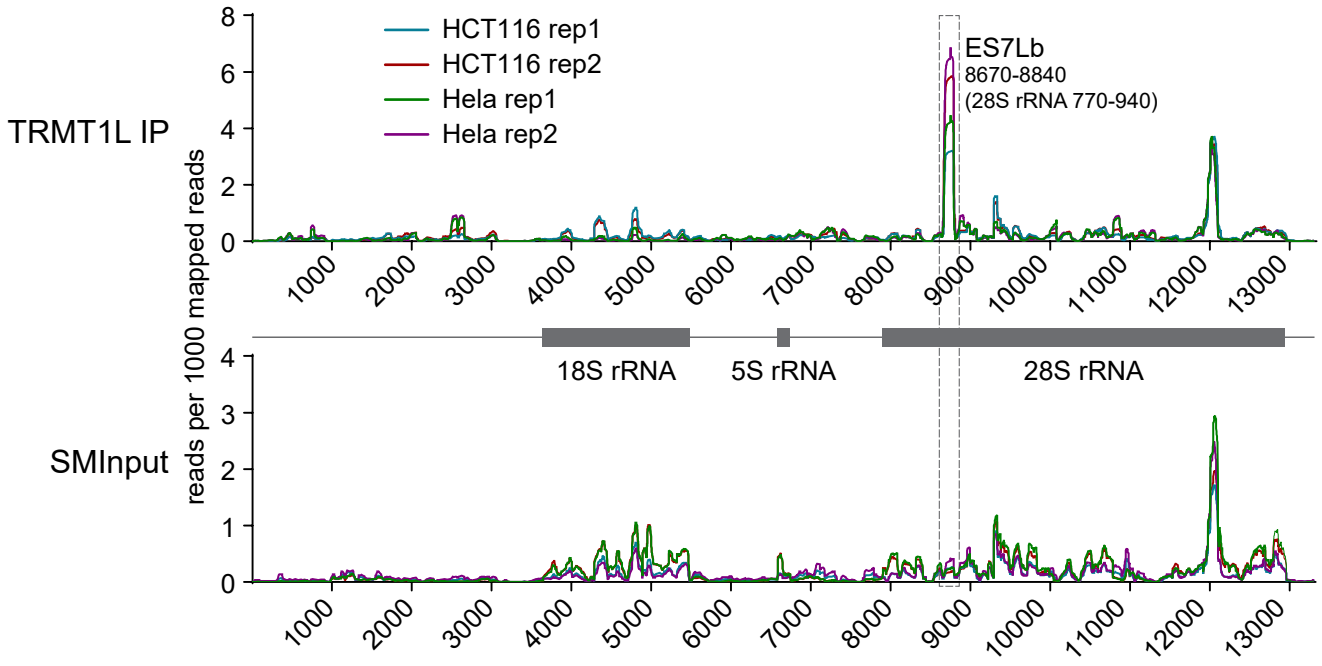

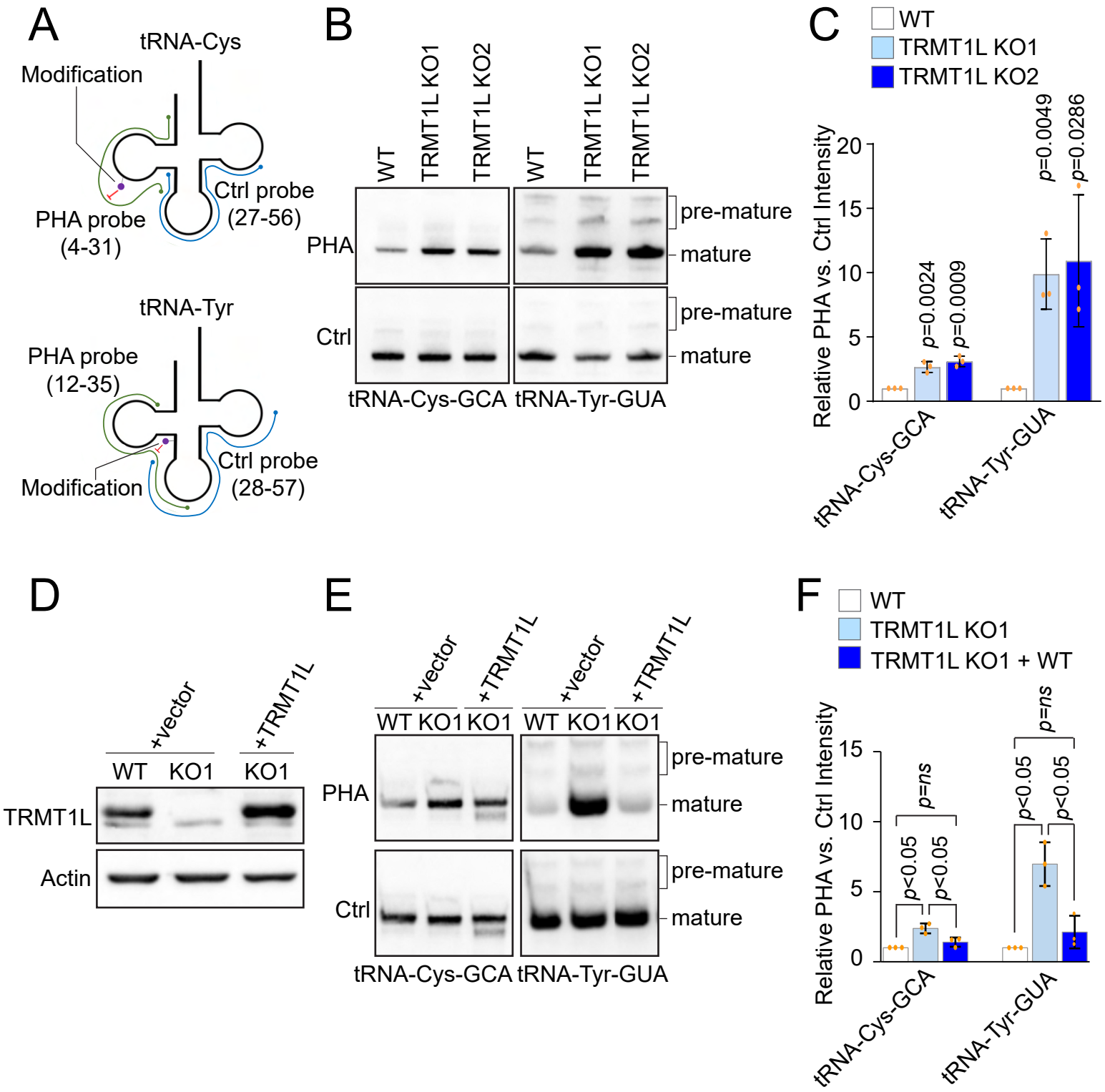
A
tRNA-Cys
Modification
Ctrl probe
(27-56)
PHA probe
(4-31)
tRNA-Tyr
PHA probe
(12-35)
Ctrl probe
(28-57)
Modification
B
WT
TRMT1L KO1
TRMT1L KO2
WT
TRMT1L KO1
TRMT1L KO2
PHA
Ctrl
pre-mature
mature
pre-mature
mature
tRNA-Cys-GCA
tRNA-Tyr-GUA
C
WT
TRMT1L KO1
TRMT1L KO2
Relative PHA vs. Ctrl Intensity
20
15
10
5
0
p=0.0024
p=0.0009
p=0.0049
p=0.0286
tRNA-Cys-GCA
tRNA-Tyr-GUA
D
+vector
+TRMT1L
WT
KO1
KO1
TRMT1L
Actin
E
+vector
+TRMT1L
+vector
+TRMT1L
WT
KO1
KO1
WT
KO1
KO1
PHA
Ctrl
pre-mature
mature
pre-mature
mature
tRNA-Cys-GCA
tRNA-Tyr-GUA
F
WT
TRMT1L KO1
TRMT1L KO1 + WT
Relative PHA vs. Ctrl Intensity
15
10
5
0
p=ns
p<0.05
p<0.05
p=ns
p<0.05
p<0.05
tRNA-Cys-GCA
tRNA-Tyr-GUA

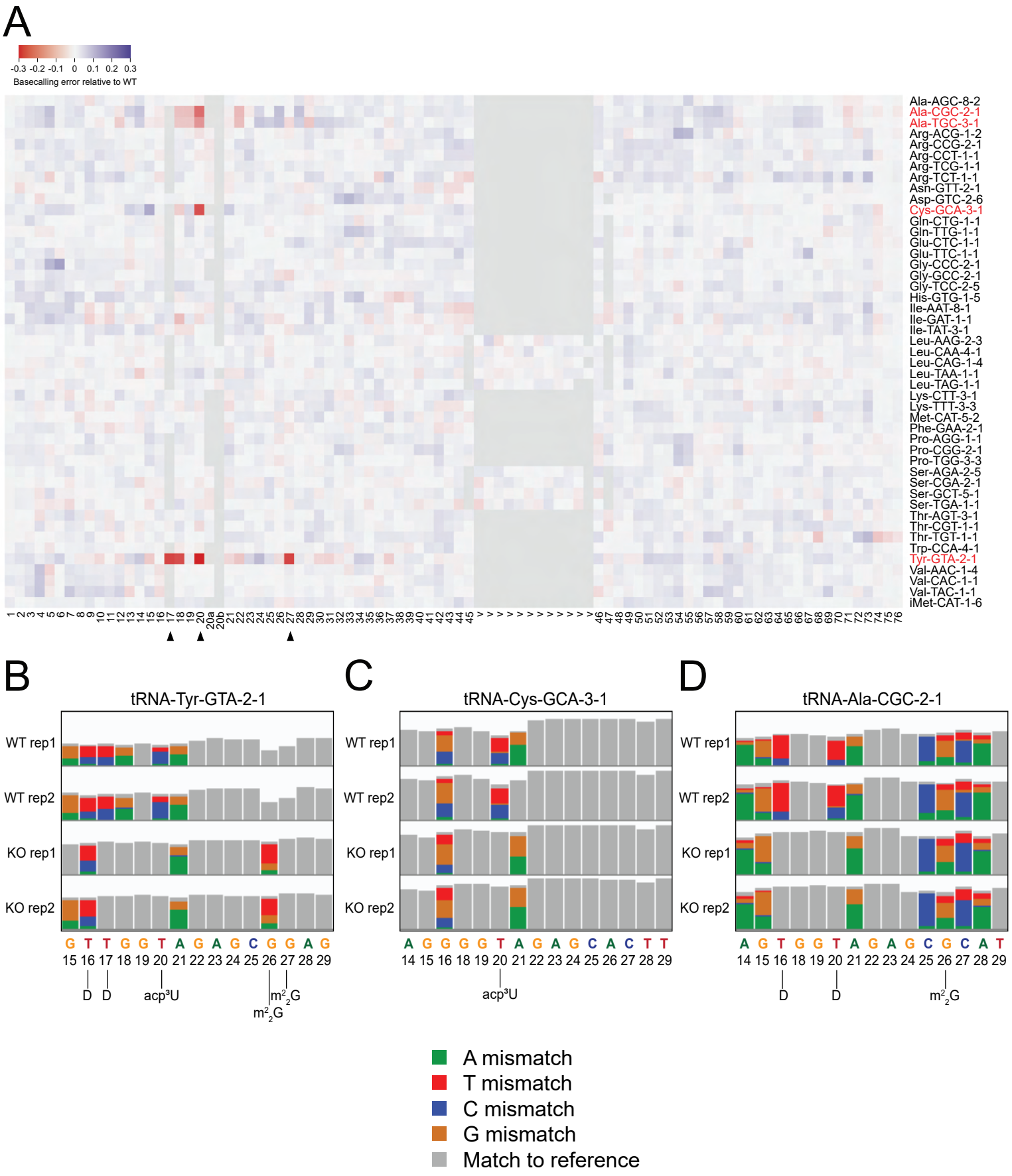
A
-0.3 -0.2 -0.1 0 0.1 0.2 0.3
Basecalling error relative to WT
Ala-AGC-8-2
Ala-CGC-2-1
Ala-TGC-3-1
Arg-ACG-1-2
Arg-CCG-2-1
Arg-CCT-1-1
Arg-TCG-1-1
Arg-TCT-1-1
Asn-GTT-2-1
Asp-GTC-2-6
Cys-GCA-3-1
Gln-CTG-1-1
Gln-TTG-1-1
Glu-CTC-1-1
Glu-TTC-1-1
Gly-CCC-2-1
Gly-GCC-2-1
Gly-TCC-2-5
His-GTG-1-5
Ile-AAT-8-1
Ile-GAT-1-1
Ile-TAT-3-1
Leu-AAG-2-3
Leu-CAA-4-1
Leu-CAG-1-4
Leu-TAA-1-1
Leu-TAG-1-1
Lys-CTT-3-1
Lys-TTT-3-3
Met-CAT-5-2
Phe-GAA-2-1
Pro-AGG-1-1
Pro-CGG-2-1
Pro-TGG-3-3
Ser-AGA-2-5
Ser-CGA-2-1
Ser-GCT-5-1
Ser-TGA-1-1
Thr-AGT-3-1
Thr-CGT-1-1
Thr-TGT-1-1
Trp-CCA-4-1
Tyr-GTA-2-1
Val-AAC-1-4
Val-CAC-1-1
Val-TAC-1-1
iMet-CAT-1-6
B
tRNA-Tyr-GTA-2-1
WT rep1
WT rep2
KO rep1
KO rep2
G T T G G T A G A G C G G A G
15 16 17 18 19 20 21 22 23 24 25 26 27 28 29
D D acp³U m²₂G m²₂G
C
tRNA-Cys-GCA-3-1
WT rep1
WT rep2
KO rep1
KO rep2
A G G G G T A G A G C A C T T
14 15 16 18 19 20 21 22 23 24 25 26 27 28 29
acp³U
D
tRNA-Ala-CGC-2-1
WT rep1
WT rep2
KO rep1
KO rep2
A G T G G T A G A G C G C A T
14 15 16 18 19 20 21 22 23 24 25 26 27 28 29
D D m²₂G
A mismatch
T mismatch
C mismatch
G mismatch
Match to reference

Hwang *et al.* Fig. 9

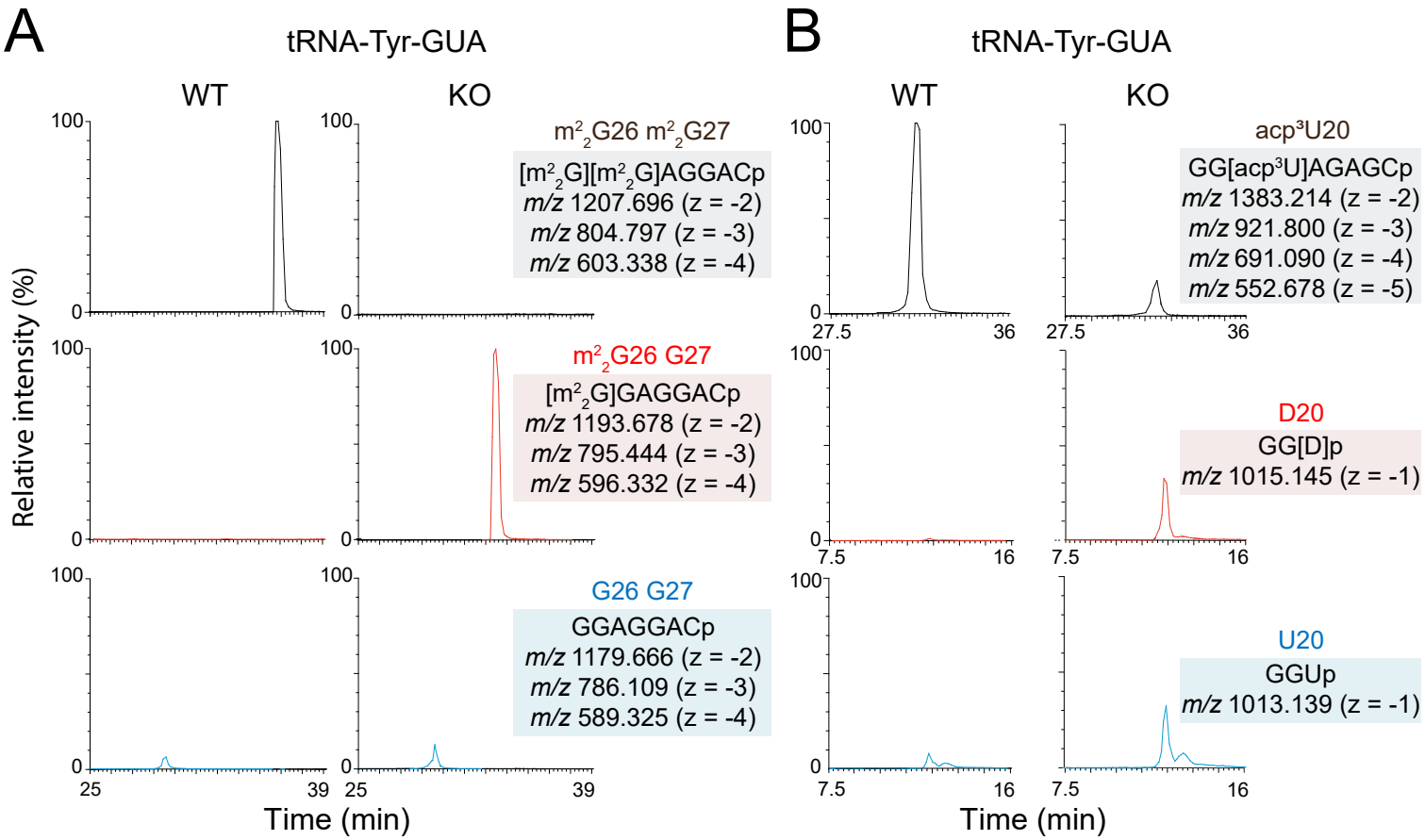

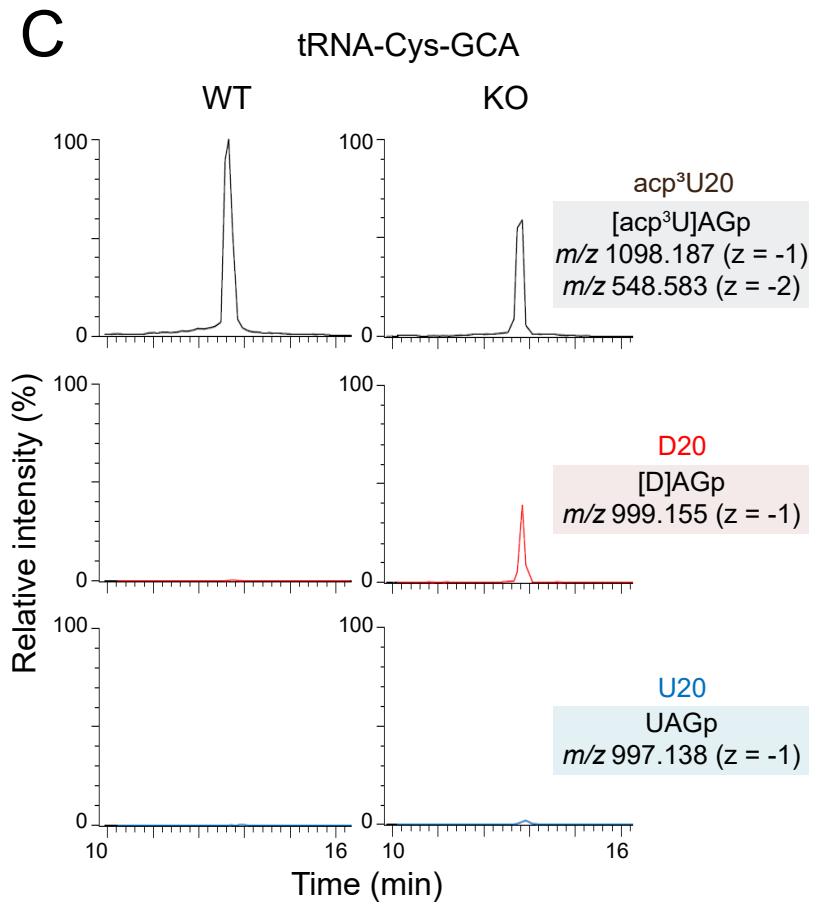

Hwang *et al*. Fig.10

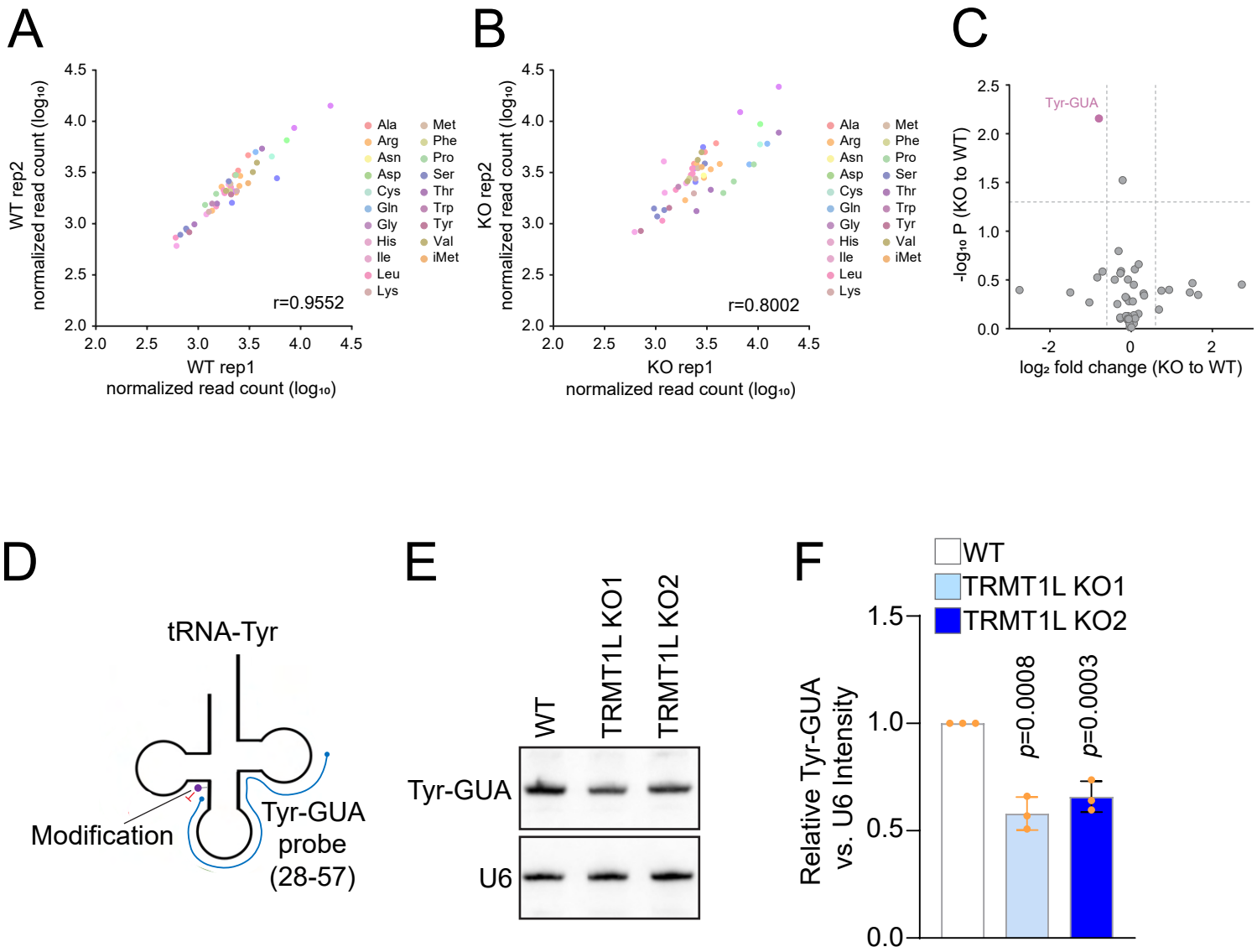

Hwang *et al.* Fig. 11

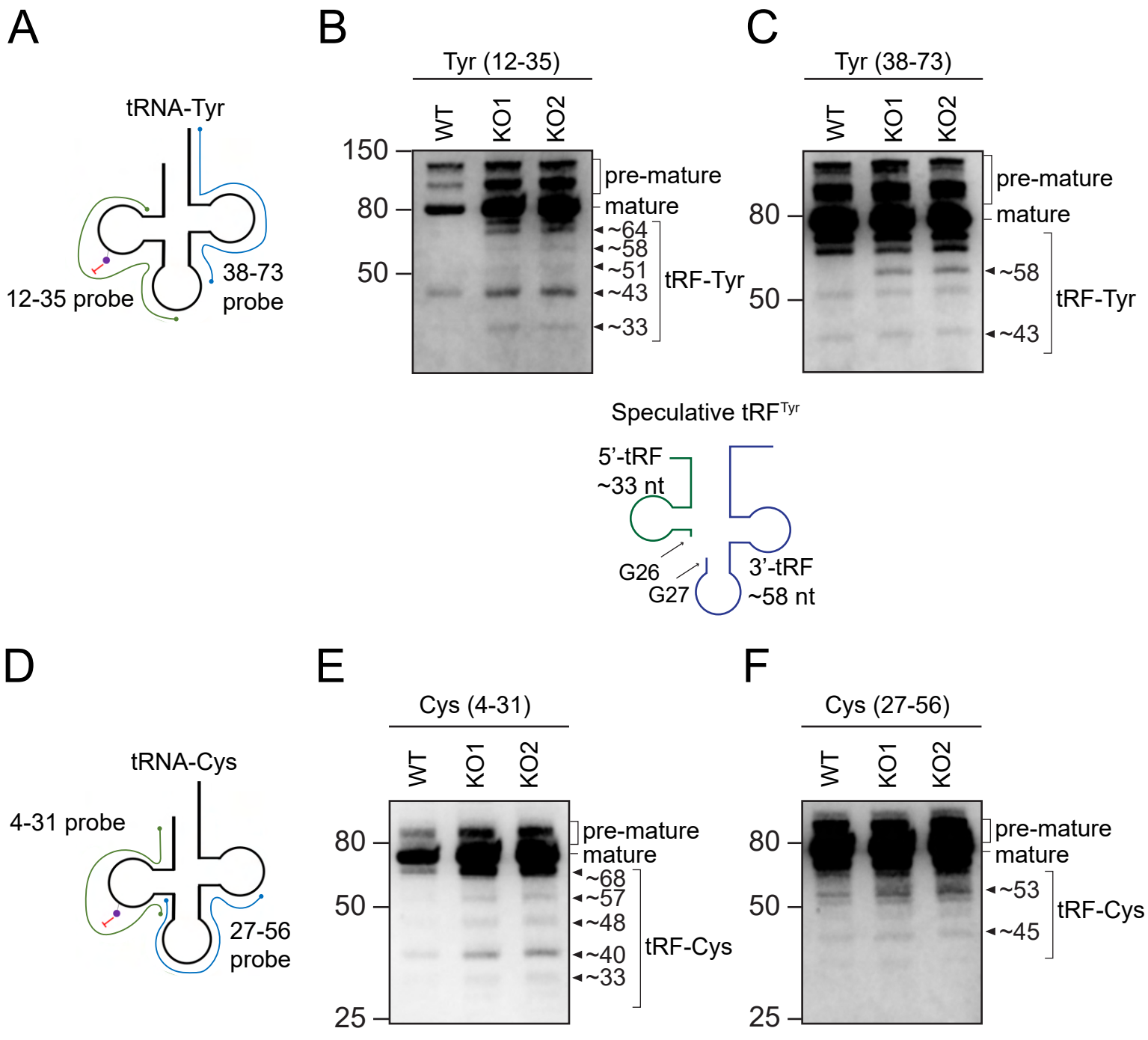

A

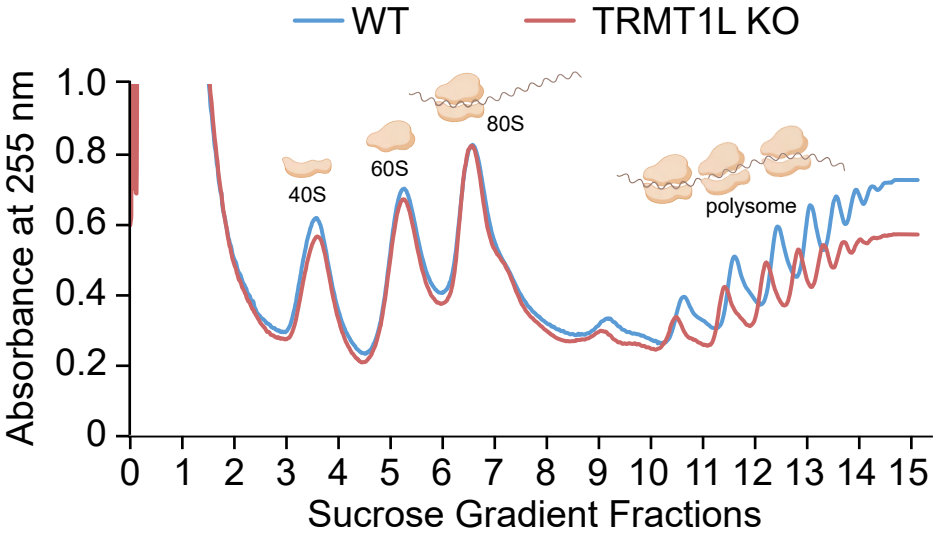
WT
TRMT1L KO
Absorbance at 255 nm
1.0
0.8
0.6
0.4
0.2
0
40S
60S
80S
polysome
0 1 2 3 4 5 6 7 8 9 10 11 12 13 14 15
Sucrose Gradient Fractions

B

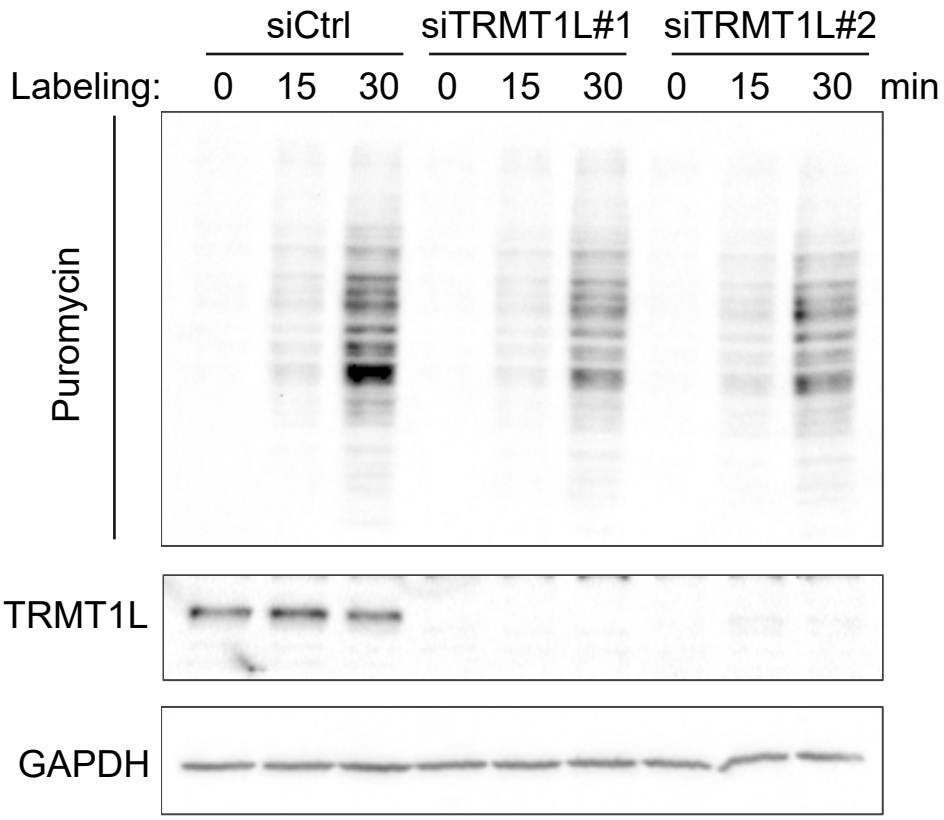
siCtrl
siTRMT1L#1
siTRMT1L#2
Labeling: 0 15 30 0 15 30 0 15 30 min
Puromycin
TRMT1L
GAPDH

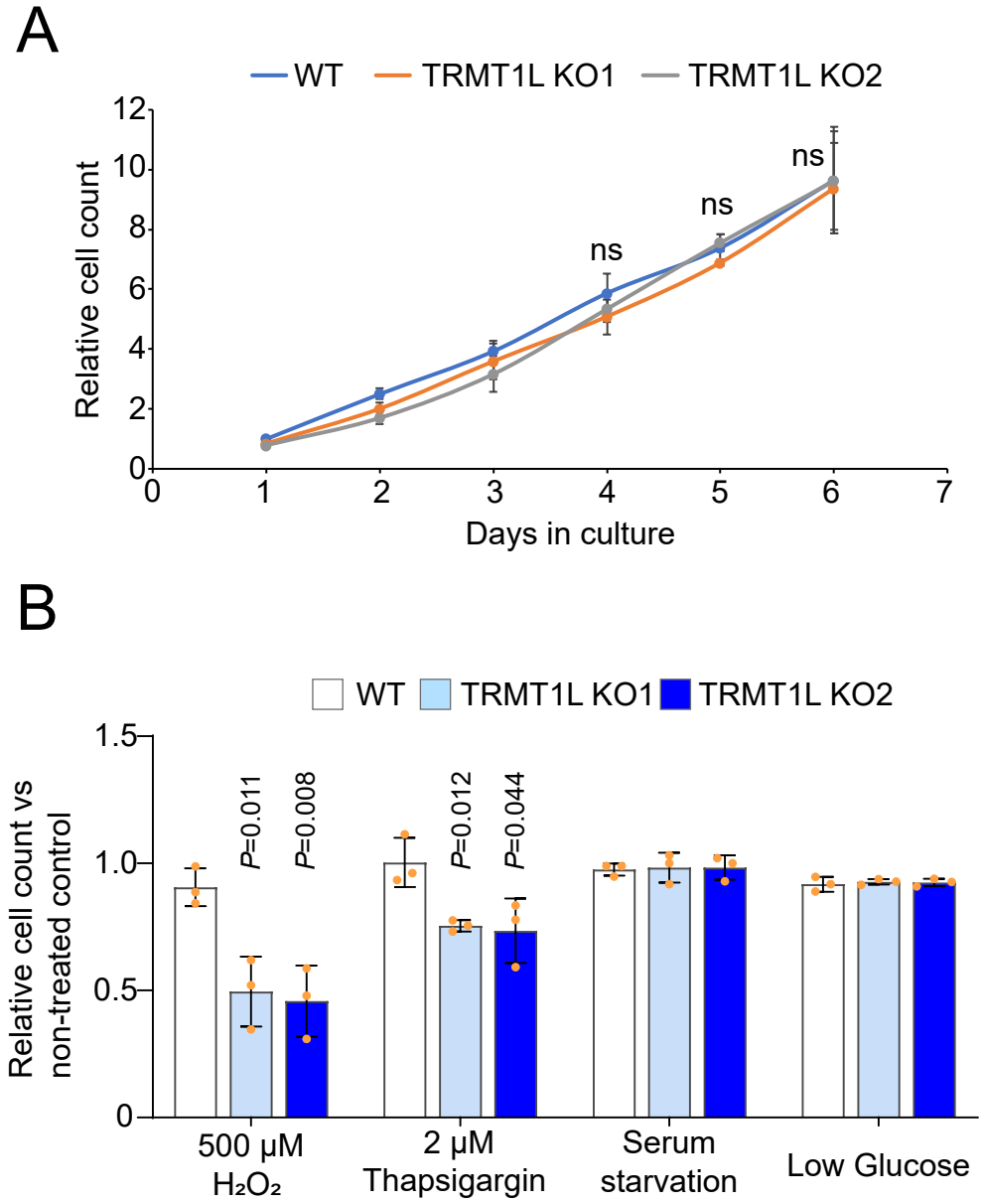
A
WT
TRMT1L KO1
TRMT1L KO2
Relative cell count
Days in culture
ns
ns
ns
B
WT
TRMT1L KO1
TRMT1L KO2
Relative cell count vs non-treated control
P=0.011
P=0.008
P=0.012
P=0.044
500 μM H₂O₂
2 μM Thapsigargin
Serum starvation
Low Glucose

A

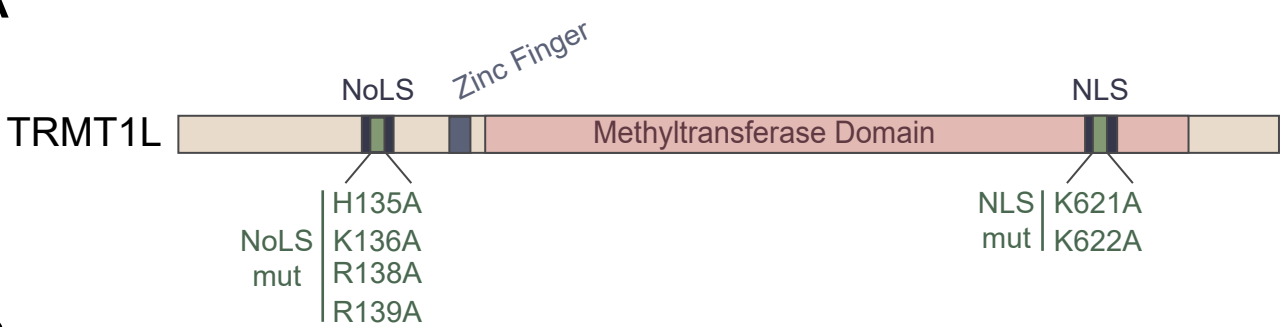
TRMT1L
NoLS
Zinc Finger
NLS
Methyltransferase Domain
NoLS mut
H135A
K136A
R138A
R139A
NLS mut
K621A
K622A

B

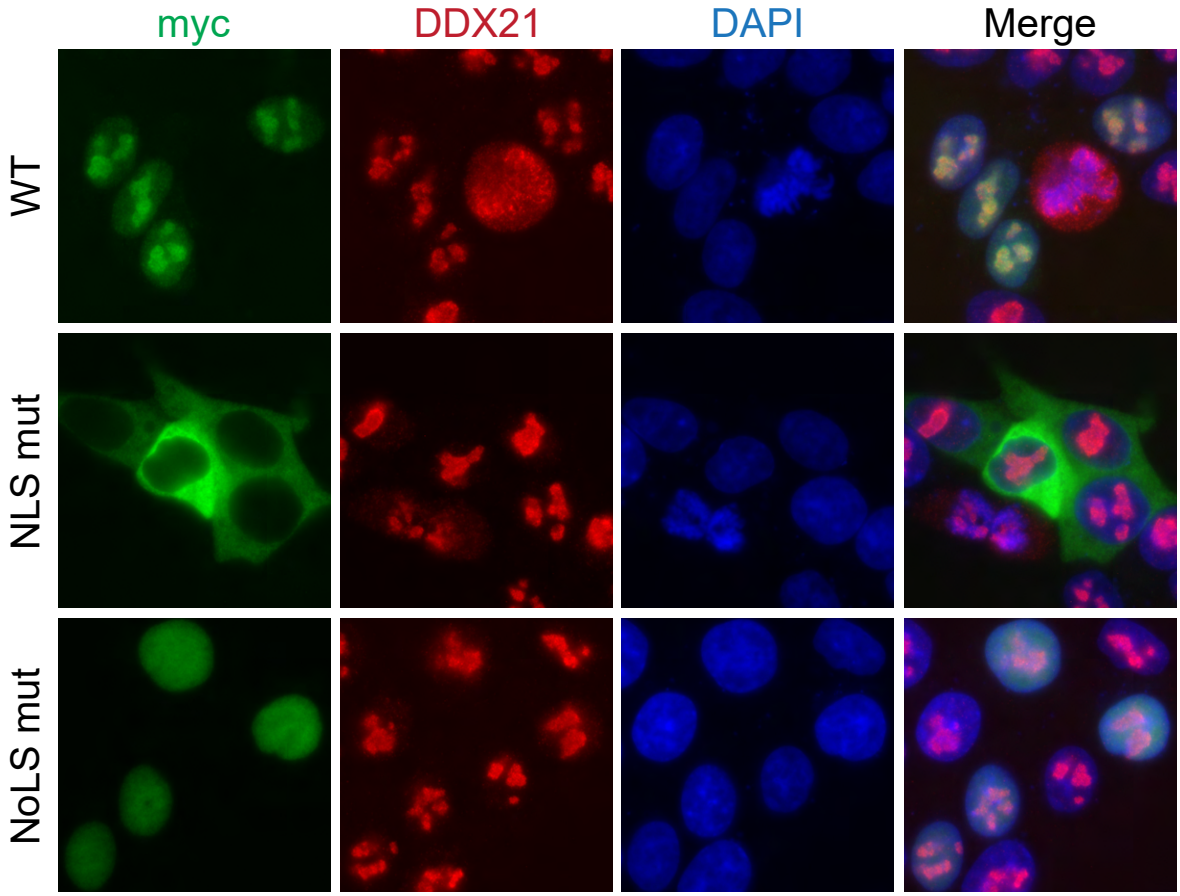
myc
DDX21
DAPI
Merge
WT
NLS mut
NoLS mut

C

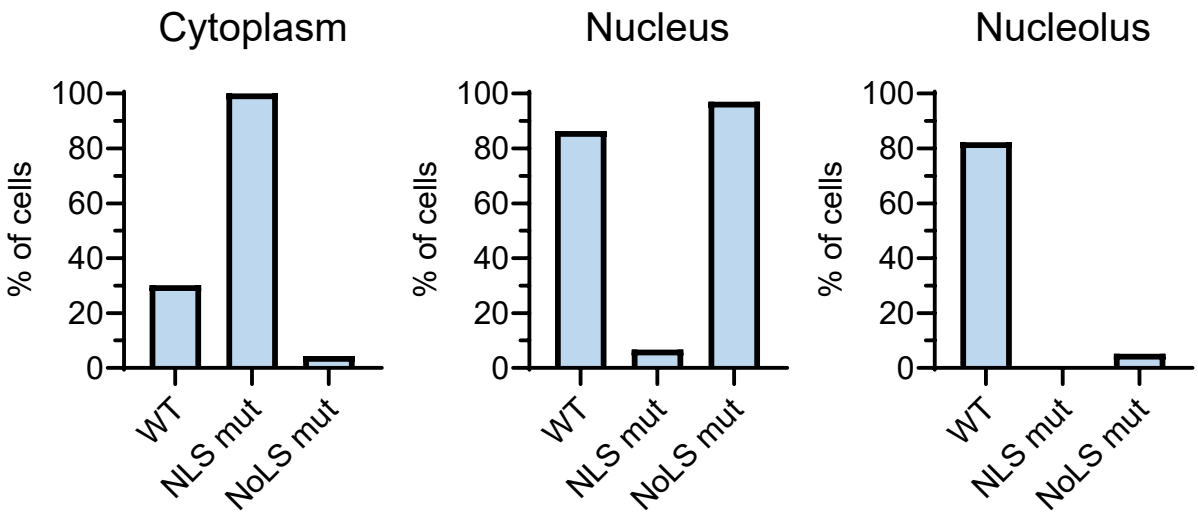
Cytoplasm
Nucleus
Nucleolus
% of cells
100
80
60
40
20
0
WT
NLS mut
NoLS mut

Hwang *et al.* SuppFig. 2

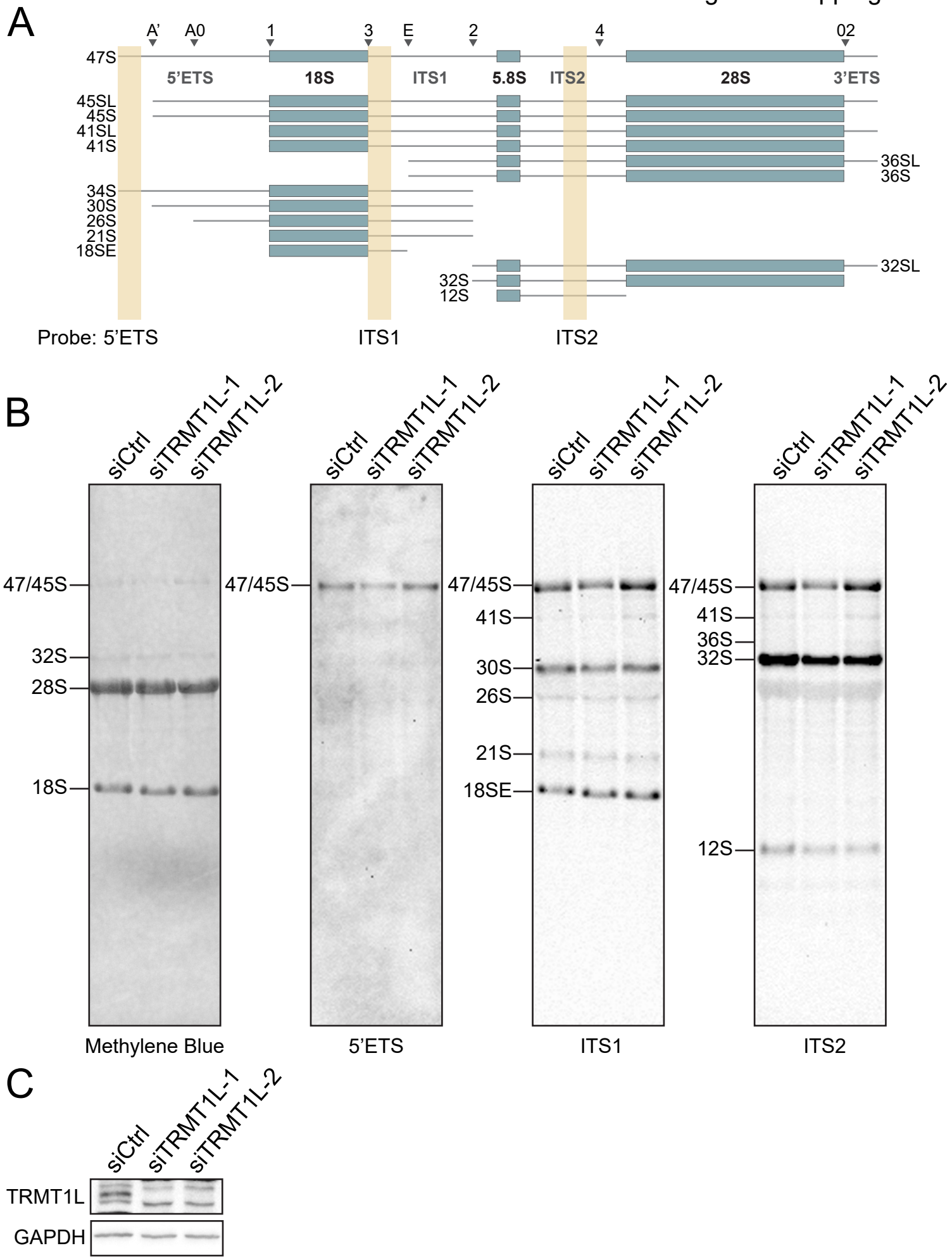

A

HCT116

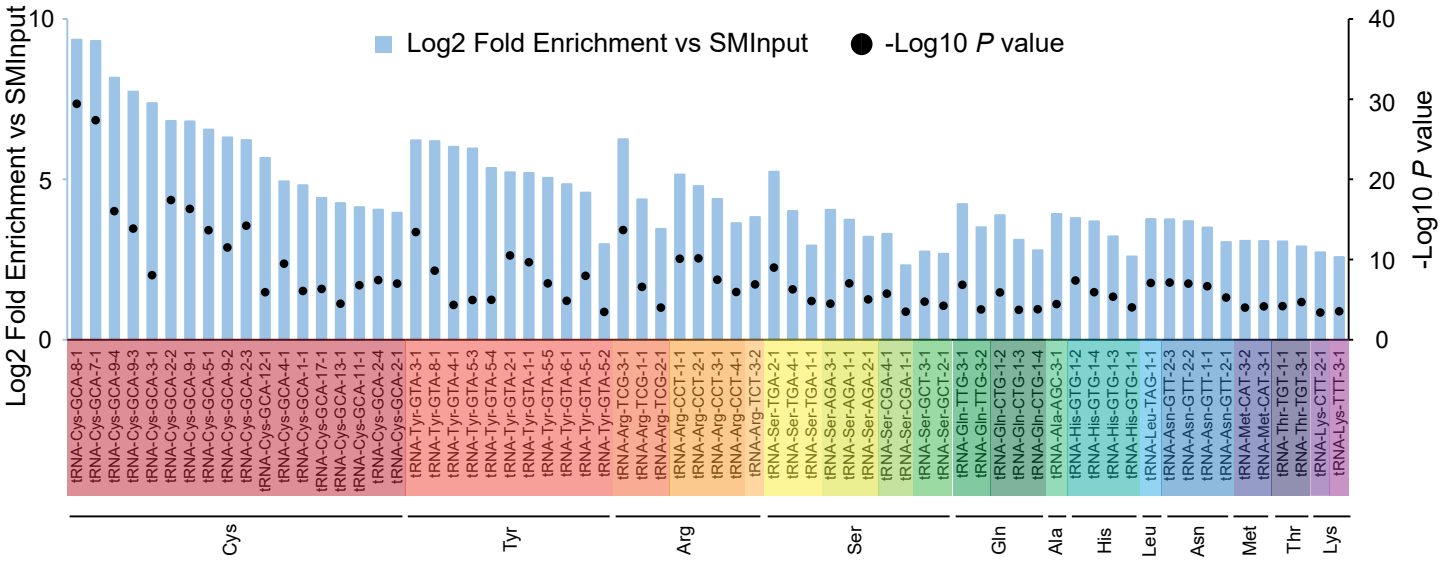

B

Hela

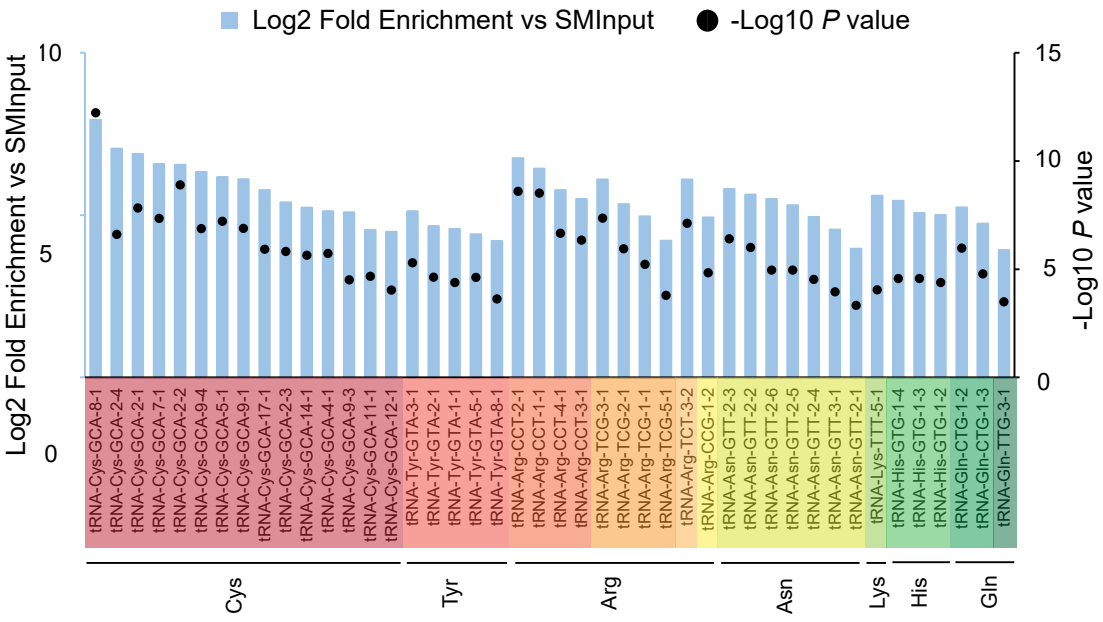

Hwang *et al.* SuppFig. 4

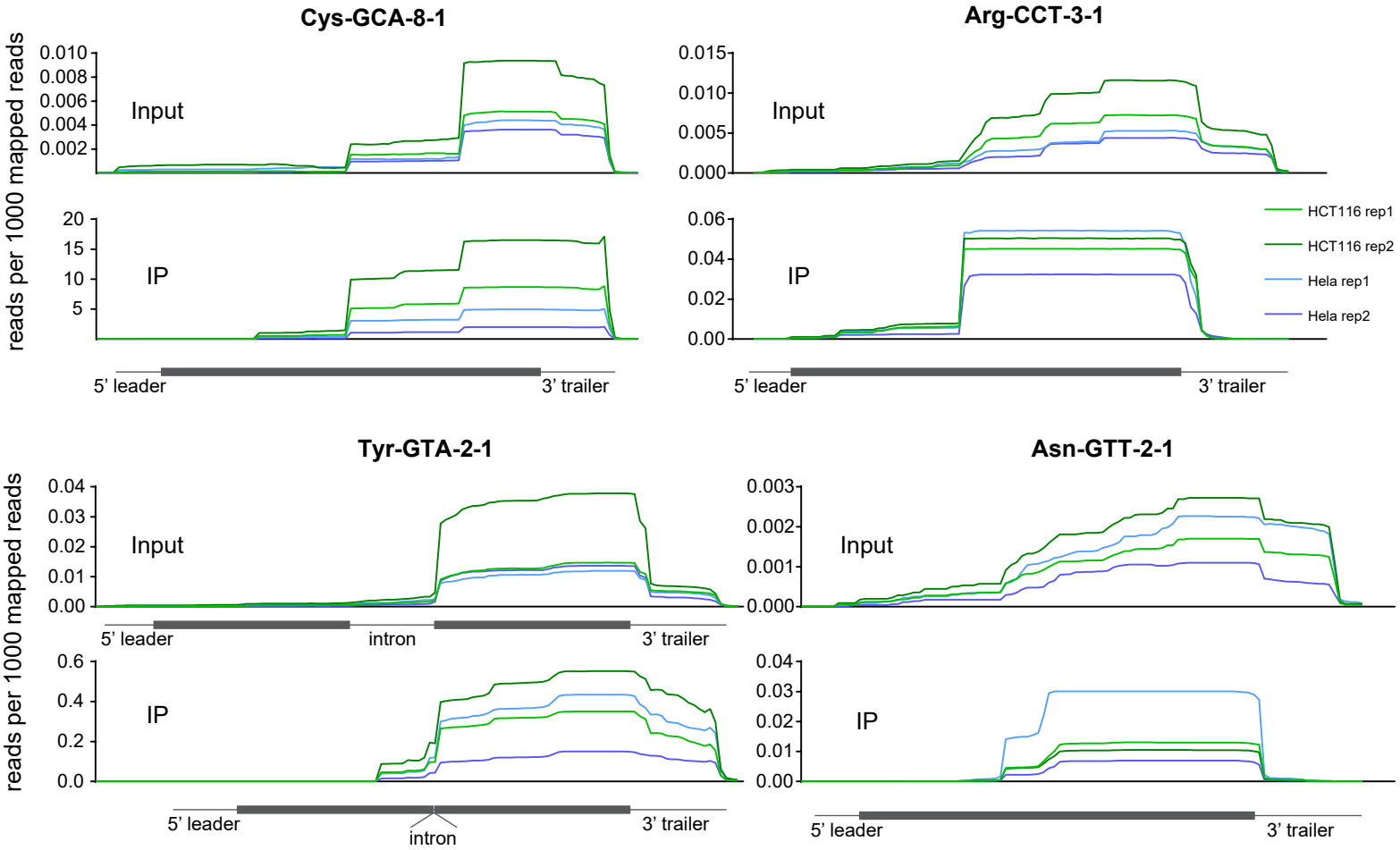

A

TRMT1L

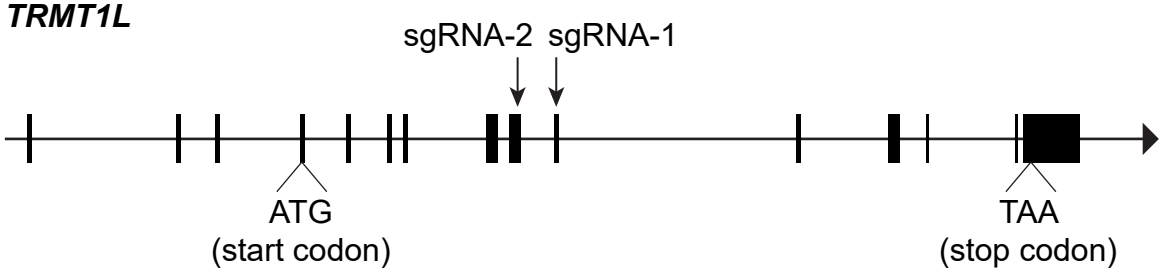

Target sequence--
sgRNA-1: GTAGTTGTGAGAGTTTTGAGGGG
sgRNA-2: TGTTACATCCGTAGTGACGCCGG

B

```
TRMT1L WT    GTGGCTCTGGAACATTTTGTGTTGGTAGTTGTGAGAGT-TTTGAGGGGACCTACTTCAGC
TRMT1L KO1   GTGGCTCTGGAACATTTTGTGTTGGTAGTTGTGAGAGTtTTTGAGGGGACCTACTTCAGC

TRMT1L WT    AAGGCACAGCATGTTGCCCGGCGTCACTACGGATGTAACATTGTCCGAACTGAATATTAC
TRMT1L KO2   AAGGCACAGCAT----------GTCACTACGGATGTAACATTGTCCGAACTGAATATTAC
```

C

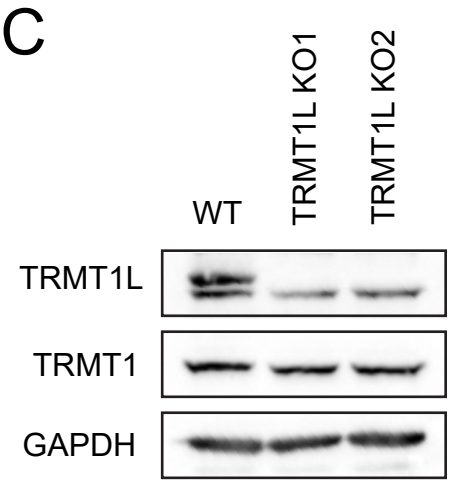

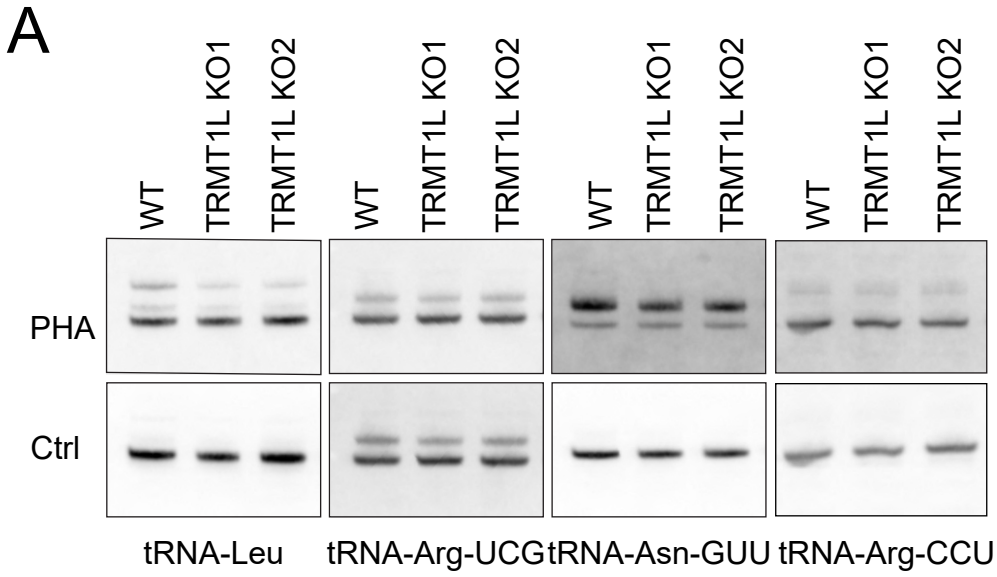
A
WT
TRMT1L KO1
TRMT1L KO2
PHA
Ctrl
tRNA-Leu
tRNA-Arg-UCG
tRNA-Asn-GUU
tRNA-Arg-CCU

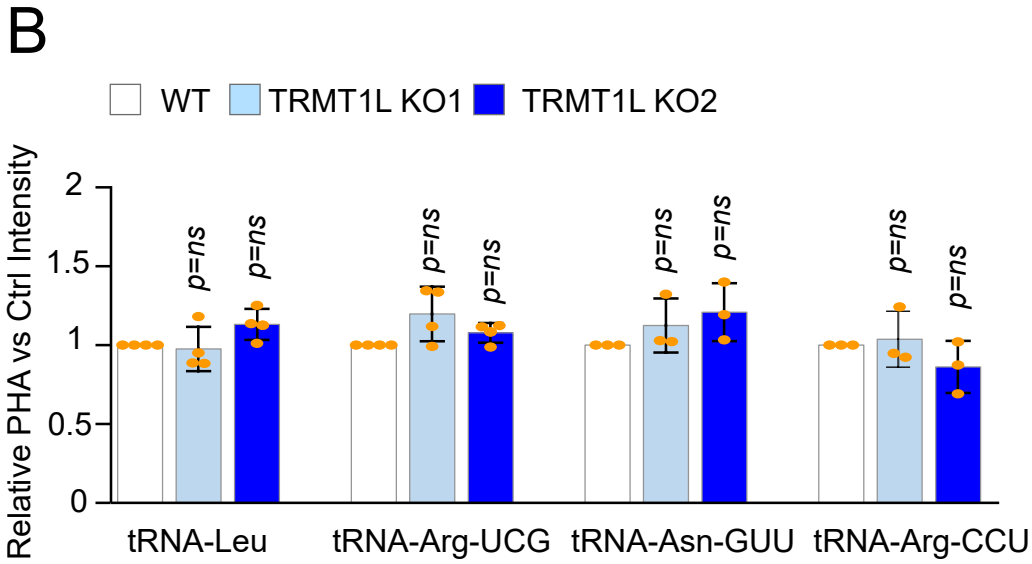
B
WT
TRMT1L KO1
TRMT1L KO2
Relative PHA vs Ctrl Intensity
2
1.5
1
0.5
0
p=ns
tRNA-Leu
tRNA-Arg-UCG
tRNA-Asn-GUU
tRNA-Arg-CCU

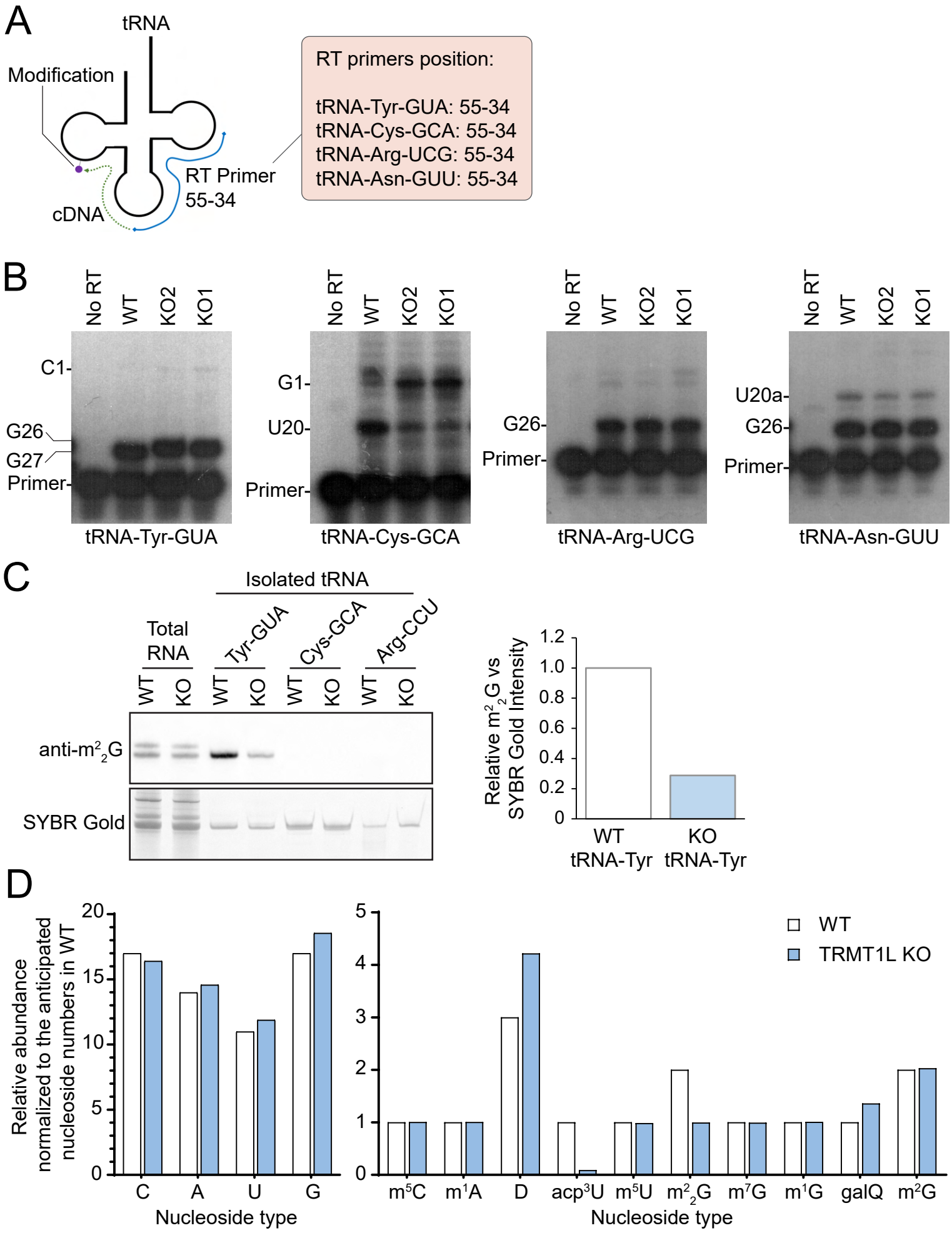
A
tRNA
Modification
RT Primer
55-34
cDNA
RT primers position:
tRNA-Tyr-GUA: 55-34
tRNA-Cys-GCA: 55-34
tRNA-Arg-UCG: 55-34
tRNA-Asn-GUU: 55-34
B
No RT
WT
KO2
KO1
C1-
G26
G27
Primer-
tRNA-Tyr-GUA
G1-
U20-
Primer-
tRNA-Cys-GCA
G26-
Primer-
tRNA-Arg-UCG
U20a-
G26-
Primer-
tRNA-Asn-GUU
C
Isolated tRNA
Total RNA
Tyr-GUA
Cys-GCA
Arg-CCU
WT
KO
anti-m$^2_2$G
SYBR Gold
Relative m$^2_2$G vs SYBR Gold Intensity
1.2
1.0
0.8
0.6
0.4
0.2
0
WT tRNA-Tyr
KO tRNA-Tyr
D
Relative abundance normalized to the anticipated nucleoside numbers in WT
20
15
10
5
0
C
A
U
G
Nucleoside type
5
4
3
2
1
0
m^{5}C
m^{1}A
D
acp^{3}U
m^{5}U
m$^2_2$G
m^{7}G
m^{1}G
galQ
m^{2}G
Nucleoside type
WT
TRMT1L KO

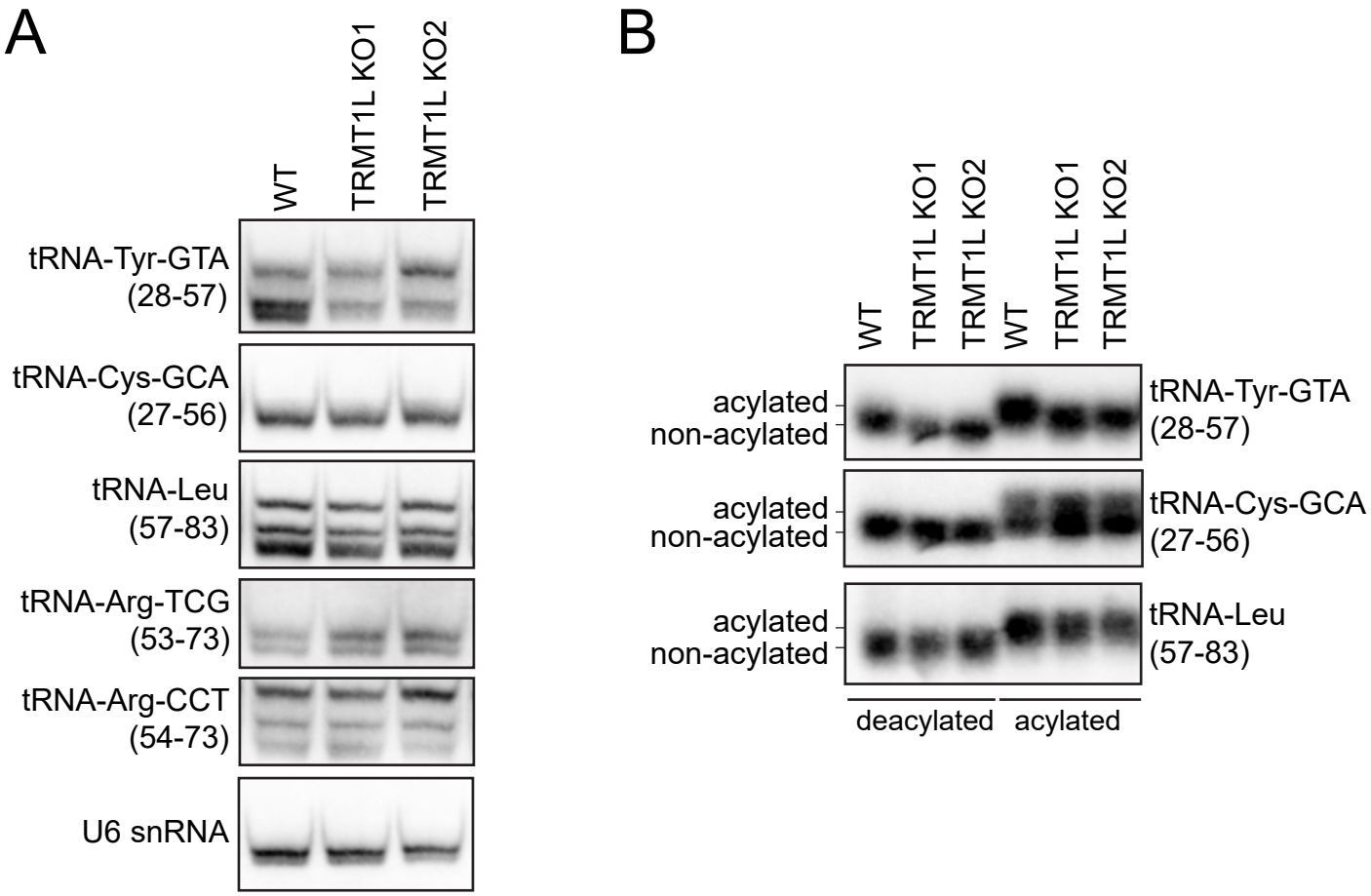
A
WT
TRMT1L KO1
TRMT1L KO2
tRNA-Tyr-GTA
(28-57)
tRNA-Cys-GCA
(27-56)
tRNA-Leu
(57-83)
tRNA-Arg-TCG
(53-73)
tRNA-Arg-CCT
(54-73)
U6 snRNA
B
WT
TRMT1L KO1
TRMT1L KO2
WT
TRMT1L KO1
TRMT1L KO2
acylated
non-acylated
tRNA-Tyr-GTA
(28-57)
acylated
non-acylated
tRNA-Cys-GCA
(27-56)
acylated
non-acylated
tRNA-Leu
(57-83)
deacylated
acylated
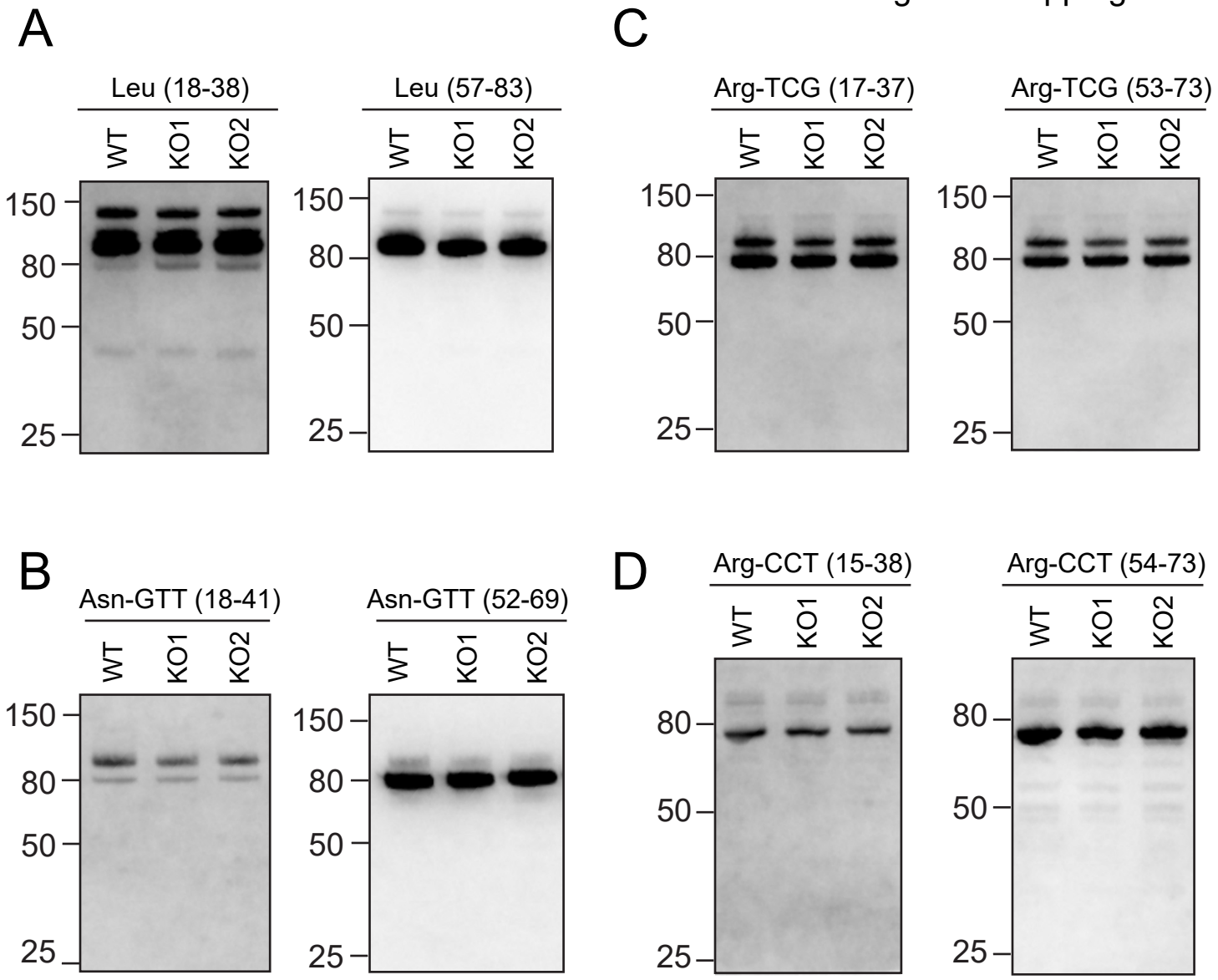
Hwang *et al.* SuppFig. 9